Development of Strategies in Finding the Optimal Cooling of Systems of Integrated Circuits

Dion L. Minter

Thesis submitted to the Faculty of the
Virginia Polytechnic Institute and State University
In partial fulfillment of the requirements for the degree of

Master of Science
In
Mechanical Engineering

Dr. E. P. Scott, Chair
Dr. J. H. Bøhn
Dr. R. L. West

May 10, 2004
Blacksburg, Virginia

Keywords: Power Electronics, Thermal Management, Electronics Cooling, Data Centers, Component Rearrangement, Multi-Scale Modeling, Zoom-in

© 2004, Dion Minter

Development of Strategies in Finding the Optimal Cooling of Systems of Integrated Circuits

Dion L. Minter

(Abstract)

The task of thermal management in electrical systems has never been simple and has only become more difficult in recent years as the power electronics industry pushes towards devices with higher power densities. At the Center for Power Electronic Systems (CPES), a new approach to power electronic design is being implemented with the Integrated Power Electronic Module (IPEM). It is believed that an IPEM-based design approach will significantly enhance the competitiveness of the U.S. electronics industry, revolutionize the power electronics industry, and overcome many of the technology limits in today's industry by driving down the cost of manufacturing and design turnaround time. But with increased component integration comes the increased risk of component failure due to overheating. This thesis addresses the issues associated with the thermal management of integrated power electronic devices.

Two studies are presented in this thesis. The focus of these studies is on the thermal design of a DC-DC front-end power converter developed at CPES with an IPEM-based approach. The first study investigates how the system would respond when the fan location and heat sink fin arrangement are varied in order to optimize the effects of conduction and forced-convection heat transfer to cool the system. The set-up of an experimental test is presented, and the results are compared to the thermal model. The second study presents an improved methodology for the thermal modeling of large-scale electrical systems and their many subsystems. A zoom-in/zoom-out approach is used to overcome the computational limitations associated with modeling large systems. The analysis performed in this paper was completed using I-DEAS©, a three-dimensional finite element analysis (FEA) program which allows the thermal designer to simulate the affects of conduction and convection heat transfer in a forced-air cooling environment.

Acknowledgements

I would like to thank my Savior to whom I owe everything. I would like to thank my wife Jessica for putting up with me during my graduate years and for sharing me with my research. I would like to thank my parents for encouraging me to always pursue education. I would like to also thank my advisor Dr. Elaine Scott for her guidance and direction and for giving me the opportunity to participate in this research and further my education and understanding. I am also tremendously grateful for the help and assistance from Ying-Feng Pang. Her helpful guidance and cheerful attitude was so very much appreciated. I would also like to thank Dr. Jan Helge Bøhn and Dr. Robert West for their guidance and assistance and for participating on my advisory board. Finally, I would also like to thank Zachary Montgomery for his help during my summer research and the Virginia Tech CAD Lab for facilitating my computational needs and access to I-DEAS software. This work was supported primarily by the ERC Program of the National Science Foundation under Award Number EEC-9731677.

Table of Contents

Abstract....ii

Acknowledgements....iii

Table of Contents....iv

Acronyms....vi

List of Figures....vii

List of Tables....x

1. Introduction....1

 1.1 Background and Motivation....1

 1.2 Research Goals and Approach....5

 1.3 Thesis Outline....6

2. Literature Review....7

 2.1 Overview of Thermal Management in Electronic Systems....7

 2.2 Overview of Thermal Modeling in Electronic Systems....13

 2.3 Significance of research....17

3. Computational Methodology....18

 3.1 I-DEAS Description....18

 3.2 Converter Geometry....19

 3.3 Boundary Conditions....21

 3.4 Computational Model Assumptions....23

 3.5 I-DEAS Simulations....31

4. Computational and Experimental Analysis of the Power Converter....36

 4.1 The Fan Arrangement Study....37

4.2 Results of the Fan Arrangement Study 39

4.3 Heat Sink Height and Heat Transfer Mode Investigations 49

4.4 Experimental Verification..52

5 Multi-Scale Thermal Modeling..63

5.1 Background and Motivation..63

5.2 Multi-Scale Modeling Methodology 64

5.3 Results and Discussion 72

6. Conclusions and Recommendations 78

References...82

Appendix A 89

Appendix B 92

Vita...99

Acronyms

AC	Alternative Current
CFD	Computational Fluid Dynamics
CPES	Center for Power Electronics Systems
DBC	Direct-Bonded Copper
DC	Direct Current
DPS	Distributed Power System
EMI	Electromagnetic Interface
ESC	Electronics System Cooling
FEA	Finite Element Analysis
FNM	Flow Network Model
IPEM	Integrated Power Electronic Module
MOSFET	Metal Oxide Semiconductor Field Effect Transistor
PFC	Power Factor Correction
VLSI	Very-Large-Scale-Integrated circuit technology

List of Figures

Figure 1.1 The growing size of air-cooled heat sinks in industry (Joshi, 2002)................4

Figure 1.2 The (a) server and the (b) industry power converter.......................................4

Figure 2.1 Software integration for electro-thermal design (Chen, et al., 2001)...............9

Figure 3.1 The (a) industry's discrete converter and (b) the outer geometry of the CPES converter..20

Figure 3.2 The (a) layout of the improved discrete version of the converter and (b) the basic function of the converter (Sewall, 2002)....................................20

Figure 3.3 The proposed layout of the integrated CPES power.......................................21

Figure 3.4 The fan curve used in the I-DEAS models for the system's two fans.............23

Figure 3.5 The (a) physical active IPEM and the (b) detailed component-level model developed by Pang and Scott (2003)..27

Figure 3.6 The simplified model of the active IPEM...28

Figure 3.7 The (a) layout of the output filter and (b) an exploded detail view of the output diodes (Components 12, 13, 17, and 18)..28

Figure 3.8 An exploded view of the rectifier model used in the present work.................29

Figure 3.9 The complete system-level thermal model of the power converter.................30

Figure 3.10 The power loss of the system's heat-dissipating components.........................30

Figure 3.11 The (a) 3D linear solid elements and the (b) 2D linear thin shell elements from the I-DEAS library of elements (I-DEAS, 2003b). The elements used in this work are circled in red...31

Figure 3.12 The meshing scheme used for the components of the output filter and The heat spreader they sit upon 33

Figure 3.13 The results of the mesh sensitivity analysis performed upon the model of Figure 3.12 33

Figure 4.1 Bottom view of the layout used in Cases 7 and 8 showing the pin-fin heat sink. Each fin is 5 mm x 14 mm..39

Figure 4.2 The thermal response of Case 1. Blue arrows indicate the direction of airflow...40

Figure 4.3 The thermal response of Case 3. Blued arrows indicate the direction of airflow...42

Figure 4.4 The velocity response of Case 1 (a) and Case 3 (b)..42

Figure 4.5 The originally proposed layout for Cases 5 and 6 that was never used...........44

Figure 4.6 The velocity vector diagram for Case 6...44

Figure 4.7 The velocity vector diagram for Case 7...46

Figure 4.8 Comparison of Cases 3, 5, and 7 with Case 1...47

Figure 4.9 The thermal response of the power converter using (a) the 18 mm tall heat sink and (b) using the 14.5 mm tall commercially available heat sink............49

Figure 4.10 The percentage of heat transferred directly to the air (through convection) versus the percentage transferred down through conduction to the heat sink ..51

Figure 4.11 The prototype DC-DC front-end power converter..52

Figure 4.12 The top view of the experimental setup without the electronic board (a), the added board (b), and the insulated converter showing the inlet fans (c) and exit vent (d). 56

Figure 4.13 The revised thermal model of the power converter showing (a) the upstream model and (b) the downstream model with thermocouple locations 56

Figure 4.14 The seven thermocouples located underneath the heat sink 57

Figure 4.15 The results of the updated computational model 60

Figure 4.16 The measured transient temperature response of the converter........................61

Figure 4.17 Comparison between numerical and experimental results...............................61

Figure 5.1 Outline of the muli-scale thermal modeling approach.....................................65

Figure 5.2 The active IPEM, output filter, and rectifier were simplified using two methods: footprints in Model A (a) and blocks in Model B (b) 67

Figure 5.3 The (a) component-level model of the output filter and (b) the air velocity contour plot immediately downstream of the passive IPEM 69

Figure 5.4 Component-level models of (a) the active IPEM and (b) the rectifier 69

Figure 5.5 The multi-device (rack) model..71

Figure 5.6 The (a) individual converter case and (b) multiple devices in a rack 71

Figure 5.7 Comparison of the temperature response between the fully detailed model (top) and Model A (bottom)..73

Figure 5.8 The temperature response of Model B..74

Figure 5.9 Comparison of Model A and Model B to the detailed model..........................74

Figure 5.10 Model B: the (a) air velocity plot and (b) a simplified version 75

Figure 5.11 Comparison of the temperature response of the output filter from (top) the detailed model and from (bottom) the component-level model.................76

List of Tables

Table 3.1 Fan operating conditions used for the fan curve of Figure 3.4 22

Table 3.2 The components in the system-level FE model of the power converter..........25

Table 3.3 The materials used in the model and their corresponding thermal conductivities 26

Table 4.1 The eight proposed layouts used in the parametric study 38

Table 4.2 The temperature responses of Case 7...46

Table 4.3 The modifications that were made to the power converter design prior to the construction of the prototype 54

Table 4.4 The location of the thermocouples with numbers corresponding to those of Figure 4.13 and Figure 4.14...55

Table 4.5 The predicted and measured component temperatures with the calculated percent differences 62

Chapter 1 – Introduction

This thesis focuses upon the development of thermal management techniques and strategies used in the thermal design of a power electronics device. The device, a DC-DC front-end power converter, is used to showcase these techniques and to address some of the problems associated with thermal management and thermal modeling.

1.1 Background and Motivation

Thermal management has always been a critical task in the design of power electronic systems. As designers work to increase power density and the integration of components, the opportunity for premature component failure due to overheating also increases. These failures are very costly to both manufacturers and consumers of electronics. It is a well-established fact that high temperature is the leading cause of component failure in power electronics (Remsburg, 1998; Yeh and Chu, 2002). It is also well established that component failure is extremely costly to both manufacturers and consumers (Quiepo et al., 1994). Thermal management is therefore a very important part of integrated circuit design and it is for this reason that this paper addresses the issue of developing efficient cooling strategies for thermal management. But cooling electrical systems can be a very formidable and complex task. When presented with various project constraints, the difficulty of this task can increase greatly. Over the years, many methods have been developed to solve the problem of cooling electronics (Aung, 1988; Azar, 1998). The job of the thermal engineer is to determine which methods will truly optimize the transfer of heat when constraints such as size, power, and cost are built into the design. Usually, for power electronic devices, the optimization of the thermal design is but one objective in a multi-objective design problem.

In 2000, Lee documented some of the biggest problems associated with the current state-of-the-art approach to power electronics design and how these problems will inevitably lead to a 'technology wall' that will significantly limit the advancement of the electronics industry (Lee, 2000). The author points out that the power electronics industry has not kept pace with other high-tech industries that use a highly automated

approach to design. The lack of standardization of components has also hurt the industry. Power electronic devices often require a high level of customization, which can require very slow turnaround times for design and very high costs of manufacturing. Because the manufacturing of these devices is so labor-intensive and because there are many companies overseas that can offer cheaper labor, the power electronics industry in the U.S.A. has suffered great losses. A more efficient approach to the design and production of power electronics is needed not only to overcome the limits of technology, but also to enhance the competitiveness of the electronics industry in the U.S.A.

To overcome these limits, many researchers have focused their efforts upon component integration and design improvement (PSMA, 2003). Despite consumer resistance to cost increases for increased product functionality (ITRS, 2003), consumers are driving the current trend toward increased standardization, package size reduction, and product efficiency. There are many challenges that lie ahead for improving power electronics technology. However, Harlow (2003) predicts that, despite these challenges, economics will drive the trend towards single-chip technology. Additionally, the increasing need for energy conservation will drive the development of more efficient power electronics devices (Bose, 2000).

Lee (2000) proposed an integration approach to electronic design similar to the circuit technology of Very-Large-Scale-Integration (VLSI). VLSI circuit technology quickly advanced the computer and telecommunications industries by increasing the level of standardization and decreasing the cost of manufacturing (Jiang et al., 2002). Similarly, an IPEM-based (Integrated Power Electronics Module) approach would increase the integration of components so that standard subassemblies of components could be used interchangeably in many different devices and applications. This approach would dramatically lower the cost of manufacturing as it would allow for faster turn-around time for custom designs and manufacturing. Furthermore, it would open up the opportunity for new applications that were before prohibited by the limits of technology. This integrated component approach is very dependant upon an equally integrated design approach requiring a high level of integration of electrical, thermal, mechanical, and materials design.

The research that is presented here was performed at the Center for Power Electronic Systems (CPES). CPES is a research center supported by the National Science Foundation and more than 80 industry partners. Five universities (including Virginia Tech) belong to the CPES partnership. The overall goal of CPES is to enhance the electronics industry in the U.S.A. by pushing for IPEM-based research and design. These IPEMs are clusters of components that work together for a common purpose or function and are but a sub-system in a much larger system of electrical components (this is analogous to a sub-routine in programming). These IPEMs, which can be used in different combinations and in different types of power electronic devices, offer modularized layouts and designs and high power densities. But while the use of IPEM technology may solve many problems in electrical design, it only makes the task of thermal management that much harder because of the high power density that comes along with this technology.

To meet the needs of integrated electrical design, new techniques in thermal management must be developed. Figure 1.1 shows the increasingly growing size of air-cooled heat sinks in the electronics industry (Joshi, 2002). Currently, air-cooled heat sinks are the tools of choice for cooling most power electronics because of their low cost and low maintenance. Obviously, air cooled heat sinks cannot continue to grow in size in order to meet the demands of technology. Eventually, if the trend of higher power density and smaller packaging continues, they will no longer be able to sufficiently cool power electronic devices (let alone do it efficiently). Other cooling techniques and strategies must be explored and employed.

The research that is presented in this thesis is centered on the thermal management techniques that were used in the design of a power converter. The use of a distributed power system (DPS) in the converter could be applied to a multitude of applications, including computers, telecommunications, networking, automotive, and aerospace. The DPS approach offers higher efficiency, higher power density, higher reliability, and lower cost than convectional approaches. Figure 1.2 shows the direct application of this research. The integrated power converter developed at CPES would be used in a telecommunications server application (Figure 1.2a) and would replace larger, less efficient, and more expensive discrete industry converters (Figure 1.2b).

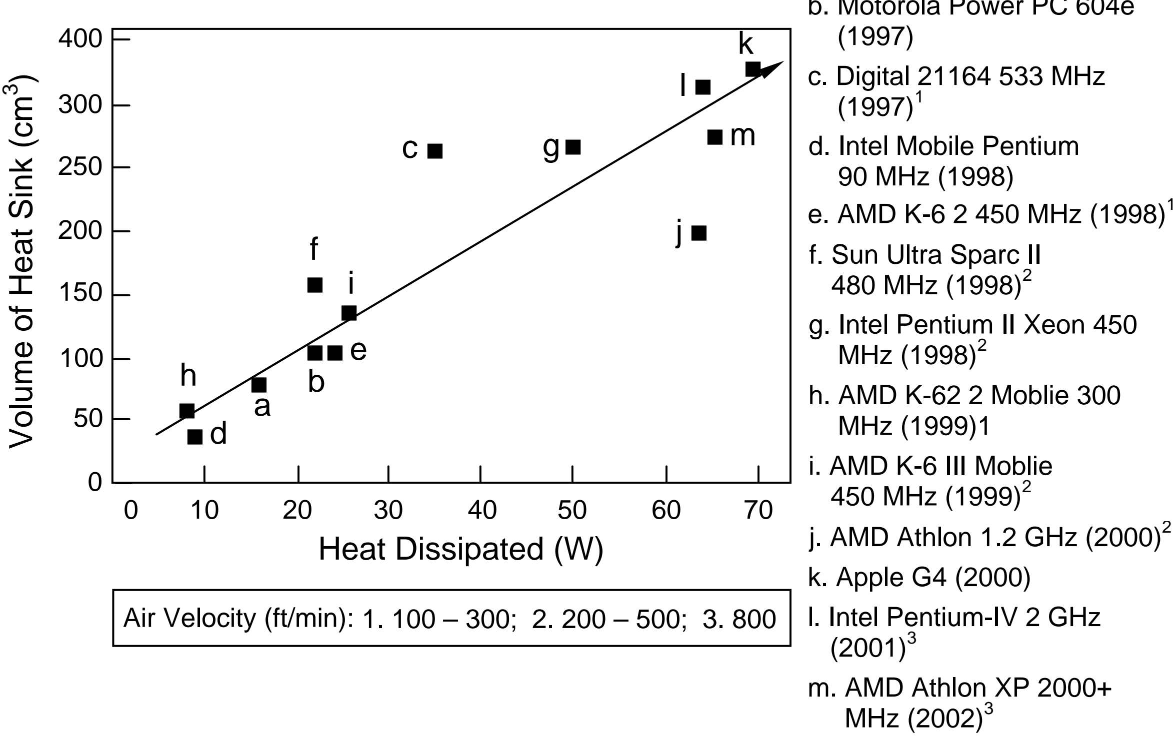

Figure 1.1 The growing size of air-cooled heat sinks in industry (Joshi, 2002).

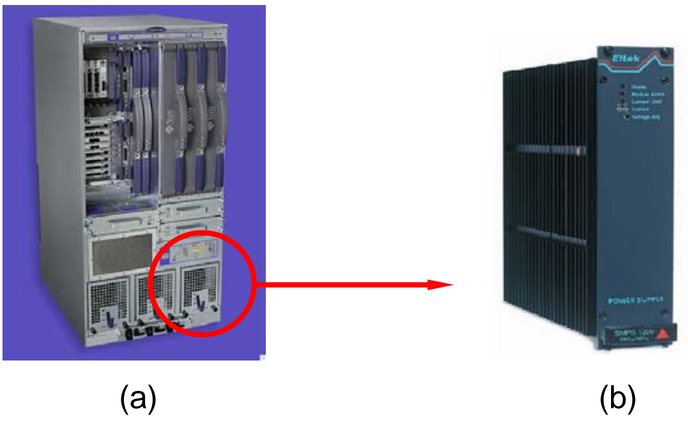

(a) (b)

Figure 1.2 The (a) server and the (b) industry power converter.

1.2 Research Goals and Approach

The goal of this research is to develop strategies for finding the optimal cooling of systems of integrated circuits. The optimizational approach used in this work did not center upon the maximization or minimization of a specific objective function, but instead upon finding the most viable solution to a multi-objective problem. This work focuses upon the thermal management of an IPEM-based power converter. However, the purpose of this research is not to simply document the thermal strategy that is used to keep the converter's component temperatures below a required limit. Instead, the design of the power converter serves as an example of thermal management techniques for high-density power electronics devices that require multi-objective optimization. This work is intended to be used as a guideline for cooling strategies and design techniques in order to increase the efficiency and effectiveness of thermal management at CPES.

There were three objectives that were established in order to accomplish the goal of this research.

1. The first objective was to develop a system-level thermal computational model of the converter and use it to investigate the system's thermal response to the location and direction of the cooling fans and heat sink fin geometry. This investigation was used to determine the most viable layout of the system that would minimize temperatures system-wide and result in an even temperature distribution.
2. The second objective was to conduct an experimental test upon a physical prototype of the converter in order to determine the true thermal behavior of the device. The results of this test would also be used to verify the computational model in order to assess the accuracy and usefulness of the model.
3. The third and final objective was to improve the approach used for system-level thermal modeling at CPES. This objective was driven by the need to overcome computational modeling limits associated with large, multi-scale electrical systems such as data centers.

1.3 Thesis Outline

This thesis contains six chapters with a common theme: developing efficient electronic cooling strategies. The first three chapters present the reader with an in-depth explanation of what is being presented in this work, why this research is significant, other research that has been performed on this subject, and the specific goals of this particular research project. The next three chapters present the actual analysis that was performed and discuss the results of that analysis.

Chapter 1 has provided a brief discussion of the background, motivation, and overall objective of the research that is presented. Chapter 2 presents an in-depth literature review of the current state-of-the-art thermal management and thermal modeling of electronic systems. Chapter 3 presents the power converter that is the focus of this work and the thermal model that was built to represent it. In Chapter 4, a parametric study that examines the effects of varying the system's fan arrangement is discussed and the results are presented. In addition, an experimental test was performed on the power converter prototype and compared to the results of the thermal model. Chapter 5 presents a more efficient methodology for modeling electrical systems, especially those that involve multiple levels of complexity. Finally, Chapter 6 presents a brief summary and discussion of the work that is presented and recommendations for future system-level thermal management.

Chapter 2 – Literature Review

This chapter presents an in-depth look at the research that has been conducted prior to the writing of this thesis on the subject of the thermal design of electrical systems. This literature review includes a discussion of current state-of-the-art issues and optimizational techniques involved with thermal management and some of the tools that are used in thermal management. These tools include thermal modeling, electro-thermal software integration, and multi-scale modeling. First, an overview of thermal management in electronic systems is presented in Section 2.1. In Section 2.2, an overview is presented of thermal modeling in electronic systems. Finally, Section 2.3 discusses the significance of the research that is presented in this thesis and how it is relevant to the electronics industry.

2.1 Overview of Thermal Management in Electronic Systems

Thermal management is an important part of the design process of most any electronic device. Thermal management is important at both the component level and the system level. It plays a crucial role in the device's quality, efficiency, and, above all, its reliability. Thermal management is only becoming more important as the trend in the electronics industry continues toward devices with higher power densities and smaller packages. As designers work to increase power density and component integration, the opportunity for premature component failure due to overheating also increases. These failures are very costly to both manufacturers and consumers of electronics. It is for this reason that the importance of thermal management cannot be underestimated, nor its necessity overlooked.

Product development involves several stages. Many times, the stages overlap and one is an integral part of the others. Likewise, thermal management can involve several integrated or overlapping stages of design. These stages can include hand calculations for initial estimates, advanced thermal modeling using commercial software, and experimental testing of physical prototypes. Minichiello and Belady (2002) showcased the thermal design methodology they employed to design a multi-processor server, the

RP8400. This methodology, first introduced by Biber and Belady (1997) three years prior and later refined (Belady et al., 1999), was used in the hope that it would help reduce the risk of product failure but at the same time minimize the cost and time required for thermal design and testing. The methodology consisted of three stages of product development: concept, design, and hardware. During the first stage, Minichiello and Belady used hand calculations and in-house spreadsheets to develop estimates and make initial design decisions. During this first stage and throughout the second, they used flow network modeling (FNM) to begin to characterize the behavior of the proposed layout(s). During the second stage, they used commercial CFD (computational fluid dynamics) software to verify the FNM results and to identify any 'holes' or wrong assumptions in their earlier predictions of the system's temperature behavior. Finally, beginning toward the end of the second stage and finishing at the end of the third, they ran tests on a prototype of the product in order to verify earlier calculations and to refine their predictions.

This methodology insists that it is much more efficient to use a variety of design tools for a given electronics cooling application or problem than to try to use only one 'best' tool. While this work does showcase the usefulness of simple in-house and/or commercial codes to predict a system's behavior quickly and cheaply, it also showcases the potential for error if proper caution is not taken. For example, because of the FNM code's inability to account for specific geometry, the results were not able to detect the presence of a crucial flow blockage. By performing CFD analysis, this blockage was detected. In a later paper published on the subject of the same methodology, Minichiello and Belady (2003) added that using a combination of diverse design tools such as hand calculations, spreadsheets, FNM and CFD analysis, and testing was four times as productive as hand calculations, spreadsheets, and testing alone.

Figure 2.1 shows the approach to electro-thermal design at CPES (Chen et al., 2001). In this integrated design approach, the program iSIGHT is used to automate the transfer of data between I-DEAS, Maxwell Q3D, and Saber. Using a diverse array of tools can dramatically reduce the risk of product failure. Indeed, the tools of thermal management should be integrated with each other for a more efficient design process. Similarly, thermal design should be integrated with electrical design.

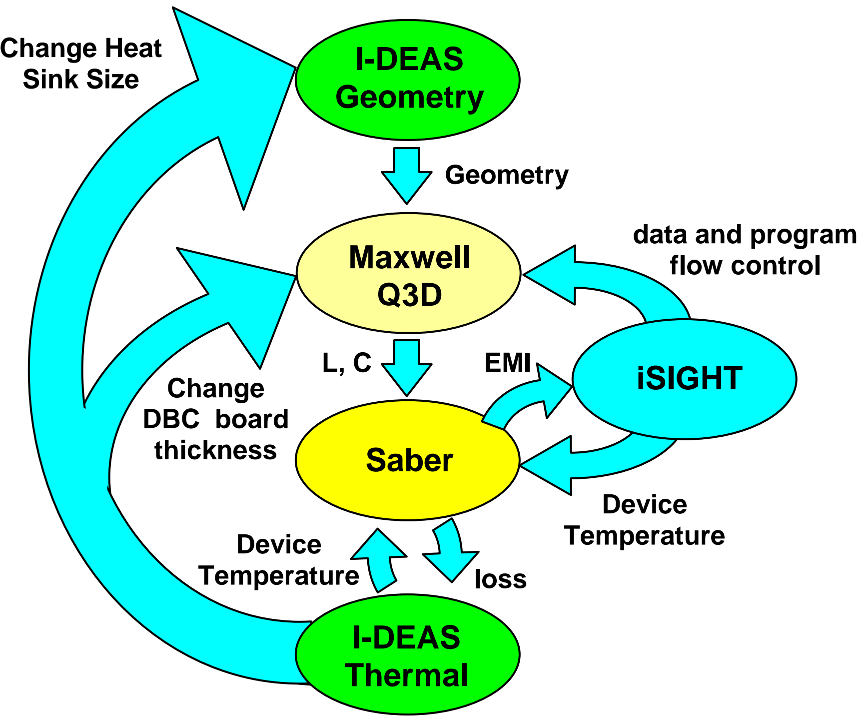

Figure 2.1. Software integration for electro-thermal design (Chen et al., 2001).

The basic goal of thermal management of electronic devices is simple: reduce the probability of component failure due to overheating by reducing the component temperatures. Deciding how to reduce component temperatures is often the most challenging aspect of the thermal design process and is the subject of the remainder of this section. The choice of the thermal management used for the electronic systems has a large impact on the size, performance, and cost of the final product. Usually, one of the first decisions made in the thermal design process of these devices is one that involves the choice of heat sink that should be used. It is now common practice to use an aluminum heat sink along with at least one cooling fan in many power electronic devices. The thermal designer must decide which type of heat sink and fan arrangement should be used for the given application. There are several types of heat sinks to choose from, including parallel-plate heat sinks, pin-fin heat sinks, and microchannel heat sinks. Lee (1995) compared the relative performance and cost of different types of heat sinks and discussed the parameters that affect their performance. In addition, Lee looked at

calculating the spreading resistances on the surface of heat sinks and documented the relationship between this resistance and the size of the base of the heat sink (Lee, 1998).

By far the most frequently used type of heat sink is the parallel-plate heat sink. Researchers have worked at characterizing their performance and optimizing the design parameters associated with them. Simons developed methods for estimating the thermal resistance associated with parallel-plate heat sinks (2003a), the pressure drop across them (2003b), and the effect of flow bypass on their performance (2004). In addition, Copeland (2000) provided a method of optimizing a parallel-plate heat sink used in forced convection environments by determining the best fin thickness and pitch to reduce the associated thermal resistance. Nagulapally and Karimanal (2002) looked at drastically simplifying the computational model by representing the entire heat sink with shell elements of zero thickness. They investigated the effects of varying parameters such as temperature, pressure, and flow rate for different fin thicknesses and spacing ratios. However, this method cannot accurately account for the volumetric flow blockage created by the heat sink. Mahalingam and Glezer (2002) looked at the benefits of using a synthetic jet with a parallel plate heat sink. The authors found that this technique significantly improved the effectiveness of the heat sink over conventional fan/heat sink arrangements.

Another popular type of heat sink commonly used in power electronic devices is the pin-fin heat sink. The pin-fin heat sink can be a very useful alternative to the parallel-plate heat sink (depending upon the application). This type of heat sink is typically used in a jet-impingement environment in which air is blown directly down on the ends of the fins of the heat sink. However, they can also be used in cross-flow environments too and are generally unaffected by the direction of airflow. Researchers (Kendo et al., 2000; Kim et al., 2002; Issa et al., 2002; Maveety et al., 2002) have developed optimization techniques for these heat sinks for various applications and cooling environments. Kim and Webb (2003) compared the performances of in-line and staggered round pin-fin heat sinks to that of a parallel-plate heat sink and an offset strip-fin heat sink in a cross-flow forced convection arrangement. They found that the parallel-plate and the staggered strip-fin heat sinks provided a significantly lower convective thermal resistance. Furthermore, they found that the staggered strip-fin heat sink slightly outperformed the

parallel-plate heat sink. While the pin-fin heat sink is typically the heat sink used in flow impingement environments, Saini and Webb (2002) compared the effects of flow impingement to duct flow for a parallel-plate heat sink and a strip fin heat sink.

Cole, et al. (1999a) presented a unique method of thermal management for electrical components in a forced-convection environment at the board level. They used experimental measurements to determine influence coefficients (such as air temperature and movement) for their resistance models. They also looked at both numerical predictions and experimental analysis of axial cooling fans and established guidelines for modeling them (Cole et al., 1999a, b). Their experimental investigation showed that the fan behavior was very sensitive to blockages near the fan and to the temperature of the air. Furthermore, outlet fans in their system produced steady, predictable flow but inlet fans produced turbulent and sometimes recirculating airflow conditions. These results agree with those obtained by Grimes and Davies (2002) when they investigated the effects of fan operating point and location. Grimes et al. (2001) also looked at the modeling of cooling fans. Their work, however, focused upon using CFD software to model radial blower fans, which can be very difficult and computationally expensive to accurately model. The authors provided a 6-step process to 'correct' the manufacturer's fan curve. They compared their numerical results to experimental results and found that they differed by approximately 10%.

Forced air is the most common method of heat removal in power electronic devices. With that said, however, it is clear that today's thermal designers are beginning to push the limits of air-cooled electrical devices. For this reason, some researchers have turned to other cooling technologies that provide an alternative to air-cooling. Bhavnani, et al. (2001) investigated immersion-cooled heat sinks using high-speed photography to capture the heat sink's interaction with its environment (i.e., location and effect of bubbles that were produced). Other researchers (Copeland et al., 1997; Jiang et al., 2002; Jiang et al., 2001; Vafai et al., 1999) have investigated the use of microchannel heat sinks in which air or liquid is used to carry the heat away from the system by flowing through small channels imbedded within a high conductive slab of material. These investigations included isothermal analysis on manifold microchannel heat sinks, closed-loop electroosmotic microchannel systems, two-phase microchannel heat sinks, and double-

layered microchannel heat sinks. The double-layered microchannel heat sink contained two sets of channels (one on top of the other) and allowed for the coolant in one to travel in the opposite direction as the other in order to enhance the removal of heat from the system.

Many researchers have investigated the use of heat pipes in electronics cooling applications (Yeh and Chu, 2002). Heat pipes work by transferring heat via boiling and condensation. While the use of heat pipes requires much more system complexity than the use of air-cooled heat sinks, heat pipes can offer a very effective and efficient method of heat removal. Some researchers (Ishizuka et al., 2003; Andreozzi et al., 2003) have also investigated the effects of inclining naturally cooled electronic devices. They have found that inclining these devices enhances the effects of natural convection (this is called the chimney effect). Closed-Loop cooling, including the use of air-to-air heat exchangers and water-to-air heat exchangers, is becoming an increasingly popular cooling technology. It can be especially useful in applications where the electronic device may be subject to contaminated air (i.e., excessive dirt and/or dust) or where conventional air-cooling is unable to efficiently remove the system's heat. Direct liquid cooling is another alternative to conventional methods and has been investigated by several researchers including Simons (1996).

This discussion is by no means complete in its content and does not begin to cover the depth of the subject of alternative cooling methods. However, its intent is to show how technology is pushing the trend to seek out innovative ways to cool electrical components. These advanced cooling technologies offer significantly improved thermal responses but their cost and complexity prohibit their widespread use in many applications. The low cost and simplicity of the forced-air cooled parallel-plate heat sink will likely allow it to remain the industry standard until the power densities of electronic devices push too far beyond its practical and efficient use.

A DC-DC power converter is an excellent example of a high-density electronic device that requires special attention to thermal design and is the subject of analysis for this thesis. Ridley, et al. (1993) performed three-dimensional thermal simulations to access the cooling requirements of DC-DC converters on high-density packaging applications. They investigated three cooling cases, the board position of the converter,

and the effect of the thermal load imposed by the components in the DC-DC converters. Their results showed the often-underestimated importance of thermal design for DC-DC converters and that seemingly minor changes in environment around heat sources can have a dramatic effect on the end temperature. More recently, Sewall et al. (2002) developed guidelines for the thermal management of DC-DC converters. They investigated the thermal effects of eight different component layouts. Similarly, Minter et al. (2003) investigated the thermal effects of the fan location on a similar DC-DC power converter. Their work showcased the system's sensitivity to fan location and insensitivity to fan direction. Montgomery et al. (2004) looked at the thermal response of the same DC-DC converter as investigated by Minter et al. (2003) when the incoming airflow is diverted to flow only in a pre-set region. This study focused on determining if it is beneficial to flow the air completely through the fins of the heat sink, completely over the top, or some percentage between the two. Their simulations showed that diverting all of the air to flow through the fins of the heat sink can significantly lower the component temperatures system-wide and is an important parameter to investigate in future thermal designs.

This section has established the importance of thermal management for power electronic systems and has showcased the research that has been conducted in this area. Thermal management encompasses all of the tools and methods the thermal designer uses to predict the thermal behavior of electrical systems. One such tool is computational thermal modeling. Thermal modeling is a crucial part of the thermal design process and is the subject of the next section.

2.2 Overview of Thermal Modeling in Electronic Systems

Thermal modeling is by far the most efficient and cost-effective tool for the thermal designer. It can bring tremendous insight to the system's behavior. The use of thermal computational modeling is becoming increasingly important as researchers continue to push the limits of conventional cooling methods and seek out new technologies to solve the problems they face. Its use as a design tool for thermal

management and optimization is now state-of-the-art (Joshi, 2001) and its importance in power electronics design will likely continue to increase with time.

There are many commercially available software packages on the market that can aid the thermal designer in thermal analysis. Some of these codes are specifically designed for electronics cooling applications. Deciding which software to use can be as difficult as deciding which type of analysis is best suited for the application (Finite Element Analysis (FEA), CFD, FNM, finite difference, etc.). It is beyond the scope of this thesis to present a comparison of the various types of analysis or commercial software packages. Choosing the best design approach and software is, however, a very important decision and depends greatly upon the specific application. Having said this, CFD has become the industry standard. Lee and Mahalingam (1994) demonstrated the usefulness of CFD as a design tool for the system-level thermal analysis of power electronic equipment. They noted its usefulness in performing analysis at both the system level and the component level. In a like manner, Linton and Agonafer (1995) used CFD software and simplifying techniques to model a heat sink. They compared the use of a course model to that of a fully detailed model and compared their results to experimental data. Yeh (2003) applied the CFD modeling approach to a telecommunications rack. Yeh discussed how CFD software was used to predict the system's thermal response to design modifications such as fan failure for each of the system's six fans. Similarly, Breier and Schlenk (2002) documented their use of CFD on a telecommunications rack. The authors showcased the usefulness of this design tool for modeling large-scale electronic systems with multiple layers of complexity.

One of the biggest difficulties associated with thermal modeling is the problem of length scale. Many applications require thermal management at several length scales. For example, a data center is a room that contains multiple racks or cabinets of telecommunication devices. Each device can itself contain multiple levels of system complexity. If the system fails, it will likely fail at the component-level due to overheating. Yet the temperature response of the components and the behavior of the airflow around them are extremely sensitive to the global-level (room) airflow and temperature conditions. For this reason, data centers and other large-scale electrical systems like them require a special approach to thermal modeling.

Data center thermal management is a new and expanding area of heat transfer research and is a very useful application of multi-scale modeling. These data centers can contain several layers of complex subsystems and a variety of equally complex airflow patterns. At IBM, Schmidt et al. have performed extensive analysis on data centers using CFD software such as Flowtherm (from Flowmerics, Inc.) and TileFlow (by Innovative Research, Inc.) (Schmidt et al., 2003; Schmidt et al., 2002; Schmidt, 2003). Flowtherm, a 3D CFD code, is one of the most widely used software packages in the electronics industry and can simulate the effects of conduction, convection, and radiation. TileFlow is another commercially available 3D CFD code that was designed specifically for the thermal analysis of raised-floor data centers. Schmidt has been at the forefront of data center thermal research. His research includes finding hot spots in data centers and characterizing the behavior of the airflow in the room, through the perforated floor tiles, and underneath the sub-floor of raised-floor data centers. Like Schmidt, Patal (from Hewlett-Packard) is also a leader in data center thermal management research. Patal et al. have also worked to characterize the thermal behavior of data centers by using CFD analysis. They have investigated solving thermal management issues using thermal load balancing analysis (Patel et al., 2002; Sharma et al., 2003) and exergy analysis (Shah et al., 2003). Patankar, et al. have also performed research in this field, including investigations in using FNM to handle thermal design/management issues (Belady et al., 1999) and controlling the rate of airflow through the perforated tiles of the data center floor (Karki et al., 2003).

Minichiello and Belady (2002; 2003) have used both CFD and FNM software to model large electronic systems. Their thermal design methodology insists that these two tools should be used together with lower-level tools (hand calculations and simple spreadsheets) for efficient product design. But their work also shows the importance of using CFD modeling and prototype testing to account for the shortfalls of FNM analysis when applied to large systems.

Large electronic systems like data centers and even the telecommunication racks they might contain are a length-scale problem as well as a complex airflow problem. To address these issues, Rambo and Joshi (2003) investigated using multi-scale CFD modeling (using the commercial finite volume solver Fluent by Fluent, Inc.) to correct

previous errors in data center thermal modeling due to the oversimplification of the individual racks. They insist that modeling is crucial at several scales and that it should be integrated. In addition, Gupta (2002) also investigated the use of multi-scale CFD modeling on a telecom rack of heat dissipating power devices. Gupta's 'zoom-in' approach involved a two-step process to handle the differences in length scales. First, he modeled the full rack but excluded component-level details. Instead, he represented groups or clusters of components with blocks and large, simple geometries. Second, after running the simulation of the full system, he was able to find where the system's hot spot was and 'zoomed-in' to this location by modeling that area or group of components. In this second model, he included the full detail of the components—but only in the vicinity of the hot spot. It was unnecessary to re-model the entire system. Instead, he extracted the results from the first model in the area of the hot spot (such as air temperature and velocity and flow blockages) as boundary conditions for the second model. Gupta then verified this method by making a third and fully detailed model of the telecom rack. He found that this two-step multi-scale modeling approach produced the same results as modeling the full system, but was a more efficient method.

Thermal modeling is indeed a necessary and useful tool in thermal management. But it should not always be used alone, nor should the results go unchecked. Computational thermal modeling is not without its own limits and its accuracy and reliability depend greatly upon the thermal designer using it. Building and testing a prototype is often a very important part of the design process as it validates the model or identifies problems in the model. One should not replace the other but the two should work together to check each other. As Azar and Rodgers (2001) showed, flow visualization can provide a tremendous amount of insight into the behavior of airflow in and around the housing of a power electronic device. Airflow can be very hard to accurately predict but is a crucial factor in the performance and reliability of electrical components.

Icoz and Jaluria (2003) presented a method of integrating numerical analysis with experimental analysis (an approach called Data Driven Design Optimization Methodology or DDDOM). This approach capitalizes on the strengths of both numerical and experimental analysis as each is used as the input for the other until an optimal

solution is found. The experimental analysis was used to handle the variations in airflow and the numerical analysis was used to investigate variations in component geometry and material. Patankar (1980) points out that both experimental and numerical analysis are important and should be used together. He adds that numerical analysis can significantly reduce the amount of experimental analysis (which is usually much more expensive and time consuming) that needs to be performed, but that experimentation cannot be ignored—especially when exploring new techniques and approaches to cooling.

2.3 Significance of Research

The significance of thermal management has already been addressed, as has the importance of thermal modeling as a thermal management tool. The necessity of thermal management for electronic systems will not go away with time but will only grow more important as the industry continues to push toward devices with higher power densities and smaller packaging requirements. Thermal management must keep pace with the changing technology. It is therefore important that new techniques to thermal management be explored and more efficient methods of thermal modeling be developed in order to allow technology to move forward. The progress of technology should not be held back by thermal constraints.

The work that is presented in this thesis is significant because it presents an improved methodology for the thermal modeling of systems with integrated electrical components. This work is also significant because it shows the efficiency of design integration. The power converter that is presented in this work was built and designed with integration in mind. Electrical and thermal analysis was integrated for a more efficient design process and a more reliable product.

Chapter 3 – Computational Methodology

Chapter 3 presents the details of the power converter that is the subject of application of the thermal management techniques presented in this thesis. This chapter also presents how a computational thermal model of the power converter was developed and simulated for thermal analysis. Chapter 3 begins with a brief description of the software that was used to model the converter. Sections 3.2 and 3.3 introduce the power converter that was analyzed and the boundary conditions associated with it. The assumptions that were used to build the computational thermal model are discussed in Section 3.4. Finally, the procedure used to mesh the geometry and to apply boundary conditions to the model is presented in Section 3.5.

3.1 I-DEAS Description

The 3D finite element analysis program I-DEAS was chosen to build, mesh, and solve the thermal models used in this research (I-DEAS, 2003a). I-DEAS can be used for many mechanical engineering applications including structural, vibrations, acoustic, and thermal. It is also able to build, mesh, and solve these types of problems as it has several sub-programs contained within the same package. Components can be easily constructed with the I-DEAS Master Modeler software, a CAD package far superior to many alternative FEA or CFD programs available on the market. For the task of electronics cooling, I-DEAS employs its Electronics System Cooling (ESC) software. In the ESC application, boundary conditions are applied to the meshed thermal model, including fans, vents, thermal contact resistances, heat loads, flow (convecting) surfaces, and flow blockages (obstructions). The I-DEAS Visualizer post-processing software allows the user to easily obtain the results of the simulation and to isolate certain aspects of the solution. I-DEAS is able to simulate the effects of conduction, convection, and radiation and contains a hybrid CFD solver coupled with its thermal solver. It solves the Navier-Stokes equations and employs an element-based finite volume approach to the 3D dynamics (EDS, 2003; Centrum Komputerowe, 2004).

I-DEAS has been the predominant thermal modeling tool at CPES. It was chosen over other alternative software because of its ability to simulate both the effects of heat transfer (including conduction, convection, and radiation) and complex fluid flow in electronic cooling applications and for its ability to interact with other electrical design software (such as iSIGHT) (Pang, 2002). Sewall (2002) used I-DEAS in a component arrangement study to predict the behavior of proposed layouts of DC-DC converters. Similarly, Pang, et al. (2002; 2003) used I-DEAS in their optimizational efforts for active IPEMs. Indeed, its use has been well established as a useful design tool at CPES by above said authors and is therefore the modeling software of choice for the research presented in this thesis.

3.2 Converter Geometry

At the time of the research that is presented in this thesis, CPES was in the process of refining the design of a state-of-the-art DC-DC front-end power converter originally developed by Eltek. The commercially available discrete power converter developed by Eltek and shown in Figure 3.1a accepted AC current at 120 V and converted it to DC current at 48 V. This industry power converter had a power density of 354 kW/m^3 (5.8 W/in^3) and a height of 66 mm (1.5 units). CPES accepted the task of improving the design and performance of the converter. The goal of this project was to increase the power density of the converter while at the same time reducing the size of the package by applying an IPEM-based design approach. The size of the converter was restricted to the dimensions shown in Figure 3.1b. CPES first developed a modified discrete version of the converter as shown in Figure 3.2a. Figure 3.2b shows the basic function of the CPES discrete power converter. This converter, which was the subject of the thermal analysis performed by Sewall (2002), had a power density of 690 kW/m^3 (11.3 W/in^3) and met the 1-unit height requirement. The electrical design team then developed a third version of the converter. This time, however, the converter contained two IPEMs – an active and a passive. This new IPEM-based power converter, which is shown in Figure 3.3 (without the heat sink) and is the main focus of this thesis, also met

the 1-unit height requirement and had a power density of 891 kW/m^3 (14.6 W/in^3)—approximately 2.5 times that of the original discrete version.

Figure 3.3 shows the actual components of the system (excluding the heat sink) and Figure 1 of Appendix A shows the system-wide flow of power as designed by the electrical and packaging teams. The details of the electrical design of the power converter are described in Dong et al. (2003). The next section of this chapter presents how this converter was represented in I-DEAS and the assumptions that were made to construct a manageable computational model for thermal analysis.

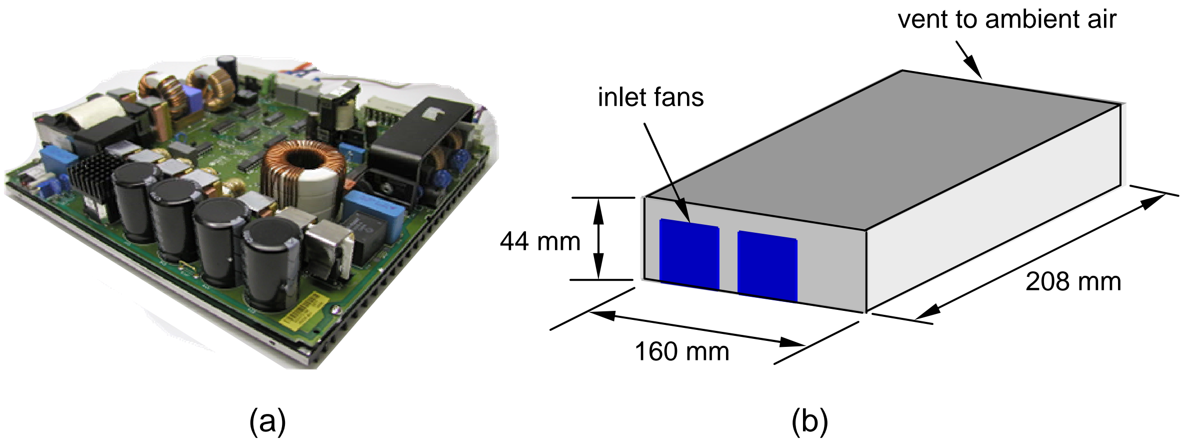

Figure 3.1 The (a) industry's discrete converter and (b) the outer geometry of the CPES converter.

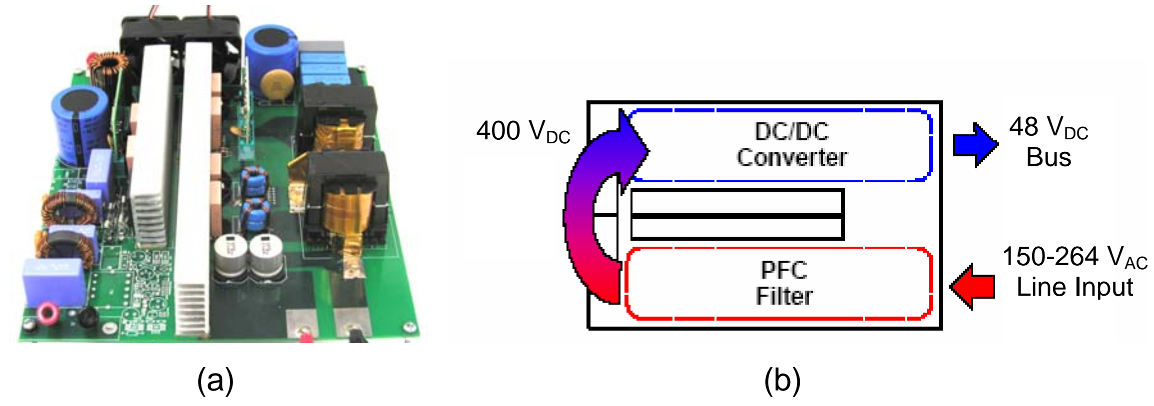

Figure 3.2 The (a) layout of the improved discrete version of the converter developed by CPES and (b) the basic function of the converter (Sewall, 2002).

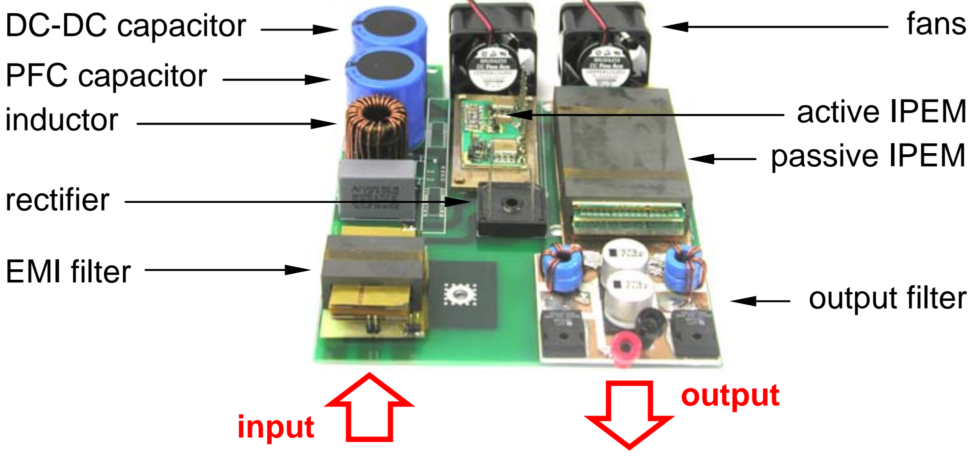

Figure 3.3 The proposed layout of the integrated CPES power.

3.3 Boundary Conditions

This section of Chapter 3 presents how the outside of the power converter was modeled and describes the system-level boundaries or constraints common to all of the computational models used in this research. These boundary conditions were dictated by the converter's proposed electrical and component design and from several necessary simplifying assumptions. The boundary conditions imposed on the components inside the converter box are discussed in Sections 3.4 and 3.5.

Two Sanyo Denki fine ace fans (109P0412G302) were incorporated into the converter's design. The fans were each 28 mm in width (jutting into the converter box), 40 mm in length, and 40 mm in height. For the purpose of simplification, the fans were modeled as simple blocks with these dimensions. Instead of including the 40 mm diameter circle with the centered 20 mm fan hub, the back square surface of the fan block was modeled as the fan surface. Thus the airflow exits the fans evenly distributed.

Figure 3.4 shows the fan curve used to describe the behavior of the fans. This same fan curve was used for all system-level simulations presented in this work. The I-DEAS ESC application can, given the input of the fan curve data, predict the operating point for each fan in the system. The fan curve describes the relationship between the

incoming airflow rate and the fan static pressure. The points of this plot were extracted from the fan curve provided by the manufacturer and are shown in Table 3.1. The actual fan curve provided by the manufacturer is shown in Appendix A. A completely open exit vent was located directly across from the inlet fans. In order to simulate a worse-case operating scenario, it was assumed that the air surrounding the power converter (that is, the air drawn into the system by the fans and the ambient air immediately downstream of the exit vent) was a constant 50°C. This assumption is commonly made when designing power electronic devices of this type (Mohan, et al., 1995).

Table 3.1 Fan operating conditions used for the fan curve of Figure 3.4.

airflow (m^3/min)	static pressure (Pa)
0	180
0.025	170
0.050	160
0.070	150
0.085	140
0.100	132
0.120	119
0.1375	110
0.145	100
0.1625	90
0.175	76
0.1875	63
0.200	60
0.2125	58
0.250	57
0.275	55
0.300	50
0.3125	42
0.350	32
0.375	21
0.400	10
0.4125	0

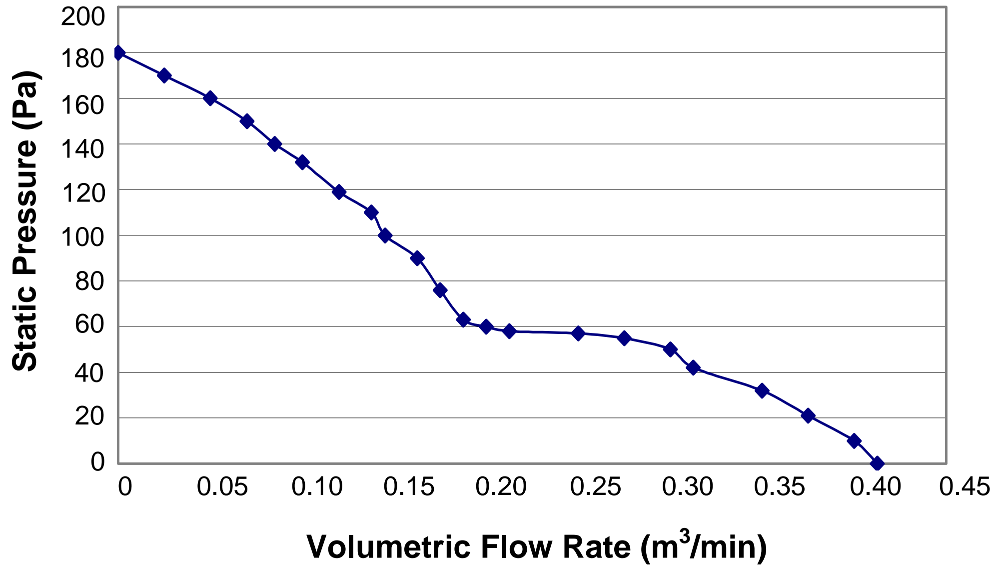

Figure 3.4 The fan curve used in the I-DEAS models for the system's two fans.

In the thermal simulations performed in this work, it was assumed that only a negligible amount of heat from the converter's components would exit out the walls of the airbox (or enter in through the walls of the airbox from surrounding heat-generating devices). Therefore, in the computational model, the walls were assumed to be adiabatic. This forced all of the heat leaving the converter system to exit through the vent. In Sewall's study (Sewall, 2002), he showed that the effects of radiation were negligible compared to those of conduction and convection. For this reason, and for model simplification and computational speed, the effects of radiation were ignored for the thermal analysis of this device.

3.4 Computational Model Assumptions

I-DEAS Master Modeling software was used to construct the geometry of the components of the converter. In system-level thermal modeling, the system's drastically different length scales coupled with the computational limits of the simulation software, prohibit the designer from including full details of the electronic device. Simplifying assumptions had to be made in order to build a model that could feasibly be solved. To

keep the system model as simple as possible, a combination of blocks and cylinders were drawn to represent simplified versions of the actual converter components. Components were modeled with perfectly smooth surfaces (zero surface roughness). Each component was drawn and assigned a specific material type with a user-specified thermal conductivity, *k*. Table 3.2 presents a complete list of the components that were included in the computational model of the power converter. This table also presents the materials and the element sizes used to represent each component (Section 3.5 provides a more detailed discussion of the meshing scheme used to represent the components). Table 3.3 lists the materials used and their assumed corresponding thermal conductivities. These materials were assumed to behave isotropically (with the exception of ESC Air). It should be noted that the material in Table 3.3 listed as "combo" is a results from the material and geometry simplification of the four diodes of the output filter. Also, a "null" material (with a thermal conductivity of zero) was assigned to the meshed surfaces of the fans and the vent and the four flow obstructions that sat to the side of the heat sink. Finally, the material used for the air inside the converter box was the I-DEAS "ESC Air" from the I-DEAS material library. Using ESC Air in the model allowed I-DEAS to automatically adjust the density of the air in the system.

Table 3.2 The components in the system-level FE model of the power converter

Component Name	Material	Mesh size (mm)
airbox	ESC air	3
fan 1	null	4
fan 2	null	4
heat sink	aluminum	5
passive IPEM	ferrite	4
Component 1 (MOSFET)	silicon	0.5
Component 2 (MOSFET)	silicon	0.5
Component 3 (DC Gate)	ceramic	2
Component 4	silicon-carbon	0.25
Component 5	silicon-carbon	0.25
Component 6 (CoolMOS)	silicon	0.5
Component 7 (PFC Gate)	ceramic	0.5
Component 8 (CoolMOS)	silicon	0.5
DC-DC Trace	copper	2
PFC Trace	copper	2
active IPEM Base	ceramic/copper	4
active IPEM Heat Spreader	copper	4
Component 11 (high snubber)	ferrite	2
Component 12 (high diode)	combo	1
Component 13 (high diode)	combo	1
Component 14 (capacitor)	aluminum	3
Component 15 (capacitor)	aluminum	3
Component 16 (low snubber)	ferrite	2
Component 17 (low diode)	combo	1
Component 18 (low diode)	combo	1
Output Filter Heat Spreader	copper	3
rectifier top coating	plastic	2
Component 19 (rectifier diode)	silicon	0.5

Table 3.2 Continued.

Component 20 (rectifier diode)	silicon	0.5
Component 21 (rectifier diode)	silicon	0.5
Component 22 (rectifier diode)	silicon	0.5
rectifier base	ceramic/copper	2
capacitor 1 (DC-DC)	null	5
capacitor 2 (PFC)	null	5
inductor	null	5
EMI Filter	null	5
vent	null	5

Table 3.3 The materials used in the model and their corresponding thermal conductivities.

Material	Thermal Conductivity, k, (W/mK)
silicon-carbon	495
copper	395
aluminum	164
combo	150
silicon	117.5
ceramic	26
ferrite	4
plastic	2

The geometrical simplicity of the passive IPEM allowed it to be modeled as a simple volumetric heat source block. The modeling of the active IPEM, however, was not so simple. Figure 3.5a shows the physical active IPEM that was to be used in the power converter and (later) constructed at CPES. The active IPEM is divided into two parts: a DC side on the left and a PFC side on the right. On the DC side, Components 1

and 2 are both MOSFETs and Component 3 is the DC gate. On the PFC side, Components 4 and 5 are silicon-carbon chips, 6 and 8 are CoolMOSs, and Component 7 is the PFC gate. This IPEM rests upon a 3 mm-thick copper heat spreader. The eight heat-dissipating components of the active IPEM were encased in a gel coating on their top surfaces. This coating created a very large thermal resistance between the components and the surrounding air. For this reason, the top surfaces of the active IPEM were modeled as adiabatic surfaces. The details of the active IPEM (minus its heat spreader and gel coating) can be seen clearly in Figure 3.5b. This detailed model of the active IPEM was used by Pang and Scott (2003) for component-level thermal analysis. Figure 3.6 shows a top view of the simplified active IPEM used in the present work. Notice that the electrical connections and ceramic top frame shown in Figure 3.5b were removed for simplicity. While the ceramic frame would hinder the removal of heat from the DC and PFC gates, it presents no resistance for the removal of heat from the other six components and therefore could be eliminated from the simplified system-level model of the active IPEM. All eight electrical chips of the active IPEM were modeled to give off heat from their top surfaces. Because the top of the active IPEM was modeled as an adiabatic surface and the heat path was specified by the use of thermal resistances, the gel coating did not need to be drawn.

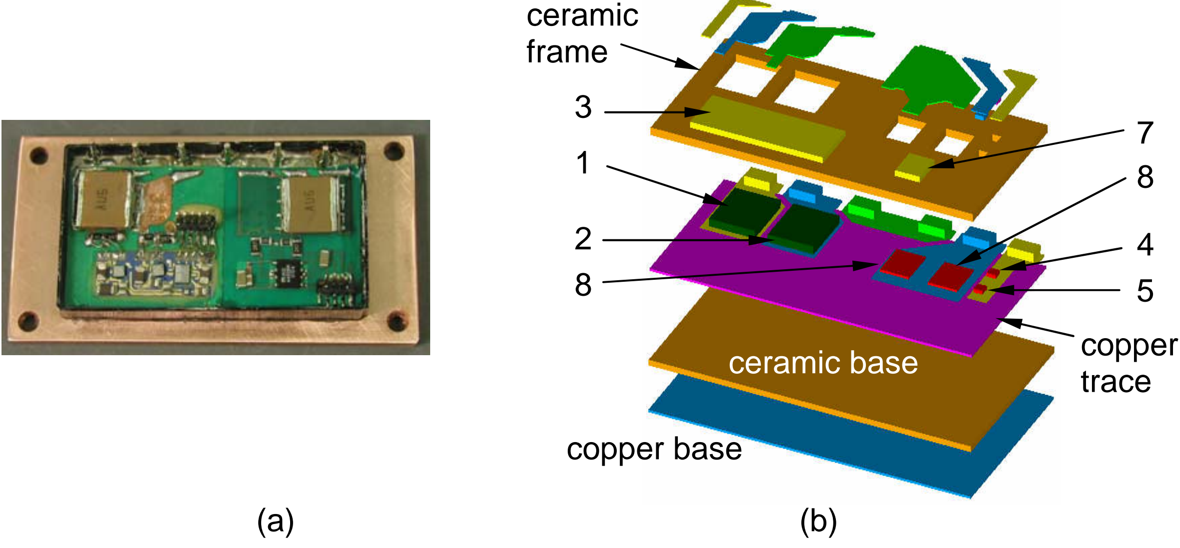

Figure 3.5 The (a) physical active IPEM and the (b) detailed component-level model developed by Pang and Scott (2003).

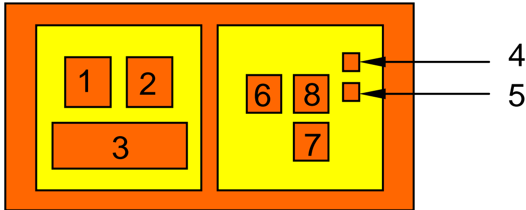

Figure 3.6 The simplified model of the active IPEM.

Figure 3.7a shows the layout of the output filter. The output filter composed of a 'high' side and a 'low' side. Components 11 – 13 made up the high side and Components 16 – 18 made up the filter's low side. As mentioned earlier, the 4 diodes of the output filter were represented as simple volumetric heat sources in order to further reduce the complexity of the thermal model. Figure 3.7b shows the detail of these components. These diodes include a small silicon chip, a copper base, and a molded plastic cover. Figure 3.8 shows an exploded view of the rectifier. The rectifier consisted of four silicon chips, a three-layer copper/ceramic/copper base, and a plastic top cover.

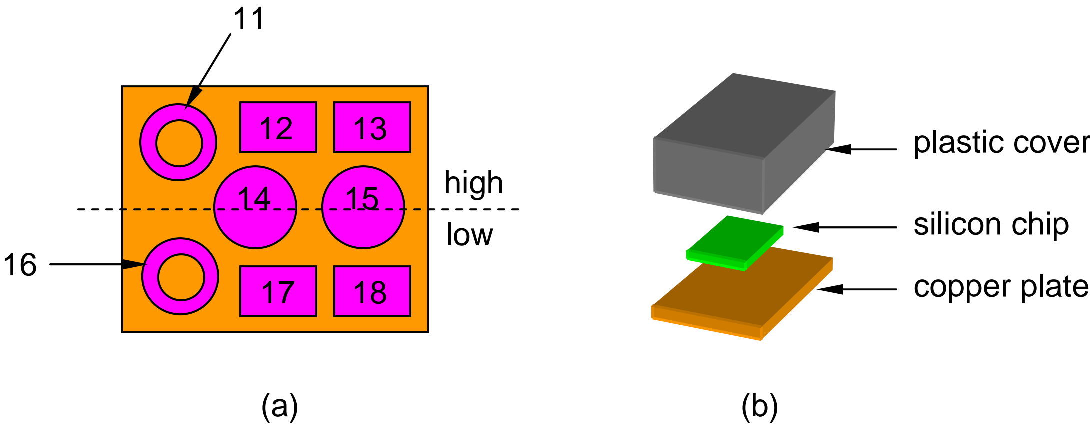

Figure 3.7 The (a) layout of the output filter and (b) an exploded detail view of the output diodes (Components 12, 13, 17, and 18).

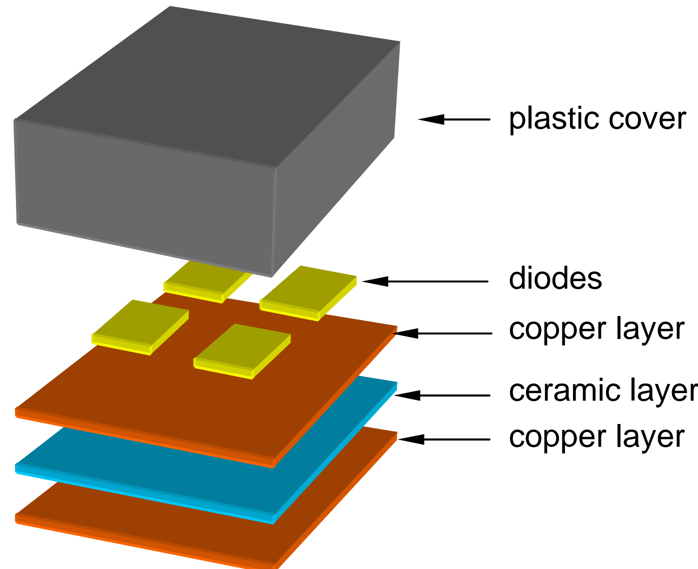

Figure 3.8 An exploded view of the rectifier model used in the present work.

Figure 3.9 shows the complete system-level thermal model of the CPES power converter as drawn in I-DEAS. The plastic top of the rectifier has been outlined in yellow to show the location and configuration of the four diodes that sit inside. The converter box (labeled as “airbox”) that contains all of the components is also outlined. Note that the passive IPEM, the active IPEM, the output filter, and the rectifier sat upon an aluminum parallel-plate heat sink. This heat sink measured 18 mm in height (the tallest allowable heat sink that could be used with the 1-unit height requirement) with a 4 mm-thick base and twenty-eight 14 mm-tall fins. Figure 3.10 shows the power losses that were used in the thermal model for the heat-dissipating components. These values were estimated by the electrical design team and were assumed to be constant. Once the components of the converter had been drawn in I-DEAS, they were each meshed, assembled together, and partitioned into the airbox. Then the boundary conditions presented in this section and the previous section were applied to the model. Section 3.5 discusses in detail the procedure used to prepare the I-DEAS model for thermal simulation.

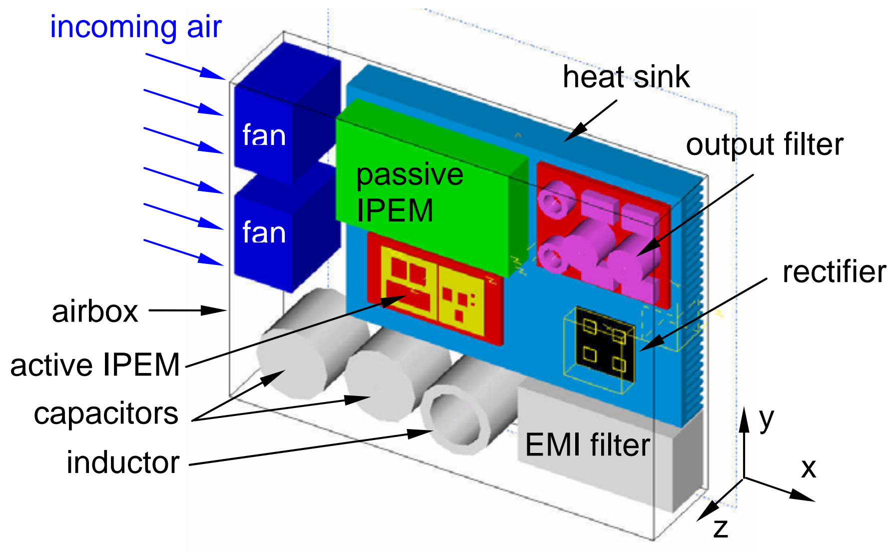

Figure 3.9 The complete system-level thermal model of the power converter.

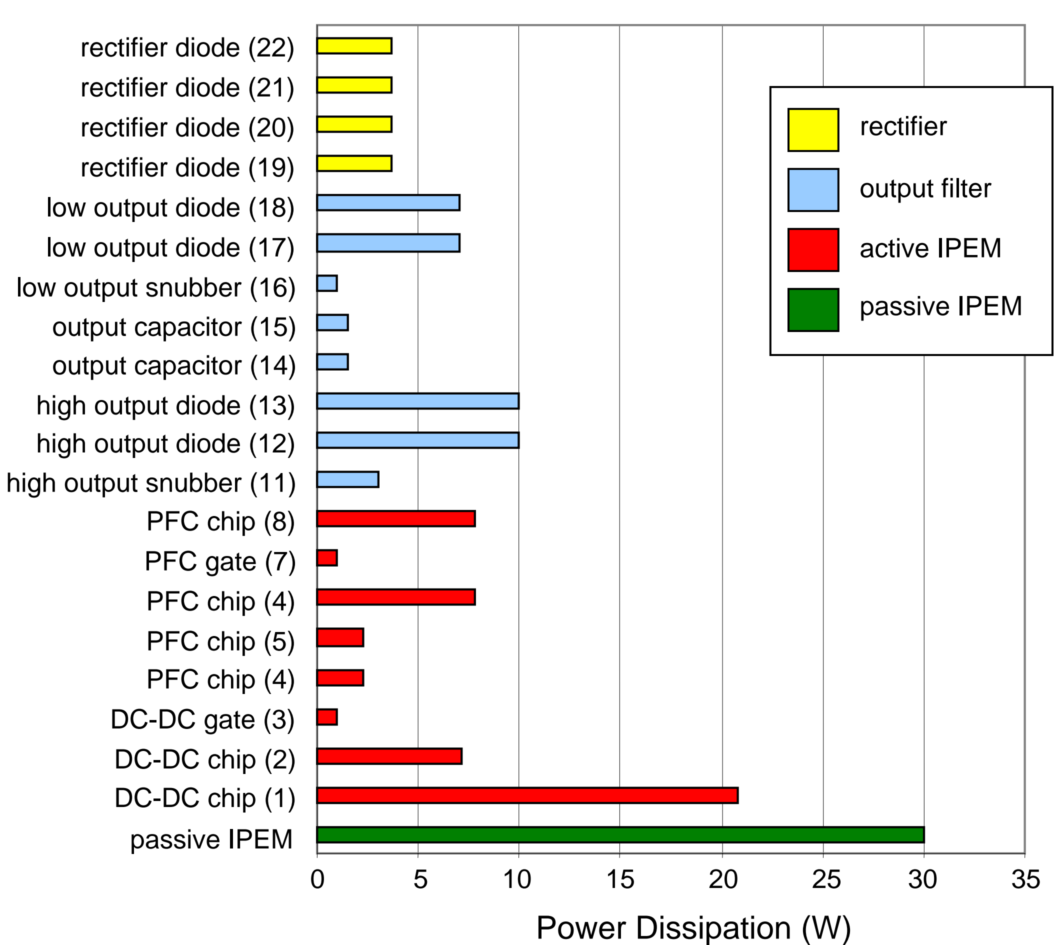

Figure 3.10 The power loss of the system's heat-dissipating components.

3.5 I-DEAS Simulations

Once each component of the power converter system was constructed, it was meshed using the I-DEAS meshing application. The element size used to mesh each component was provided in Table 3.2 of Section 3.4. The 3-noded linear triangular shell element (circled in red in Figure 3.11a) was used to mesh the top, bottom, and side surfaces of components. The 4-noded linear tetrahedron 3D element (circled in red in Figure 3.11b) was used to solid mesh the components. These triangular-shaped elements allow the software to easily mesh irregular-shaped geometry but generally produce less accurate results than the alternative brick element used commonly in ANSYS for 3D meshing. However, as pointed out by Cook, et al. (2002), finite element models are generally less sensitive to element size and type for thermal analysis than for stress analysis.

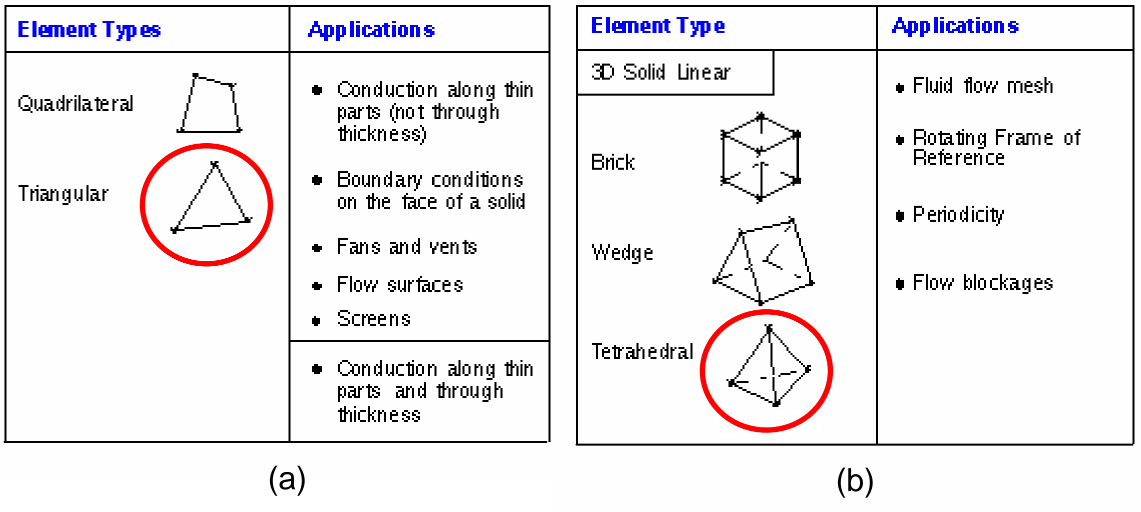

Figure 3.11 The (a) 3D linear solid elements and the (b) 2D linear thin shell elements from the I-DEAS library of elements (I-DEAS, 2003b). The elements used in this work are circled in red.

A fine meshing scheme was used to represent the components of the power converter system. The small geometry of the individual heat-dissipating electronic chips dictated the local and global meshing schemes. In order to determine the model's sensitivity to element size, a mesh sensitivity analysis was conducted. The entire model of Figure 3.9 was not used in this analysis because doing so would have been extremely computationally expensive and would have required a tremendous amount of solve time. Instead, a representative region was used in the analysis—the output filter (as shown in Figure 3.12). Figure 3.12 shows the final meshing scheme that was used to mesh the components of the output filter and the heat spreader they sit upon. The two snubbers are shown in red, the two capacitors in green, and the four diodes in blue. A relatively fine mesh was also used for the air. Figure 3.13 shows the results of the mesh sensitivity analysis. It should be noted that beyond a certain point (indicated by the red vertical line), the meshing scheme was observed to be overly refined, preventing solution convergence. While an overly course meshing scheme can produce inaccurate temperatures, an overly fine meshing scheme can be computationally hard (or impossible) to solve and can lead to solution divergence. In this case, this divergence is likely due to round-off error associated with the software's solution precision. The results of this mesh sensitivity analysis were used to justify the meshing scheme used in the full system-level model.

Once the individual components were meshed, the airbox was partitioned to account for the solid objects in the model. Partitioning the airbox informs the software where to (and where not to) include the solid air mesh. Once the airbox was partitioned, it too was meshed with a fine mesh and included in the assembly. The solid elements of the air were then checked for deformations, mesh modifications were made as needed, and the components of the converter were assembled together as one part.

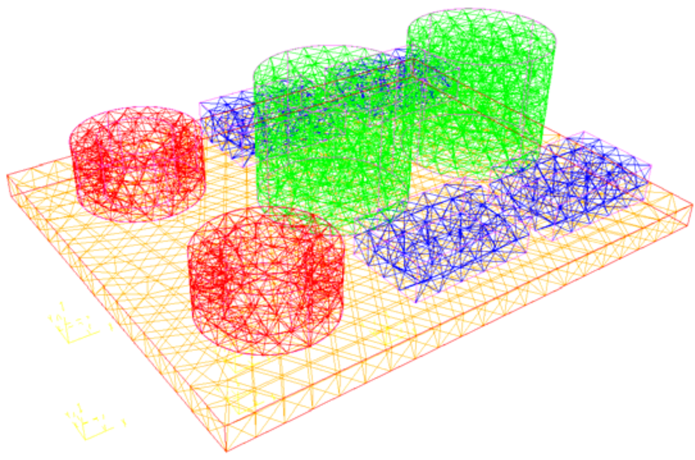

Figure 3.12 The meshing scheme used for the components of the output filter and the heat spreader they sit upon.

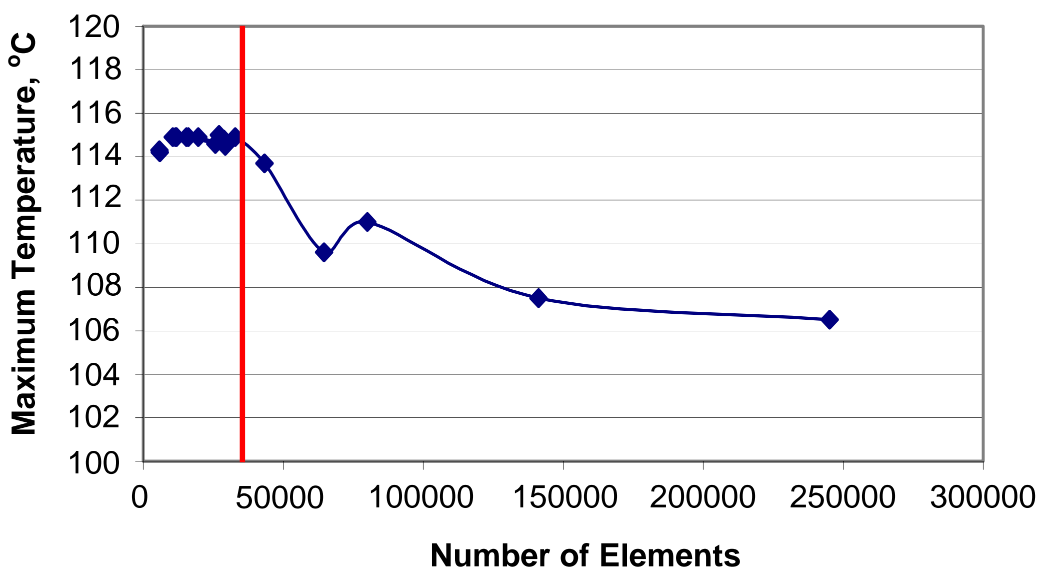

Figure 3.13 The results of the mesh sensitivity analysis performed upon the model of Figure 3.12.

Before the model could be simulated, boundary conditions had to be applied to the components of the model. Section 3.3 discussed the outer boundary conditions imposed on the system, including the fans, the vent, the surrounding air, and the transfer of heat to and from the system. Section 3.4 discussed the materials, mesh size, and the estimated power loss for each component. Additional boundary conditions were applied to the components of the power converter, including flow surfaces, flow blockages, and thermal contact resistances. Flow surfaces were used to specify which surfaces convected heat directly to the air. Flow blockages were used to specify which components served as obstructions to the airflow. Thermal resistances were also used in the model to account for the contact resistance between the surfaces of the components due to epoxies, thermal pads, and thermal pastes. The thermal model's flow surfaces, as well as the resistance values used in the model, are listed in detail in Appendix A.

Once the boundary conditions had been applied to the finite element model of the power converter, the model was simulated. All of the simulations presented in this work were run at steady-state. While transient analysis can provide a tremendous amount of insight to the physics of the problem being solved, computational limits (i.e. computational expense and required solve time) prevented system-level transient investigations. The I-DEAS ESC flow solver and thermal solver offer several options including results specification, fluid flow specifications, buoyancy effects, and convergence criteria. The mixing length turbulence model (which is the default setting) was chosen to allow the software to determine the behavior of the fluid flow and allow for laminar, transitional, and turbulent flows. Buoyancy effects (which includes the effects of natural convection and gravity) were neglected as they were assumed negligible in the forced-convection environment inside the converter. Furthermore, the software's default convergence settings were used in the simulation of the converter model. These default convergence settings required a temperature change of less than 0.1, RMS flow residuals of less than 0.0002, normalized convective heat imbalance less than 0.01, and normalized global imbalance less than 0.02. The simulations for the analysis of Chapter 4 were solved in I-DEAS 9 using the Unix operating system and were represented by over 360,000 elements. The simpler simulations performed for the analysis of Chapter 5

were solved in I-DEAS 10 using the Windows 2000 operating system and were represented by less than 31,000 elements.

Once the simulations had converged to a solution, the results were extracted using the I-DEAS post-processing software Visualizer. Visualizer allows the user to easily explore the results of the simulation with color coded temperature, velocity, and pressure results, contour, arrow (vector), and cutting plane plot options, result probes, and material filters. These plots were used in the following chapters to allow the user to quickly and easily distinguish between various simulation results. The results obtained from these simulations and presented in this thesis provide tremendous insight into the thermal behavior of the components and the complex fluid behavior of the air inside the power converter. The work presented in the following two chapters involved the use of numerical analysis and was performed using the assumptions discussed in this chapter.

Chapter 4 – Computational and Experimental Analysis of the Power Converter

A parametric study was performed on the power converter described in Chapter 3 and is presented in this chapter. In this study, the issues involved with thermally controlling a system of integrated circuits with various fan arrangements are investigated using the thermal computational model created in I-DEAS (also described in Chapter 3). As described in Chapter 3, some of the more complex electrical components were reduced to simpler volumetric heat sources in order to capture the general temperature response of the system. Chapter 3 presented the first layout that was proposed by the electrical designers of the converter (hereafter referred to as the layout of Case 1 or the base model). The objective of this study was to use the I-DEAS model to predict the converter's temperature response and to determine if an alternative fan configuration would improve (reduce) the system-wide temperature response. The overall goal of the thermal management of this power converter was not only to simply find one configuration that allowed component temperatures to meet the required 125°C maximum temperature limit, but also to explore several possible layout configurations that would allow the lowest possible system-wide temperature and the most even temperature distribution.

This chapter presents the numerical analysis that was performed to solve this multi-objective problem and the experimental analysis performed to assess the results of the numerical analysis. First, the procedure and the results of the parametric study investigating the system-wide effects of fan rearrangement and airflow direction are presented in Sections 4.1 and 4.2, respectively. Then, additional follow-up analysis is presented in Section 4.3. Finally, in Section 4.4, the procedure for the experimental testing that was performed on the prototype of the power converter is presented and the results are compared to those obtained from the computer simulations.

4.1 Parametric Analysis

Once the thermal model of the first proposed layout had been modeled and simulated in I-DEAS, a parametric study was set up and performed to determine the best geometric arrangement to enhance cooling. Table 4.1 presents the eight proposed layouts that were simulated in I-DEAS as part of this study. The first layout (Case 1) was the first proposed layout previously discussed in Chapter 3. The seven additional layouts were proposed based upon the recommendations of several team members and upon the electrical and packaging constraints bound on the system. This study was heavily restricted by the electrical and packaging design teams in order to achieve the best flow of power in the required space. Figure 1 of Appendix A shows the electrical layout and the system-wide flow of power. In order to achieve this power flow, the electrical components in this study were restricted to maintain their present positions. Instead, the main focus of this investigation was upon the fan arrangement—looking at how the system's temperatures responded to where the fans were located. Also included in this study was a look at how the system would respond if the fan direction was simply reversed. For example, the only difference between Cases 1 and 2 is the direction of the airflow. In Case 1, the system has inlet fans to draw in air and in Case 2 the system has outlet fans to blow air out of the system. Also included in the study was a brief look at using a pin-fin heat sink as opposed to a parallel-plate heat sink. The layouts of Cases 1 through 6 include the 28-fin parallel-plate heat sink described in Chapter 3 while the layouts of Cases 7 and 8 include the 200-fin pin-fin heat sink shown in Figure 4.1.

Table 4.1 The eight proposed layouts used in the parametric study

Case	Layout	Description
1		Parallel-plate heat sink with inlet fans on the left and outlet vent on the right.
2		Parallel-plate heat sink with outlet fans on the left and inlet vent on the right.
3		Parallel-plate heat sink with inlet fans on the right and outlet vent on the left.
4		Parallel-plate heat sink with outlet fans on the right and inlet vent on the left.
5		Parallel-plate heat sink with inlet fan on the left and outlet fan on the right.
6		Parallel-plate heat sink with inlet fan on the right and outlet fan on the left.
7		Pin-fin heat sink with inlet fans on the left and outlet vent on the right.
8		Pin-fin heat sink with outlet fans on the left and inlet vent on the right.

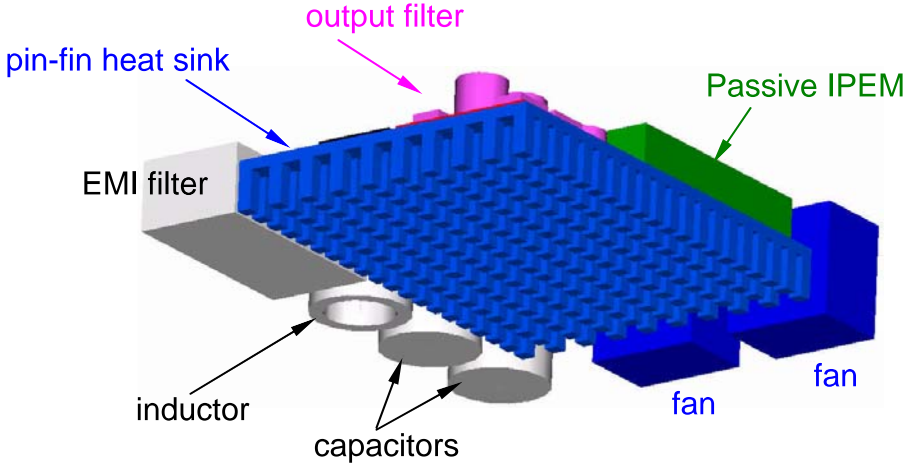

Figure 4.1 Bottom view of the layout used in Cases 7 and 8 showing the pin-fin heat sink. Each fin is 5 mm x 5 mm x 14 mm.

4.2 Results of the Fan Arrangement Study

The eight cases presented in Table 3.1 were simulated in I-DEAS and the results are presented in this section. It should first be noted that, according to the I-DEAS simulations, the effects of simply switching the fan direction were negligible. The layouts of Cases 1 and 2, for example, produced nearly identical component temperatures and heat distribution. For this reason, only the odd-numbered cases (Cases 1, 3, 5, and 7) will be showcased in this section. Figure 4.2 shows the results from the simulation of Case 1. The temperature of the five components that gave off the most heat and/or were consistently the hottest components in the system are highlighted. Note that, generally, there is a good distribution of heat across the components and heat sink. All of the components remained below the 125°C limit. The passive IPEM, which has the highest power loss (30 W), remains relatively cool. This is due to the large amount of surface area it has for transferring heat directly to the air via convection and to the heat sink via conduction. Component 1 also has a high loss (20.8 W) but, because of its adiabatic top surface, is at a disadvantage in that it cannot give that heat directly to the air. However, because of its close proximity to the fans, there is an abundant supply of cool air blowing through the fins of the heat sink underneath it. The four diodes in the rectifier

(Components 19, 20, 21, and 22, not shown in Figure 4.2) were also well below the required temperature limit with a steady state temperature of approximately 89°C.

Despite the fact that it only gives off 3 W of heat, Component 11 (the high snubber in the output cluster of components) is the hotspot of the system. Because the snubber is immediately downstream from the passive IPEM and is much smaller than its upstream neighbor, it is blocked from receiving a substantial amount of airflow. The snubber's geometry also contributes to its thermal problems as it is shorter than the adjacent passive IPEM, which subsequently blocks the airflow, and its lack of top surface area limits the amount of heat it can convect. To make matters worse, the air that does reach Component 11 is warm due to the heat transferred to it from the passive IPEM.

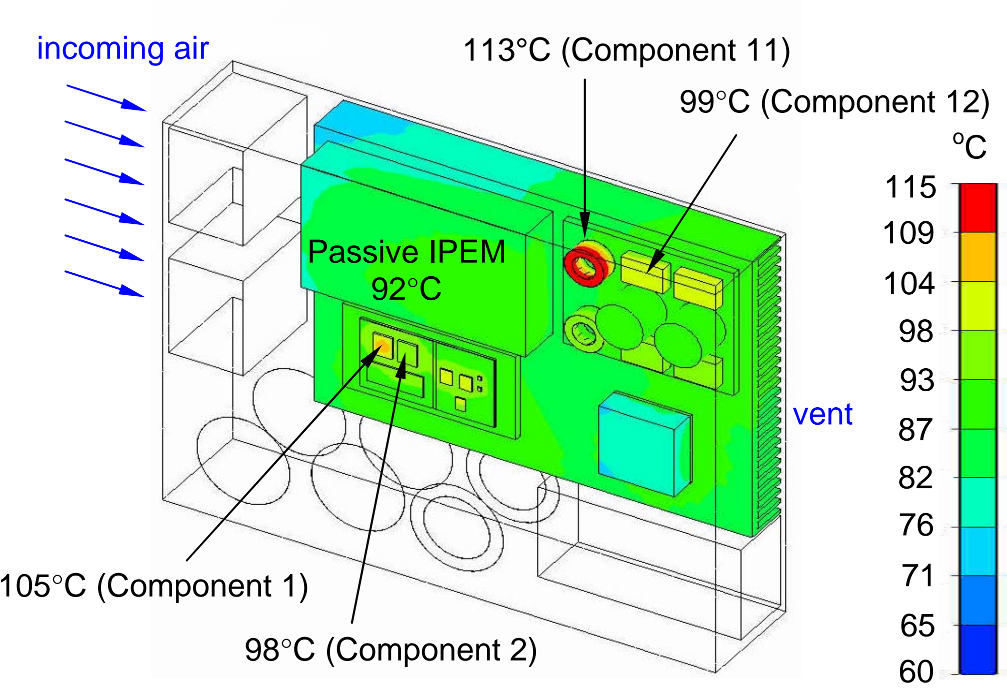

Figure 4.2 The thermal response of Case 1. Blue arrows indicate the direction of airflow.

Case 3 proved to be the best scenario from the parametric study. For this orientation, the cooling fans were moved to the opposite side of the air box from Case 1. As a result, the system's hotspot has the coolest air blowing directly on it. Although there are still components partially blocking the upstream air (this time, it is the two diodes Components 12 and 13), the snubber is subject to a much higher flow rate than was found for Case 1. This difference in layout results in a significant reduction in temperature. Figure 4.3 shows that the maximum temperature of Component 11 was reduced by approximately 10°C from the results of Case 1. It should be noted that, again, the temperature of the four silicon chips (diodes) inside the rectifier maintained a steady-state temperature that was well below the maximum limit (approximately 85°C).

Notice that while there was a significant decrease in temperature for the output components in Case 3, there was only a slight increase in temperature for the active IPEM components. This unexpected result can be explained by the active IPEM's adiabatic top surface. Because its surface is adiabatic, all of the heat produced by its components is forced down to the heat spreader and then (most of that) down to the heat sink. Therefore, the active IPEM depends upon the heat sink to dissipate the vast majority of its heat. And, as long as there is a significant amount of air running through the fins of the heat sink underneath the area that the active IPEM sits, the active IPEM will be sufficiently cooled off. Similarly, the temperatures on the surface of the passive IPEM remained relatively unchanged due to its high level of surface area. The change of layout did not reduce the amount of air flowing around or underneath it. Also unchanged from the layout of Case 1 was the airflow around the components that sit off of the heat sink. Figure 4.4 shows the velocity diagram of the air in the converter box for Cases 1 and 3. While the direction of the air is opposite between the two, both layouts allow for the vast majority of the air to flow around the heat-dissipating components and ignore the non-heat dissipating components that sit off to the side.

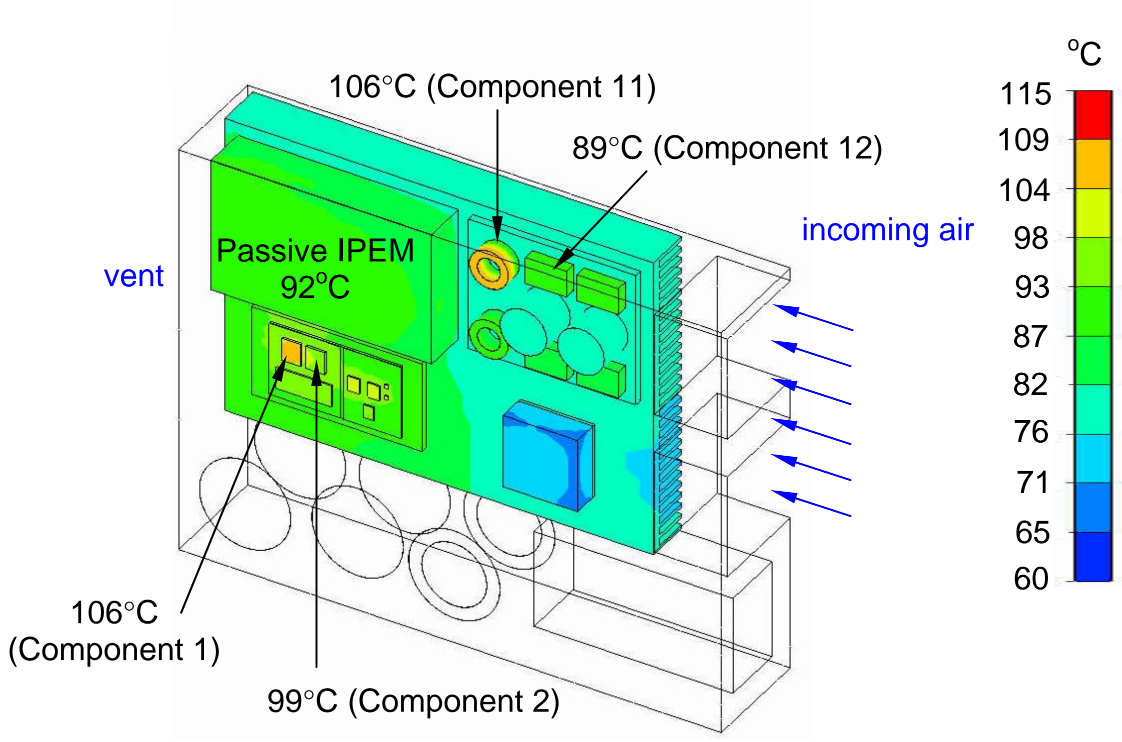

Figure 4.3 The thermal response of Case 3. Blue arrows indicate the direction of airflow.

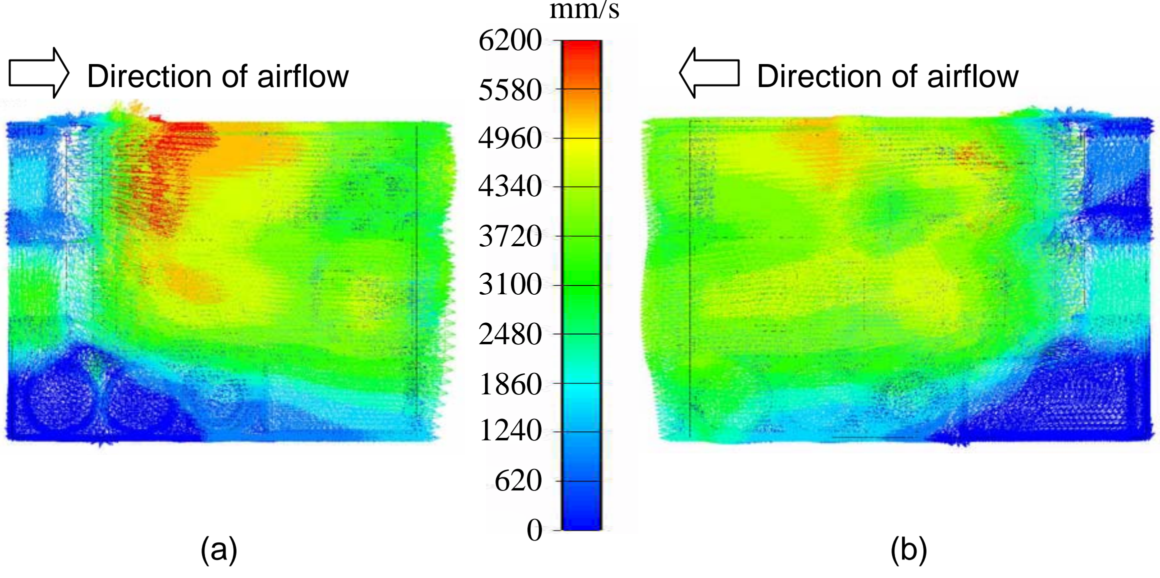

Figure 4.4 The velocity response of Case 1 (a) and Case 3 (b).

While there was not a noticeable difference between the temperature response of Cases 1 and 2 and between Cases 3 and 4, there was noticeable difference between Cases 1 and 4 and between 2 and 3. For example, Case 2 (where the air is being pulled out) and Case 3 (where the air is being pushed out) have fans at opposite ends of the air box but the direction of the air is the same. According to the results obtained from the I-DEAS simulations, it is not the direction of the air that significantly affects the system's temperature response but the location of the fans.

As expected, Case 5 proved to be the worst case among the eight scenarios. In this case, the two fans were positioned directly across from each other on opposite ends of the heat sink. The original proposal for this layout involved using one fan to blow air directly on the output components and a second fan to blow directly on the active IPEM (as shown in Figure 4.5). However, due to packaging constraints, this layout was not a practical solution and so the layout was altered to the form shown in Table 4.1. For Case 5, the surface temperatures of some components reached nearly 360°C. While there is some uncertainty whether the temperature responses of Cases 5 and 6 are thermally accurate, a close look at the velocity diagram provides insight into why temperatures would increase so dramatically given this specific fan arrangement scenario. Figure 4.6 shows the velocity diagram for Case 5 (looking underneath the heat sink). Unlike the other cases where the incoming air had the freedom to circulate throughout the box, the fans in these two cases acted together to draw cool air in and immediately force it out. The air had little chance to properly flow over most of the surfaces (including the heat sink fins) in the box. Most of the air movement was restricted to a small channel under the heat sink, leaving most of the components to transfer heat via natural convection. One method that could be used to reduce the outlet fan's ability to force air out immediately is to reduce the size (and/or power) of the outlet fan. A second method would be to relocate both fans so that one fan is blowing (or drawing) air directly over the output components and the other fan is blowing (or drawing) air directly over the active IPEM.

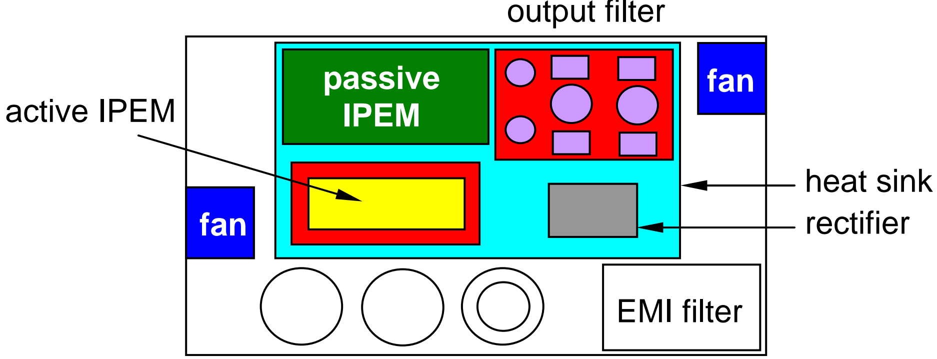

Figure 4.5 The originally proposed layout for Cases 5 and 6 that was never used.

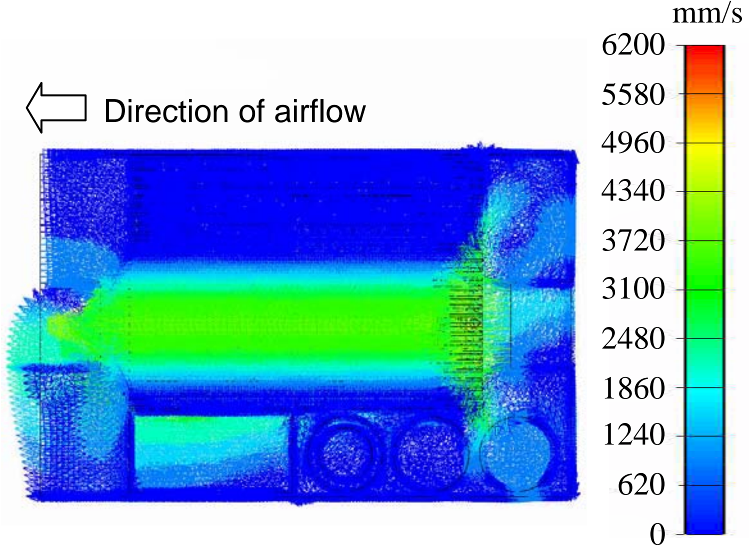

Figure 4.6 The velocity vector diagram for Case 6.

The purpose of simulating the layout of Case 7 was to determine how the system would respond if the parallel-plate heat sink used in the other cases was replaced with a pin-fin heat sink. The particular pin-fin heat sink used in Case 7 was not necessarily optimized for this system. Instead, the heat sink was limited to 200 fins in order to avoid building a model that would require a large amount of small elements that would be too cumbersome for I-DEAS to handle. Determining the optimal fin geometry and distance and location of the fans could itself be the subject of its own parametric study. Such is beyond the scope of this research. Furthermore, using a flow impingement arrangement to blow cool air directly on the bottom of the pin-fin heat sink or to draw hot air off was suggested and could have been included in the study. However, placing the fans on the bottom or top of the air box would prevent the power converter from meeting its 1 unit (44 mm) height requirement and thus was never investigated as a potential feasible solution.

As was predicted by simple (1D) hand calculations, the layout of Case 7 produced system temperatures greater than that of Case 1. Table 4.2 presents the temperatures of the five major components (the diagram of the temperature spread is not shown but is similar in appearance to that of Case 1). Only the passive IPEM remained below the 125°C limit. To find out why this was the case, it is useful to look at the velocity vector plot of Figure 4.7. Figure 4.7 shows the air flowing underneath the pin-fin heat sink. It was first thought that using a pin-fin heat sink would help promote convection because the air would be allowed to flow in both the x- and y-directions. Notice, however, that the air between each fin (in the y-direction) appears to have a very low velocity and is nearly still. In fact, the geometry of the fins creates a scenario in which air gets trapped into eddies in between the fins, filling in the gaps and creating a wall such that air can only move in the x-direction. As a result, the velocity plot of Case 7 is similar to that of Case 1 in that the air is primarily moving in the x-direction. The air behaved as it would had a parallel-plate heat sink been used. In essence, the parallel-plate heat sink of Case 1, with a significant chunk of material removed, was used for Case 7. Consequently, the heat sink's convective area has been dramatically reduced and the system's components respond with increased temperature. It is very likely that the use of a staggered pin-fin or staggered strip-fin arrangement would have helped to alleviate this problem.

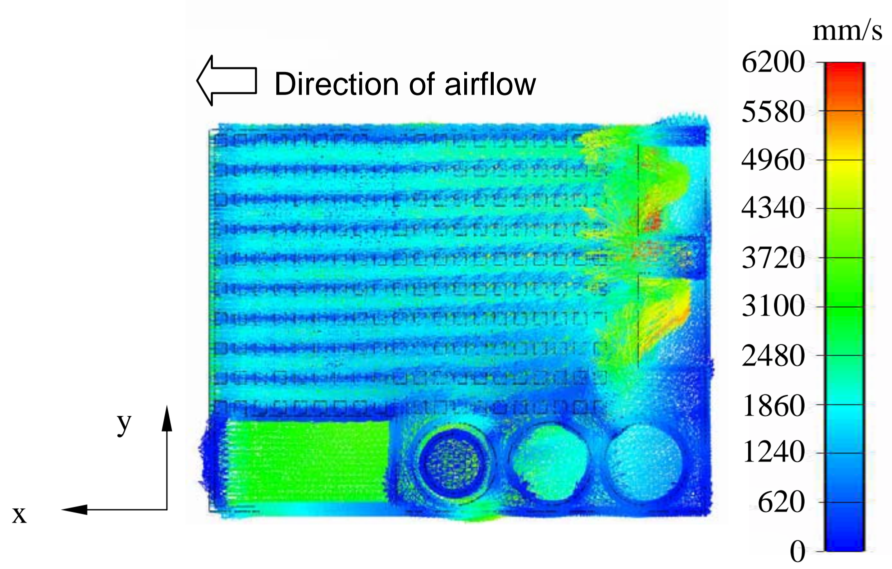

Figure 4.7 The velocity vector diagram for Case 7.

Table 4.2 The temperature responses of Case 7.

Component	Maximum Temperature (°C)
1	138
2	127
11	142
12	127
Passive IPEM	117

To compare the results from the study, Cases 3, 5, and 7 were compared to Case 1. The results of Cases 2, 4, 6, and 8 were insignificantly different from Cases 1, 3, 5, and 7, respectively, and therefore they were ignored for this comparison. The following

five components were used in this comparison because they were consistently the hottest and/or produced the most power in each case: Components 1, 2, 11, and 12, and the passive IPEM. The following equation was used for the comparison:

$$\%\ Change\ From\ Case\ 1 = \frac{T_{case\ i} - T_{case1}}{T_{case1}} \quad (1)$$

where $T_{case\ 1}$ is the maximum temperature of each component in Case 1 and $T_{case\ i}$ is the maximum temperature for each component for some case other than Case 1. Figure 4.8 shows the results from this comparison. While Case 5 only provided a slight temperature improvement over Case 1 (relative to the scale of the graph), it was the only scenario where the maximum temperature was reduced from that of Case 1.

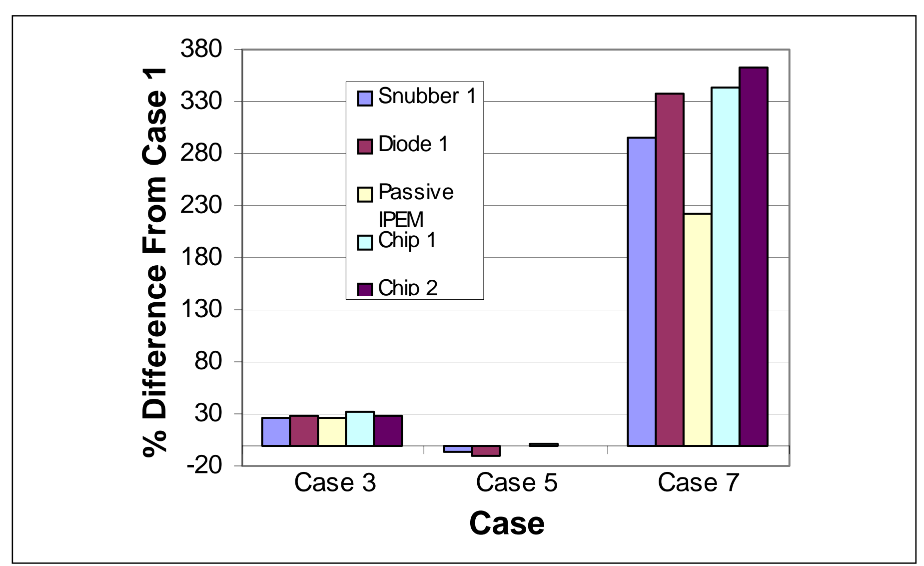

Figure 4.8 Comparison of Cases 3, 5, and 7 with Case 1.

While the temperature response of Case 5 was somewhat improved over Case 1, the location of one of the fans of Case 5 was later found to conflict with the converter's output connection. And, because the benefits of the layout of Case 5 over those of Case 1 were not significant enough to warrant a redesign, the layout of Case 1 was used for the final design.

This study was heavily restricted by electrical and packaging constraints. Had the system-level thermal design of the power converter been included as an integral part of

the design process early on, the rearrangement of individual electrical components could have been investigated. Such an investigation would have likely led to an overall improved layout. This suggests the importance of integrating thermal design with electrical and packaging design early in the design process and throughout all of the design stages.

4.3 Heat Sink Height and Heat Transfer Mode Investigation

This section presents some of the additional analysis that was performed using the power converter thermal model. As was mentioned in Chapter 3, the parallel-plate heat sink that was used to cool the components of the power converter was 18 mm tall with a 4 mm base and 14 mm-tall fins. This particular heat sink was the tallest heat sink that could be used in order to meet the 1-unit height restriction. However, when a shorter commercially available heat sink was found, the thermal model was used in order to determine if would be feasible to use it. This shorter heat sink was 14.5 mm in height with a 3.7 mm base and 10.8 mm tall fins. Figure 4.9 compares the temperature response of the power converter system using (a) the 18 mm tall parallel-plate heat sink and (b) the shorter, commercially available heat sink. Notice that while the temperatures do increase when the shorter heat sink is used, the temperatures still fall below the maximum required limit of 120°C.

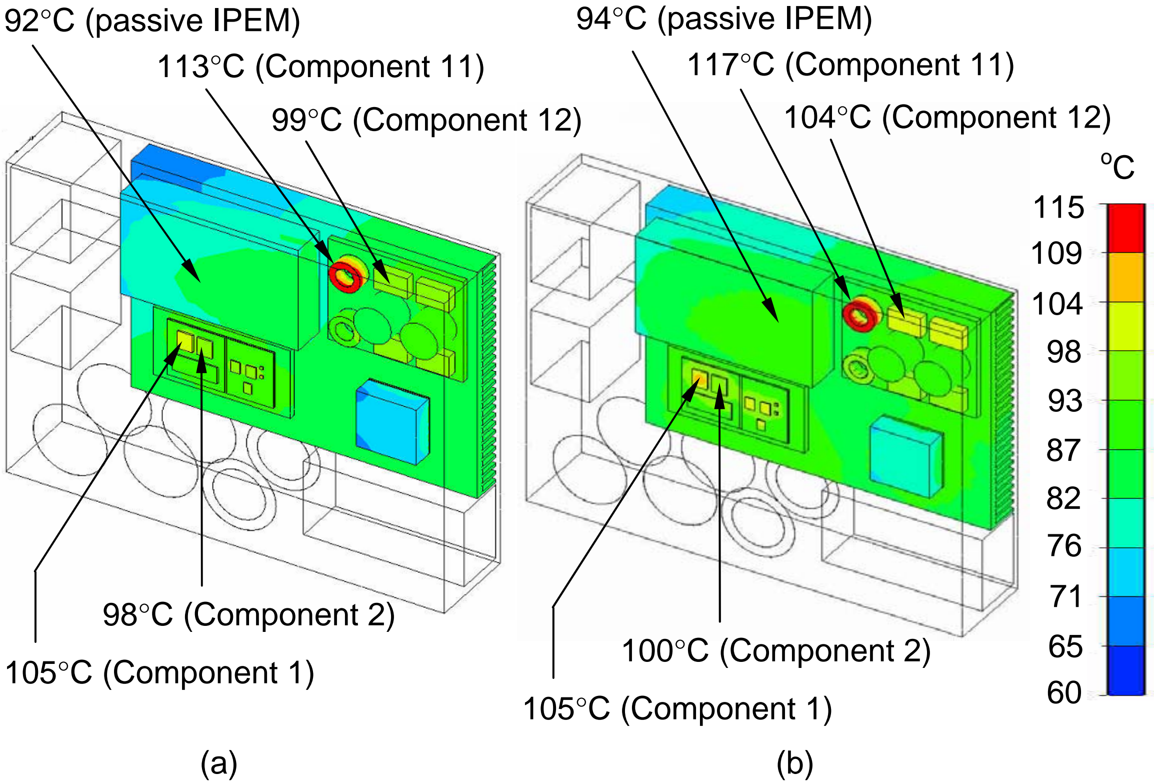

Figure 4.9. The thermal response of the power converter using (a) the 18 mm tall heat sink and (b) using the 14.5 mm tall commercially available heat sink.

The results of the parametric study outlined in Section 4.2 showed that most of the components in the system were strongly dependent upon the heat sink to rid them of the heat they dissipated. From the results obtained from the model of Figure 4.9b, the heat spreader that the active IPEM sits on gives only 10% of the heat it receives directly to the air. The rest of the heat is transferred down to the heat sink. This is not surprising as only 38% of the active IPEM's heat spreader is exposed to the air. Similarly, the rectifier gives off almost 90% of its heat directly to the heat sink. This too is not surprising as its plastic top coating is a very poor conductor of heat. Figure 4.10 summarizes the heat convected directly to the air versus the heat conducted to the heat sink for the passive IPEM and the output heat spreader for the eight output components. Notice that the passive IPEM gives off about half of its heat directly to the air due to the large amount of surface area it has. The two capacitors in the output component cluster (Components 14 and 15) give off approximately 80% of their heat directly to the air. This is in stark contrast to the other output components around them. Their geometry explains this difference in heat transfer. Unlike the two snubbers and four diodes around them, Components 14 and 15 are much wider and taller and can convect heat to the air that flows over the output components in the wake of the passive IPEM. It should be noted that only about 9% of the heat from the output components is transferred to the air from the heat spreader. The other 91% is transferred to the heat sink. A redesign of the converter housing could open the way for double-sided cooling. Included in this redesign could be the addition of an airflow diversion apparatus that could channel air to the components or clusters of components that need it the most.

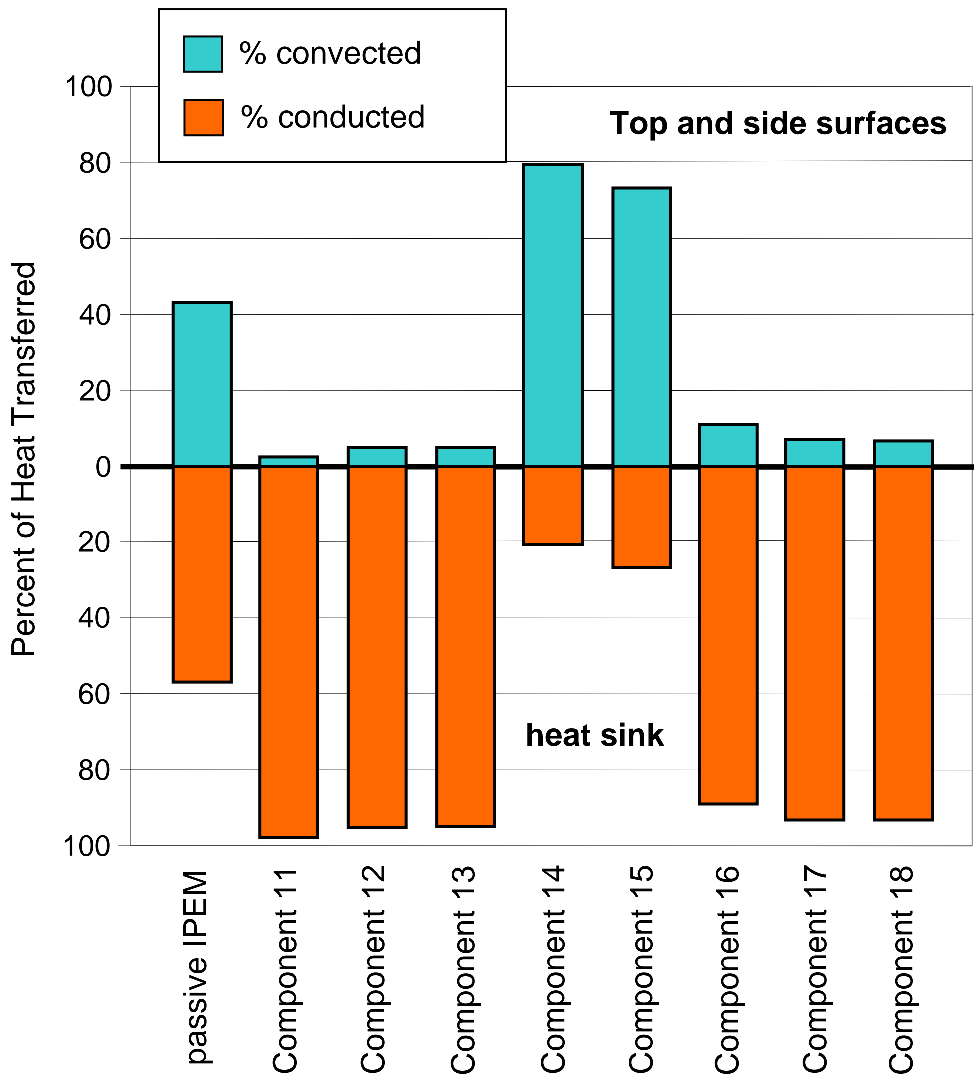

Figure 4.10. The percentage of heat transferred directly to the air (through convection) versus the percentage transferred down through conduction to the heat sink.

4.4 Experimental Verification

The finite element model of the DC-DC front-end power converter played a significant role in the design process and was used not only to predict the temperature response of the electrical team's converter layouts, but also to perform additional thermal analysis and investigations. Once the design process was complete and final decisions had been made concerning the converter's electrical and physical layout, a functional prototype of the power converter was built. The prototype is shown in Figure 4.11. In order to determine the converter's true thermal behavior, an experiment was set up to measure the temperature response of the actual converter. This test was important not only to insure that the temperature of the components remained within the recommended limits, but also to test the accuracy of the numerical predictions and investigate the converter's transient response. This section describes the experimental setup and compares the results to those obtained from the finite element model.

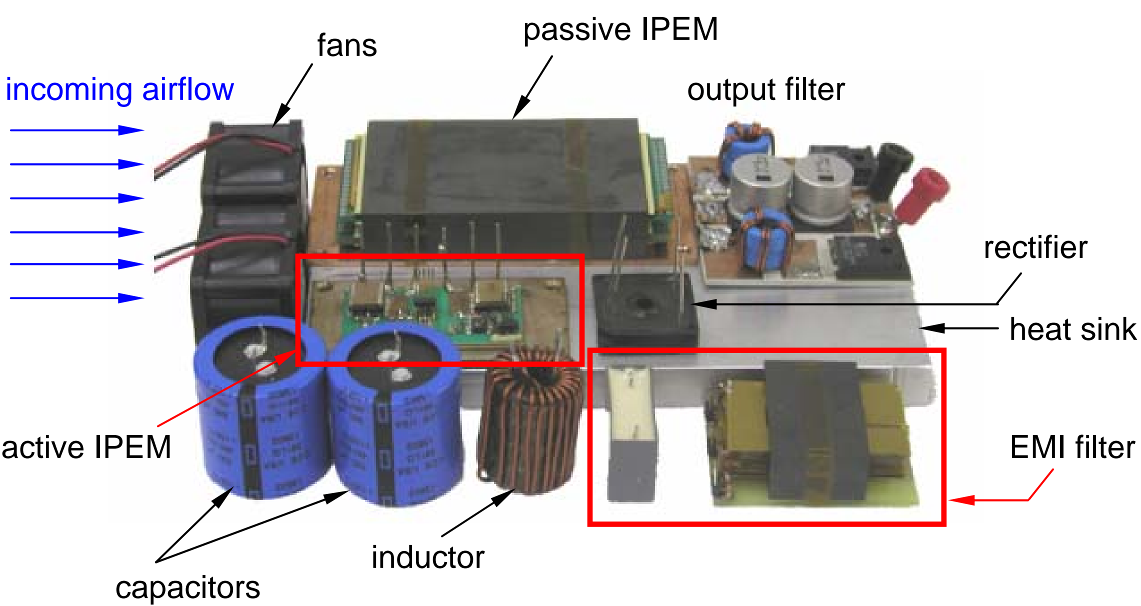

Figure 4.11 The prototype DC-DC front-end power converter

A comparison between Figures 4.11 and 3.9 reveals that there were several changes made to the final design of the power converter prior to its construction. These changes primarily involved the electrical and component layouts and are summarized in Table 4.3. It should here be noted that, for purposes of simplification, the thermal model described in Chapter 3 did not account for the presence of the converter's electronic board (shown in Figure 4.12b). This board was used as the top lid of the converter box and served as the connection apparatus for the electrical probes and power input. Furthermore, the two capacitors and the inductor hung down from the board in the empty space shown in Figure 4.12b. The board allowed some of the heat given off by the components to escape via pin connections and small gaps. However, given the forced-convection environment that the components were subjected to and given that the converter was well insulated during the experiment, it was assumed that only a negligible amount of heat could escape through the board. Figure 4.12c and Figure 4.12d show the insulated power converter. The insulation used was a 0.5 in. thick asbestos-free ceramic fiber wrap. Two layers were used on every side of the converter excluding the vent.

Table 4.3 The modifications that were made to the power converter design prior to the construction of the prototype

Location	Modification
fans	moved closer to the heat sink
passive IPEM	moved closer to the active IPEM to provide air to Component 11
	1.5 mm-thick copper heat spreader added underneath the passive IPEM
output filter	snubber heights doubled (Components 11 and 16)
	output diodes reduced from four to two (10 W high diode, 7 W low diode)
	the thickness of the heat spreader was reduced from 3 mm to 1.5 mm
active IPEM	top gel coating was not used for the experiment
	active IPEM moved closer to the fans
rectifier	reduced in height by approximately 3 mm and moved closer to the fans
heat sink	number of fins reduced from 28 to 25
EMI filter	removed – not necessary for experimental testing

As Figure 4.12b shows, the presence of the electronic board prevented an IR camera from being used to collect data. It was therefore decided to use 20 Type-K 36 gauge thermocouples to measure the temperature response of the system. Figures 4.13 and 4.14 show the location of the thermocouples above the heat sink and below the heat sink, respectively. Table 4.4 lists the locations according to number. These locations were based primarily upon the results presented in Section 4.2. Figures 4.13 and 4.14 also show the updated finite element model that was built to account for the changes that were made to the converter design. The geometry and location of the components for this model were measured directly from the prototype power converter.

Table 4.4 The location of the thermocouples with numbers corresponding to those of Figure 4.13 and Figure 4.14.

number	location
1	ambient air outside the power converter
2	top surface of the passive IPEM (centered)
3	surface of the heat sink, directly underneath the center of the passive IPEM
4	the top surface of the active IPEM's heat spreader
5	top surface of the passive IPEM
6	top surface of the output heat spreader, immediately downstream from Component 11
7	top surface of the high output diode
8	top surface of Component 15 (one of the output capacitors)
9	top surface of the low output diode
10	side surface of Component 16 (low output snubber)
11	top surface of Component 2 (active IPEM chip)
12	top surface of Component 6 (active IPEM chip)
13	surface of the heat sink, directly underneath active IPEM (DC-DC)
14	surface of the heat sink, directly underneath active IPEM (PFC)
15	side surface of Component 11 (high output snubber)
16	surface of the heat sink, directly underneath Component 11
17	surface of the heat sink, directly underneath the high diode
18	top surface of the passive IPEM's heat spreader
19	heat sink fin, downstream of the active IPEM and rectifier
20	heat sink fin, downstream of the passive IPEM and output components

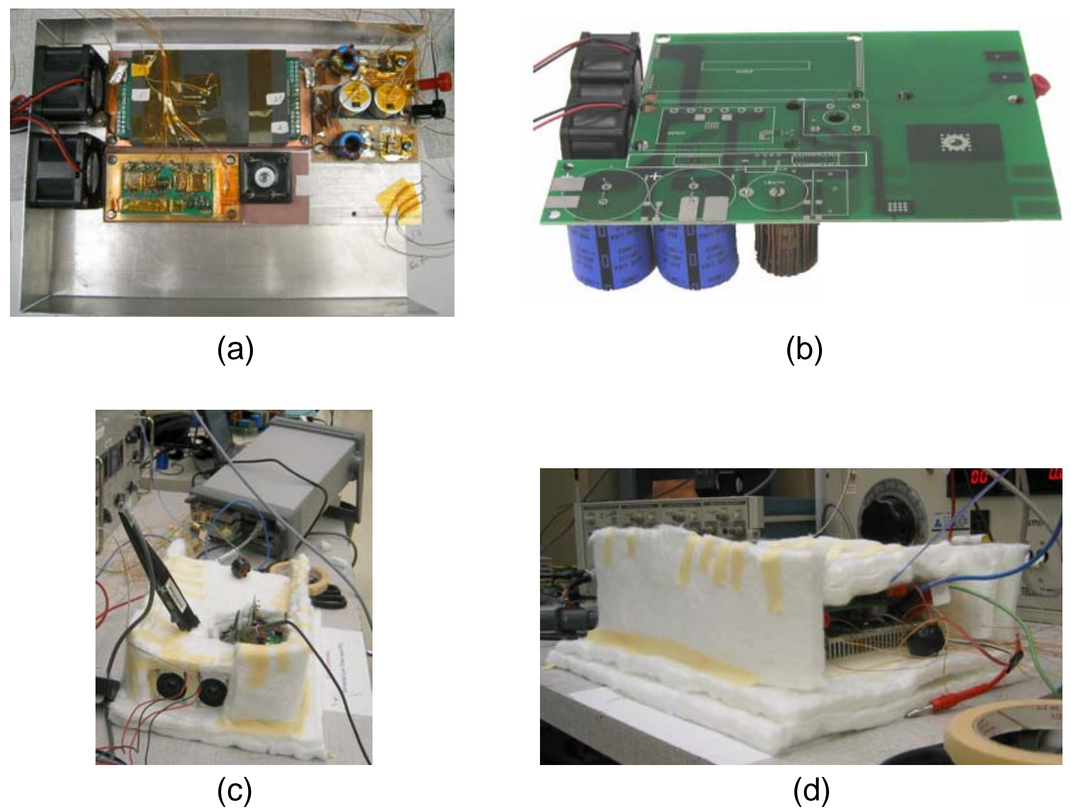

Figure 4.12 The top view of the experimental setup without the electronic board (a), the added board (b), and the insulated converter showing the inlet fans (c) and exit vent (d).

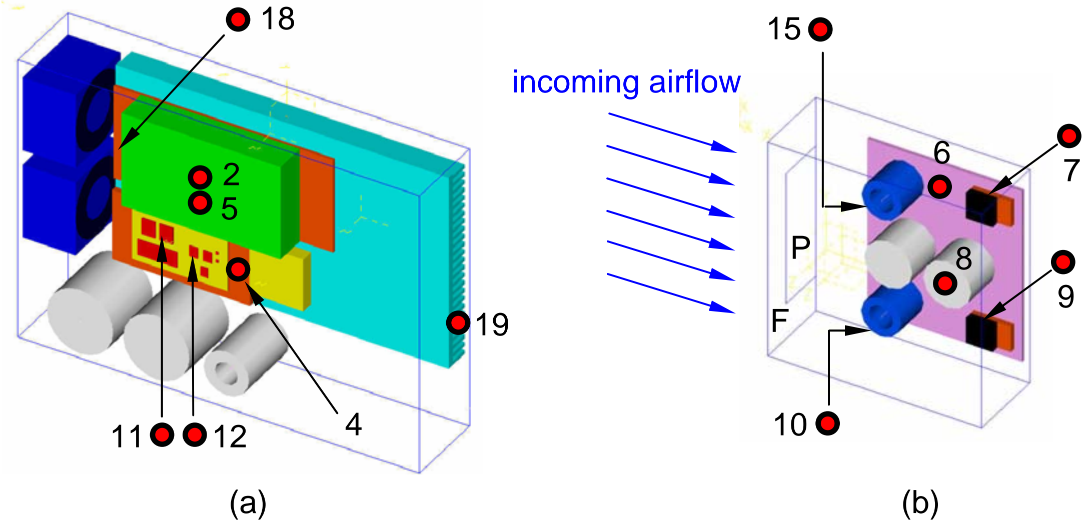

Figure 4.13 The revised thermal model of the power converter showing (a) the upstream model and (b) the downstream model with thermocouple locations.

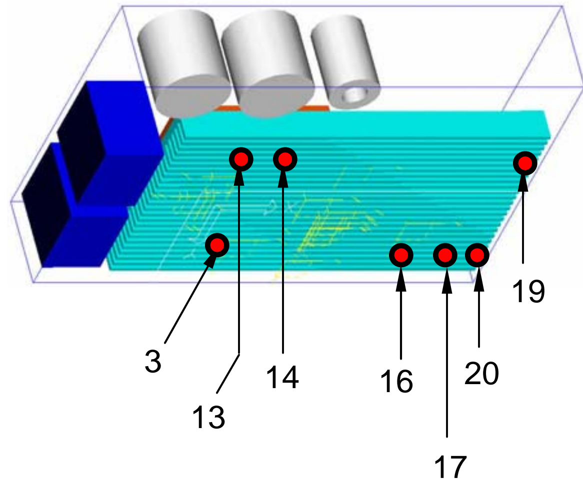

Figure 4.14 The seven thermocouples located underneath the heat sink.

The experiment had to be conducted without damaging or permanently altering the two IPEMs. This meant that a hardening, permanent epoxy could not be used on the components themselves. For this reason, the 19 thermocouples used inside the converter were attached to the components using two methods. Thermocouples 2, 4, 6 – 12, 15, and 18 – 20 were all attached in a non-permanent manner using a combination of Kapton tape and Omegatherm 201. The highly conductive silicone-based paste allowed for an improved contact between the tip of the thermocouple and the surface of the component. The Kapton tape was used to ensure that the thermocouples did not move or blow away due to the force of the incoming air. Each thermocouple tip was sandwiched between two layers of tape and surrounded by Omegatherm paste. Thermocouple 5 was placed beside Thermocouple 2 and attached in a slightly different manner (its tip was left untapped) to verify the consistency of the results.

A second and permanent method of attachment was used for the rest of the thermocouples. Thermocouples 3, 13, 14, 16, and 17 were used to record the surface temperature of the heat sink directly underneath certain components. To do this, holes were drilled into the base of the heat sink where the thermocouples would be placed. The thermocouples were inserted into the holes and a hardening epoxy was used to fill the holes and keep the thermocouples rigidly in place. The surface of the heat sink was then carefully sanded to ensure that the tips of the thermocouples and the epoxy were flush

with the rest of the heat sink. The 20 thermocouples were attached to a data acquisition unit (that back of which is pictured in the upper half of Figure 4.12c), which was connected to a Dell Latitude laptop computer for data recording. The power converter was run at approximately 70% power.

To increase computational efficiency and reduce model complexity, the revised thermal model of the power converter was divided into two parts: an upstream model and a downstream model. The upstream model, shown in Figure 4.13a, included the fans, heat sink, flow obstructions (hanging down from the electronic board), the passive IPEM, the active IPEM, and a simplified version of the rectifier. It was assumed that the temperature response of the two IPEMs would not be significantly affected by the components downstream (the rectifier and the output filter). Therefore, the output filter was eliminated from the model. However, the rectifer was included (although only a simplified version) to account for the presence of a flow blockage immediately downstream of the active IPEM. It was believe that this flow blockage could create a recirculation of warm air near the components of the active IPEM and was therefore necessary for accuracy. Note that the fans were modeled in more detail to account for their hubs and circular openings. To increase the efficiency of the finite element model, the airbox was partitioned in order to allow for a fine air mesh around the active IPEM and a courser air mesh elsewhere. It should be noted that the same boundary conditions mentioned in Section 3.3 were applied to this model.

The downstream model, shown in Figure 4.13b, included just the output filter. The results of the upstream model were used as boundary conditions for the downstream model. These boundaries included the temperature and average velocity of the air immediately upstream of the output filter. The rectangular area on the upstream surface (denoted as P) represented the flow blockage due to the passive IPEM and its heat spreader. The remaining area (denoted with an F) represented the inlet fan. The bottom surface of the output filter's heat spreader was set at a constant 58°C based upon the results of the upstream model shown in Figure 4.13a. Because this model was so small, the details of the output diodes (shown in Figure 3.7b) could be added for increased accuracy. This method of modeling is explained in more detail in Chapter 5.

Figure 4.15 shows the results of the two finite element models of Figure 4.14. This figure also shows the approximate locations of the nodes that were used to query the temperatures of the computational model. These locations correspond to the locations of the thermocouples in the physical device. With the inlet and outlet (ambient) temperatures lowered to 26°C and the power dissipation for each component reduced to 70%, temperatures were drastically reduced (as would be expected) from the results of Sections 4.2 and 4.3. And, as predicted earlier in this chapter, Component 11 was found to be the system's hotspot. Figure 4.16 shows the temperature response of the physical prototype as measured by the 20 thermocouples. Notice that the system's hotspot is at Components 11 and 16. While the thermal model did not predict that the two snubbers would be so close in temperature, it did predict that Component 11 would be significantly hotter than the rest of the system's components. Notice also that Thermocouple 4 drastically varies as it approaches its steady-state reading. This is likely due to the thermocouple's location between the active IPEM and the rectifier. As the velocity plot of the model showed, this area in the system is susceptible to recirculation of warm air coming off of the active IPEM mixing with the surrounding cool air. Also note that Thermocouples 2 and 5 gave very close temperature readings.

Figure 4.17 shows a graphical comparison of the numerical and experimental results and Table 4.5 lists the predicted and measured temperatures with the calculated percent differences. Note that Thermocouple 20 is not included in the comparison as the temperature of the heat sink fins in that area was not simulated in the thermal model. Although the numerical model consistently over-predicted all but two of the component temperatures, the thermal model of the power converter provided a good prediction of the behavior of the true converter. It was able to detect the location of the system's hotspots and predict general trends in temperature and air movement. Component 6 (measured by Thermocouple 12) was the most accurately measured component. The greatest difference between prediction and measurement occurred at Thermocouples 8, 9, and 16. Error bars indicate the error associated with the thermocouple measurements as specified by the manufacturer (±2.2 ^{o}C). It should be noted that the error due to the variance of the data was much smaller than this error. Differences in temperature can primarily be attributed

to the estimates in power loss and thermal contact resistances. It should also be noted that the test results were used for comparison and not for a full-scale model verification.

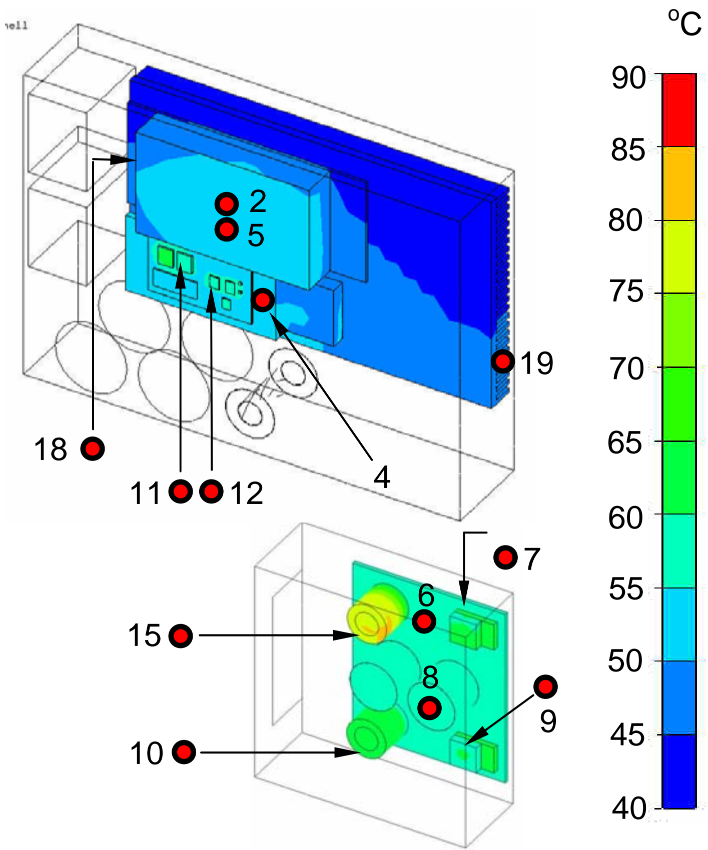

Figure 4.15. The results of the updated computational model.

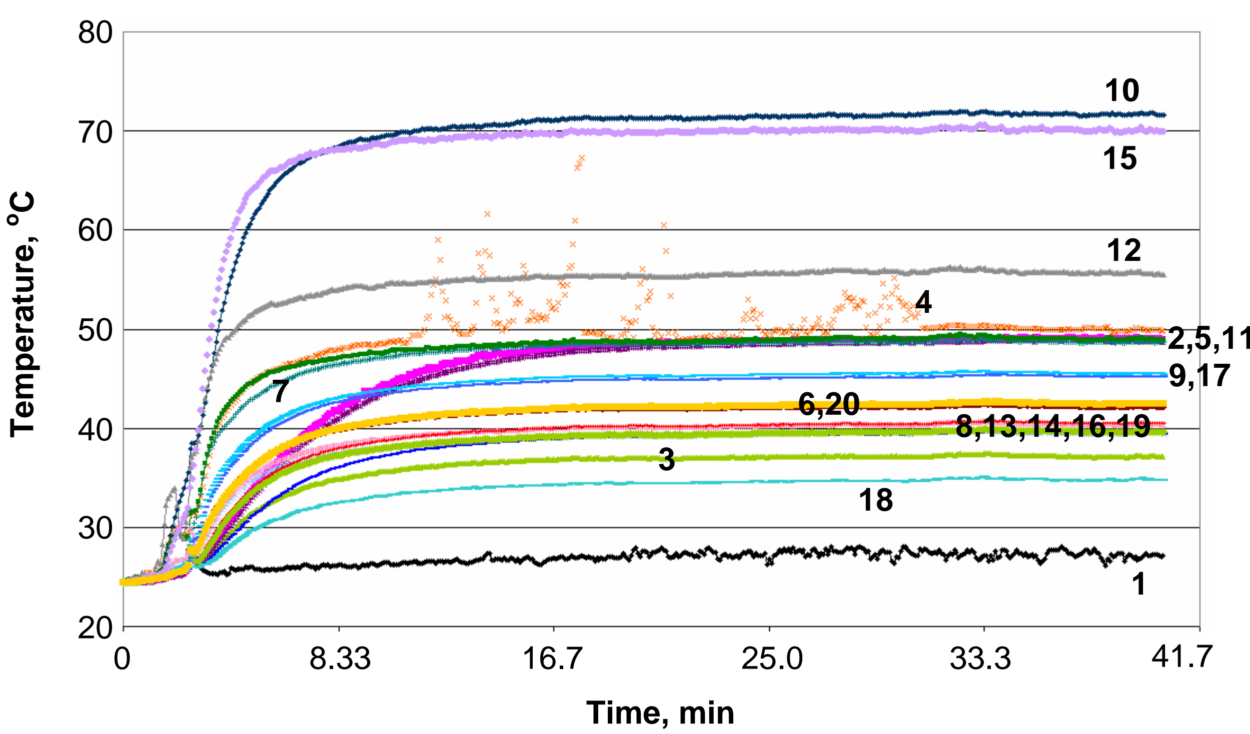

Figure 4.16 The measured transient temperature response of the converter.

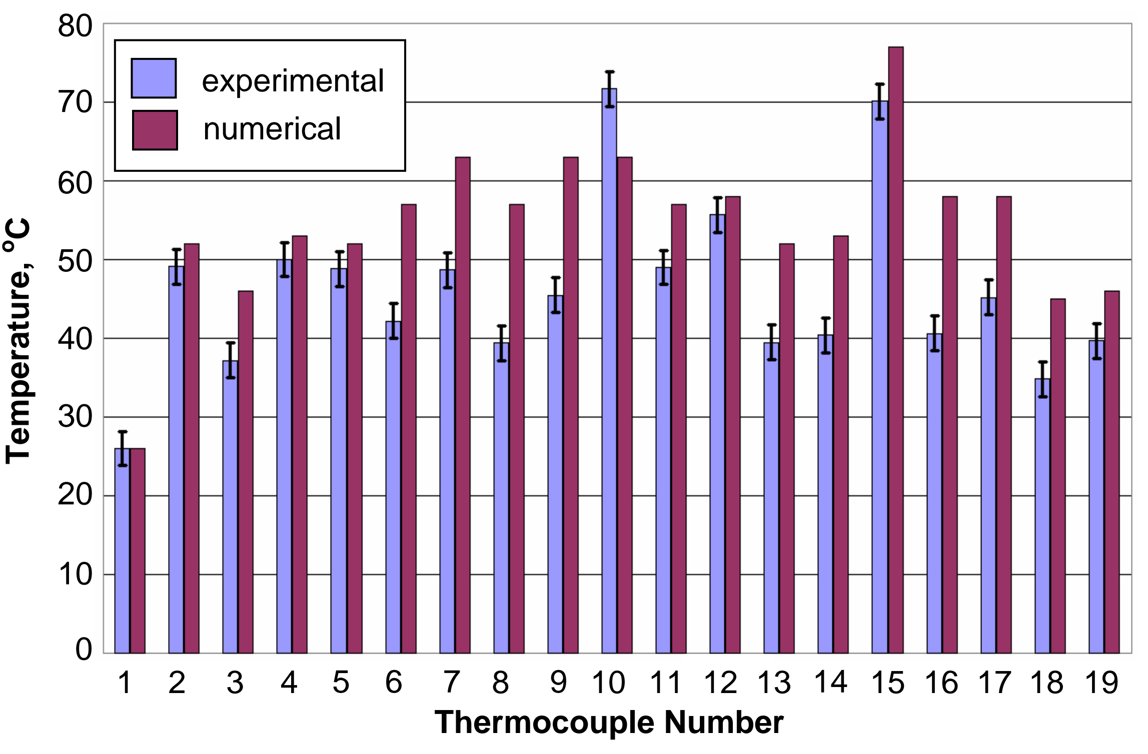

Figure 4.17 Comparison between numerical and experimental results.

Table 4.5 The predicted and measured component temperatures with the calculated percent differences.

Thermocouple	Predicted (^oC)	Measured (^oC)	% Difference
1	27	27.2	-0.7
2	52	49.1	5.6
3	46	37.2	19.1
4	53	50.0	5.7
5	52	48.8	6.2
6	57	42.2	26.0
7	63	48.7	22.7
8	57	39.4	30.9
9	63	45.5	27.8
10	63	71.7	-13.8
11	57	49.0	14.0
12	58	55.7	4.0
13	52	39.5	24.0
14	53	40.4	23.8
15	77	70.1	9.0
16	58	40.6	30.0
17	58	45.2	22.1
18	45	34.8	22.7
19	46	39.7	13.7

Chapter 5 – Multi-Scale Thermal Modeling

In Section 4.4, a unique method was used to model the updated finite element model of the power converter. This method involved splitting the modeling into two parts: an upstream and system-level model and a downstream component-level model. It was assumed that the results of the upstream model did not depend upon the results of the downstream model but that the downstream model did depend upon the results of the upstream model. The results from the upstream model were input as boundary conditions to the downstream model. This method allowed for much faster run times than the fully detailed model and produced equally accurate results. In this chapter, this method (known as 'zooming-in') will be discussed in more detail and will be applied to systems with much larger length-scale problems.

5.1 Background and Motivation

Chapter 4 presented the parametric study that was performed as part of the design process for a DC-DC front-end power converter developed at CPES. To perform this study, a thermal model was built, meshed, and solved using I-DEAS. This model played a crucial role in the design process and was used not only to predict the temperature response of proposed converter layouts, but also to perform additional thermal analysis and investigations in other studies. Later, it was proposed to use that same thermal model to model a rack holding several such power converters. It was also desired to eventually be able to model an entire room of these racks, such as a telecommunications or internet data center. In order to do so, the original thermal model would require significant simplification. For this reason, the work that is presented in this chapter began as a study to determine the best strategy for thermal model simplification. However, when it was realized that the need existed, emphasis shifted from the ultimate goal of modeling a data center to the refinement of system-level thermal modeling at CPES. The thermal management of data centers or racks of power electronic devices is not the main objective of this work, but merely one application of multi-scale modeling. The objective of the

work that is presented in this chapter is to determine how best to model systems of power electronic devices that have several layers of system complexity.

5.2 Multi-Scale Modeling Methodology

5.2.1 General Description

It was proposed that the problems of data center thermal modeling could be solved by using the approach outlined by Gupta (2002). Furthermore, it was decided to see if his approach could be expanded in such a way that it could be used to zoom both in and out (Gupta's work focused only upon zooming-in). Figure 5.1 shows the outline of the proposed methodology. First, a system-level base model of the proposed layout of a single device is created using a commercially available electronics-cooling package. This package should be able to perform CFD analysis. The thermal modeling process should start at the base model. Once the base model has been simulated, the designer can then zoom-in on a particular area or subsystem (typically the predicted hot spot) of the system or zoom-out to include several such systems. In both cases, the results obtained from the base model are used as boundary conditions for the scaled-up and scaled-down models.

The remainder of this section will present how this methodology was applied to the task of modeling the power converter presented in Chapter 3. The detailed system-level model showcased in Chapter 3 will be used for comparison to verify the accuracy of this methodology. Also included in this section is the 'zooming-out' approach and how it can be applied to the modeling of large, multi-scale systems such as data centers.

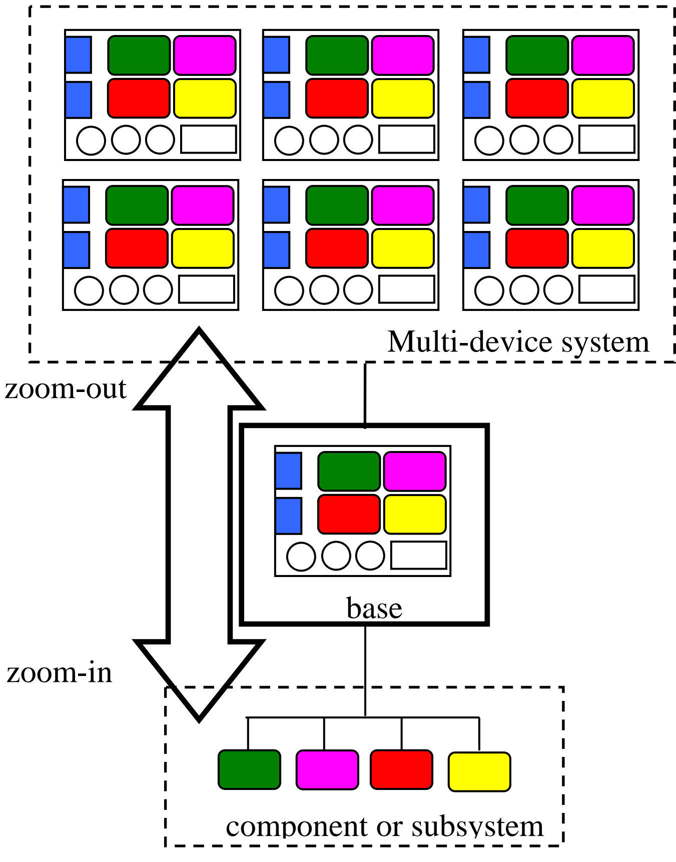

Figure 5.1 Outline of the multi-scale thermal modeling approach

5.2.2 The Base Model

The base model of the proposed methodology can be used to quickly determine the overall behavior of the system. Furthermore, it can be used to quickly investigate how the system will react if its layout is drastically changed from component rearrangement or fan location changes. The base model will not be able to provide the temperatures of the components themselves. For this reason, component-level modeling is a crucial and integral part of this approach.

The original thermal model (presented in Chapter 3) was itself a simplified model. Many simplifying assumptions were made in order to build a manageable model in I-DEAS. For example, the active IPEM model was greatly simplified from its proposed physical construction. Likewise, the four diodes in the output cluster were modeled as

simply volumetric heat-generating blocks with an equivalent thermal conductivity. In reality, these diodes were part silicon, part copper, and part plastic – three materials with three very different thermal conductivities. When the original model was built and simulated, there was concern whether the model was over-simplified or not simplified enough. During this study, it was found that the original model could indeed be further simplified without jeopardizing the integrity of the results.

Figure 5.2 shows the two versions of the base model that were used in this study. These models are simplifications of the model presented in Chapter 3. The differences between the two models are subtle. In both models, the passive IPEM, the fans, the heat sink, and the components that sit off to the side of the heat sink were modeled as they were originally. Both models were meshed using a course meshing scheme (an element length of 10 mm for all shell and 3-D elements for both the solid components and the air). In addition, the details of component geometry were eliminated. Instead, components and/or clusters of components were lumped together and represented as a single group. But the model of Figure 5.2a (Model A) uses 'footprints' to represent the active IPEM, the output component filter, and the rectifier. The use of the footprints assumes that the heat from the components is evenly spread by the time it reaches the heat sink and that there is only a negligible thermal resistance produced by the presence of the copper heat spreaders (for the active IPEM and the output filter) and the rectifier base. A uniform heat load (equal to the total heat dissipated by the actual electrical components) is applied to the footprint surfaces. In comparison, the model of Figure 5.2b (Model B) uses blocks (like the passive IPEM) to represent these groups. The two copper blocks that represent the active IPEM and the output filter are the same dimensions as their respective heat spreaders and have a uniform heat load (equal to the total heat dissipated by the actual electrical components) applied to their top surface. The plastic block that represents the rectifier has a uniformly distributed heat load applied to its bottom surface equal to the total heat dissipated by the four rectifier diodes. In Section 5.3, the results of the two models will be shown and discussed.

The base model will only provide a general idea of how the system will respond as most of the details of the components that sit on top of the heat sink have been left out. But the details in the rest of the system have been left in (the fans, the heat sink, and the

non-heat generating components). For the base model, the emphasis is not so much upon the temperature-sensitive components that give off heat, but upon the other components that contribute to the complexity of the system's airflow (i.e., fans, heat sink, and flow blockages). Once these components have been characterized in the base model, there should be no need to include them in subsequent models. The results from the base model should tell the designer how these components interact with the heat-generating components. This information will, in turn, be used as boundary conditions in any additional thermal modeling.

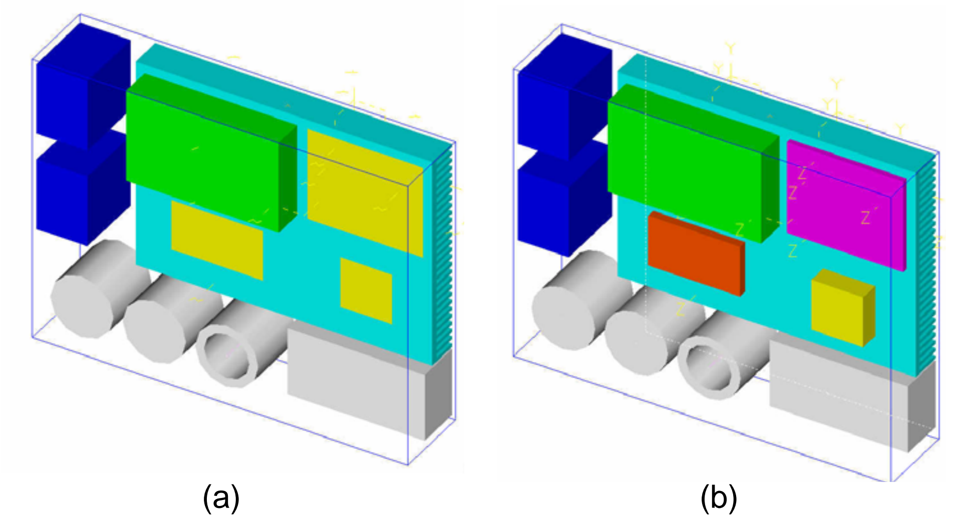

Figure 5.2 The active IPEM, output filter, and rectifier were simplified using two methods: footprints in Model A (a) and blocks in Model B (b).

5.2.3 Zooming In: Component-Level Modeling

The zoom-in approach gets its name from the designer looking at the base model and zooming in, if it were, on the groups of components in the system that get the hottest. The designer builds and meshes a second model of the system's hot spot. This second model is a component-level model and contains the details of the components (geometry, heat loss, contact resistances, surface characteristics, etc.) only in that group. As was done by Gupta (2002), the results from the base model become the boundary conditions for the second model. In the present application, only three values needed to be transmitted from the system-level model to the component-level model: the average upstream air velocity, the average upstream air temperature, and the local surface temperature of the heat sink. This information was transmitted by hand from the first model to the second. By isolating individual regions or clusters of components, details can be added to the model without worrying about the problems associated with an overly large, cumbersome model. Furthermore, a fine mesh or grid spacing can be used to increase the accuracy of the results. A zoomed-in model can be created for any of the system's subsystems or component clusters in order to determine the exact temperature responses of the components and to refine the accuracy of the results.

Figure 5.3a shows the component-level model of the output component cluster. The rectangle denoted as 'P' is a flow blockage that represents the backside of the passive IPEM immediately upstream of the output components. This area was set at a constant temperature representative of the steady-state temperature of the backside of the passive IPEM. The area denoted as 'F' was the air inlet of this model and was given a constant temperature and a constant air velocity. These temperature and velocity values were obtained from the results of the base model in that same area. For example, Figure 5.3b shows the air's velocity in the region immediately after the passive IPEM. The average air velocity here was calculated to be 4500 mm/s. The bottom surface of the heat spreader was also set at a constant temperature (88 ^{o}C) based upon the results of the base model. Additional component-level models could be made for the active IPEM and the rectifier (Figure 5.4).

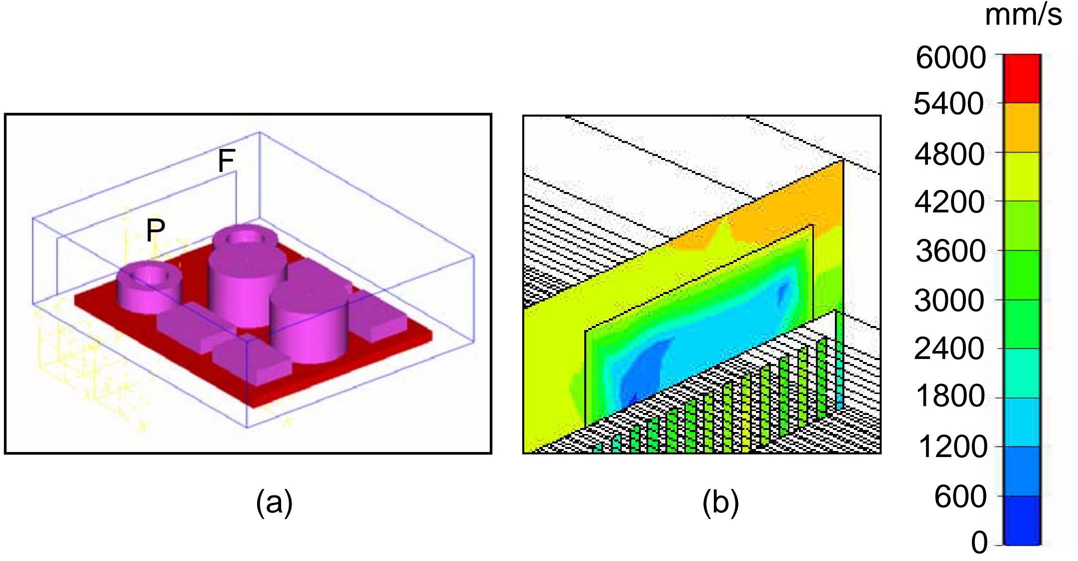

Figure 5.3 The (a) component-level model of the output filter and (b) the air velocity contour plot immediately downstream of the passive IPEM.

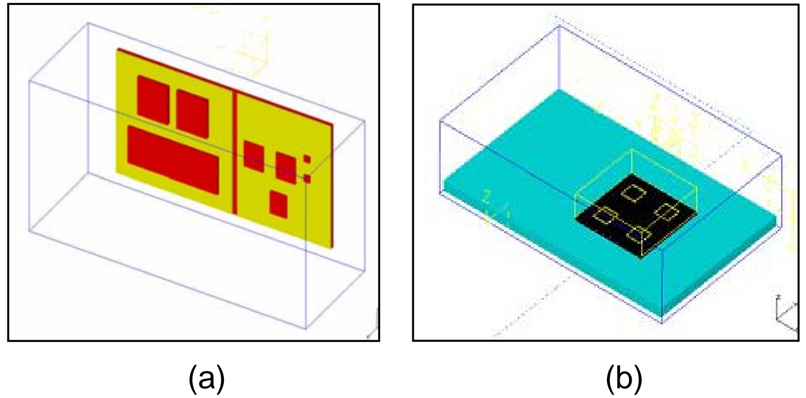

Figure 5.4 Component-level models of (a) the active IPEM and (b) the rectifier.

5.2.4 Zooming-Out: Multi-Device Level

Because the initial intent of this work was to determine how several power converters would thermally respond to being grouped together in a rack configuration, a model was built as part of this study to represent this scenario. Figure 5.5 shows the model that was created to represent a section of the rack of power converters. The proposed configuration called for the power converters to be installed side-by-side in the rack (horizontally). This is in contrast to a rack that has its heat-dissipating devices stacked on top of each other (vertically). In such an arrangement, the temperature will be hotter toward the top of the rack. But with the power converters stacked side-by-side, the temperature response will be nearly the same for the inner converters. Taking advantage of the symmetry this configuration provides, only three converters were included in the rack model. The outer-most sides of the outer power converters were adiabatic. Note that the model of Figure 5.2a was used to model the rack. As will be shown later in this section, the model of Figure 5.2b could have also been used for slightly more accurate results.

The modeling approach of Figure 5.5 is limited in that there is a practical limit as to the number of (even simplified) power converters that can be modeled. For this reason, a ‘zoom-out’ approach should be used to model multiple devices. Figure 5.6a shows a box that represents the power converter unit. Like the zoom-in approach, the results from the base model are obtained and applied to this model. When several power converters are modeled together (as in Figure 5.6b), the results will indicate how much heat the converters are contributing to each other and how hot the sides of each case will get. Then, the base model can be simulated once again but with additional heat sources representing the surrounding power converters.

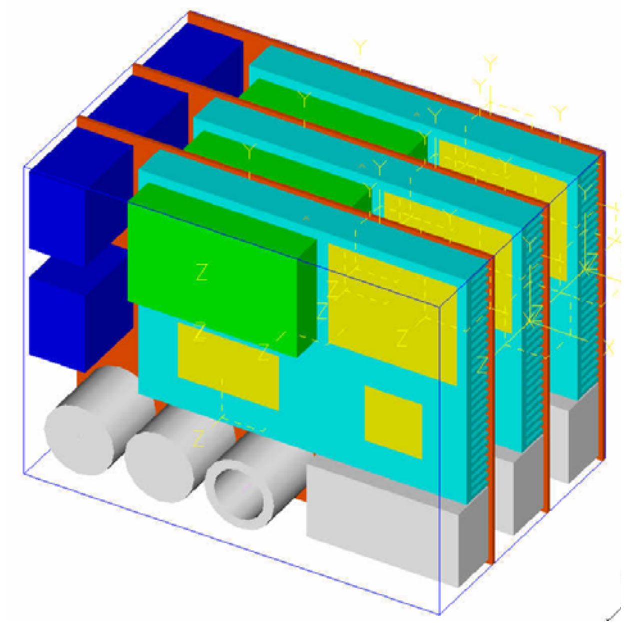

Figure 5.5 The multi-device (rack) model

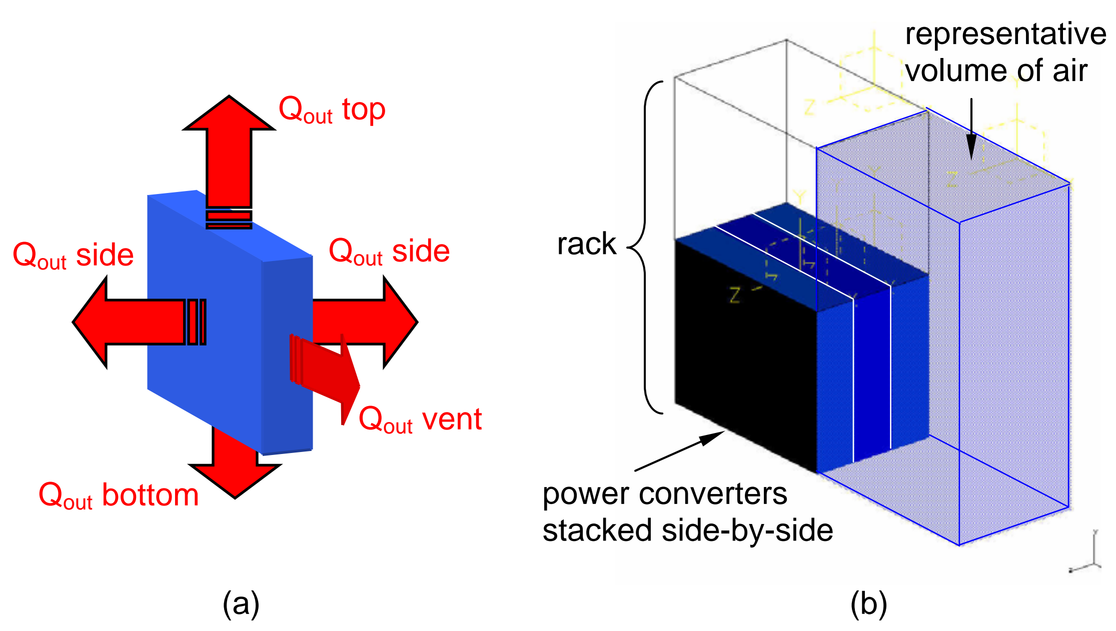

Figure 5.6 The (a) individual converter case and (b) multiple devices in a rack.

5.3 Results and Discussion

5.3.1 Base Model Comparison

Figure 5.7 compares the temperature response of the detailed model of Case 1 in Chapter 4 to the temperature response of Model A. In both cases, only the temperature response of the heat sink is shown for proper comparison. The top (original) model has a maximum temperature of 92°C around the area of the active IPEM and the output component cluster. Model A, however, has a maximum temperature of 98°C but a similar temperature spread. In the bottom model, the footprint areas on the surface of the heat sink representing the active IPEM and the rectifier were adiabatic because most of the heat from these components is forced down to the heat sink via conduction. The output component cluster footprint, however, convected heat to the air as well as conducted heat to the heat sink and is therefore cooler. The cause for the differences in temperatures is the bottom model's lack of area to convect heat.

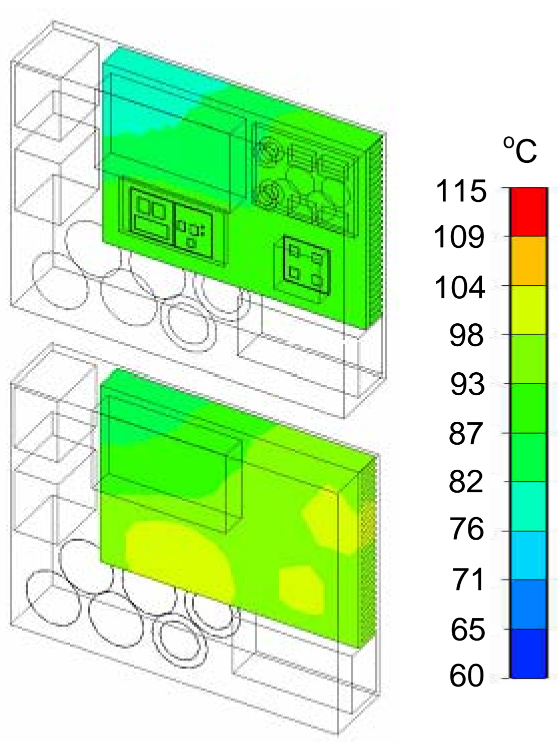

Figure 5.7 Comparison of the temperature response between the fully detailed model (top) and Model A (bottom).

Figure 5.8 shows the temperature response of Model B. Model B produced more accurate results than Model A. The maximum temperature of Model B was 90°C and the temperature spread more closely matches that of the original model. The differences between Model B and the fully detailed model can be attributed to the increase in flow surfaces and the lack of flow obstructions in Model B due to the absence of the individual electrical components. Still, the differences are nearly negligible. Model B gave more accurate results than Model A because it accounted for the heat that was absorbed by the heat spreaders. Figure 5.9 provides a graphical comparison of Models A and B to the fully detailed model at five locations in the system. Figure 5.9 references the temperature of the bottom surface of the devices or the top area of the heat sink directly underneath them.

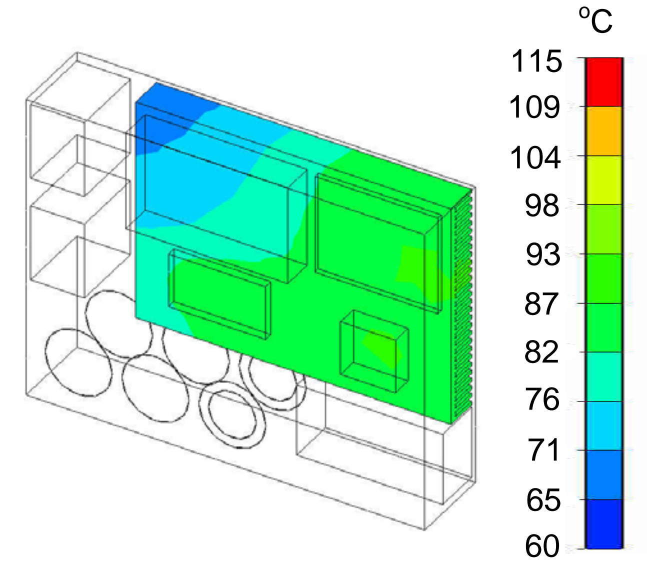

Figure 5.8 The temperature response of Model B.

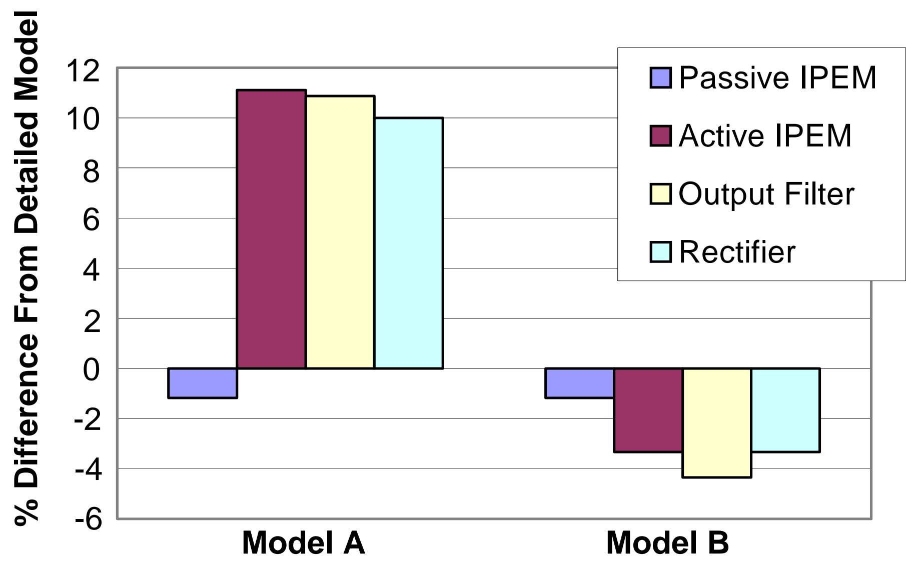

Figure 5.9 Comparison of Model A and Model B to the detailed model.

Should additional analysis be needed on the base model itself (i.e., optimization of the layout of the components on the surface of the heat sink or the location of the fans), a reduced or simplified version of the base model could be used for faster results. Once the base model was run, it was observed that there is very little movement of air around the two capacitors, the inductor, and the EMI filter that sit off to the side of the heat sink. The same condition was observed in the results obtained in Chapter 4. This is shown in Figure 5.10a. In the plane, the areas of little or no fluid (air) movement are indicated by blue and the areas of maximum air velocity are indicated by yellow. Because these components have a negligible contribution to the behavior of the airflow in the system and give off no heat, they can be eliminated from future base models for further simplicity (Figure 5.10b). The temperature response of the model of Figure 5.10b is identical to that of Model B in Figure 5.8.

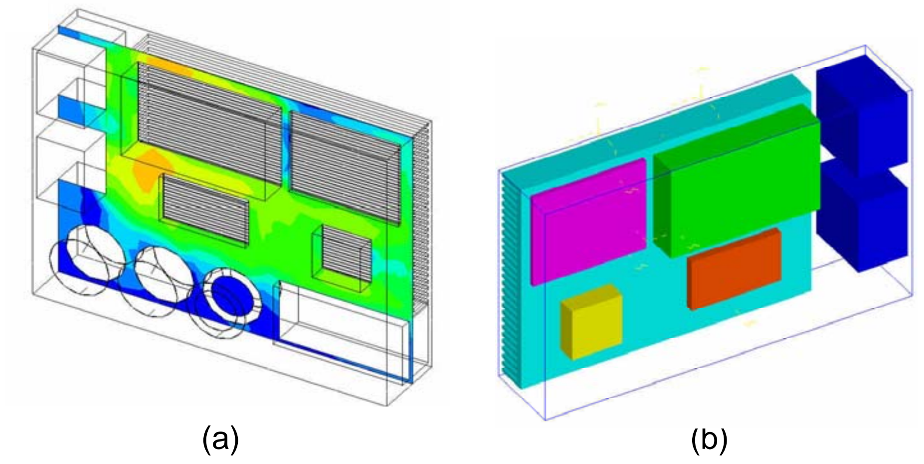

(a) (b)

Figure 5.10 Model B: the (a) air velocity plot and (b) a simplified version.

5.3.2 Component-Level Model Comparison

Figure 5.11 shows a comparison of the temperature response of the output component cluster from (top) the full-scale detailed original model and (bottom) the component-level model of the proposed methodology. The temperature response is nearly identical. It should also be noted that the fully detailed model of Figure 5.11 was

represented by over 360,000 elements while the component-level model of Figure 5.11 was represented by less than 31,000 elements. Should the design team need to perform a parametric study on this group in order, for example, to see if rearranging the components would further drive down temperatures, the analysis should be performed on the component-level model. This approach will give equally accurate results in much less time. Furthermore, in their parametric study, the designers could add more detail to the component-level model (such as the detail missing from the diodes) and refine the solid and air mesh. This will increase the accuracy of their results without adding a significant amount of solve-time.

For the purposes of this work, it is not necessary to examine a component-level model of the passive IPEM, the active IPEM, or the rectifier. The passive IPEM was modeled in the base model because of its already simple geometry. Furthermore, because it is in a forced-convection environment and because the vast majority of the air in the system moves in the x-direction only, the heat generated by components around it or down stream of it will have a negligible effect on its temperature response.

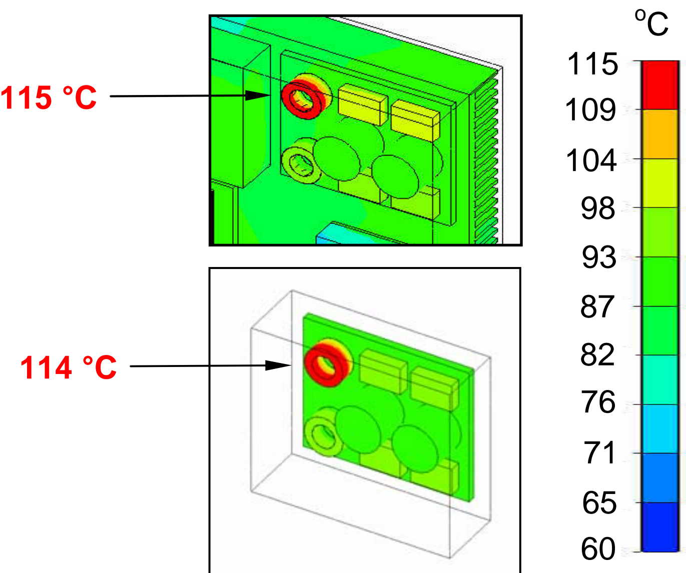

Figure 5.11 Comparison of the temperature response of the output filter from (top) the detailed model and from (bottom) the component-level model.

5.3.3 Multi-Device Methodology

The temperature response of the rack model of Figure 5.5 was lower than expected with a maximum temperature (on the surface of the heat sink) of only 99°C. In this model, heat could be transferred freely between the converters but was restricted to exit the system only through each of the converter's vents. A 2 mm aluminum plate, representing the top and bottom of the case or box, separated each converter. Further analysis should be performed in order to verify that this model does indeed accurately describe what would happen if three power converter devices were placed on their sides side-by-side. It is the designer's responsibility to make sure that this model is an accurate representation of the real system or if the model needs to be modified or radically changed. A good way to verify the accuracy of these results is to build and run the models of Figure 5.6. The zoom-out approach of Figure 5.6 should produce the same results but with much less time required. In addition, experimental analysis should be performed to verify that the computational model accurately predicted the behavior of the three converters stacked side-by-side. Furthermore, this approach should be used to model multiple racks of power converters.

Chapter 6 – Summary

The importance of thermal management in the design of power electronic devices has been well established by many of the researchers referenced in this work. As the industry continues to push toward devices with higher power densities, increased component integration, and smaller packaging, it faces increasingly difficult challenges associated with thermal management. Many researchers have devoted their efforts to solving thermal management problems in electronics cooling applications. In her work, Pang (2002) validated via physical testing the use of I-DEAS as a useful thermal modeling tool and established the importance of the accuracy of input parameters in thermal modeling. In addition, Sewall (2002) established I-DEAS as a useful system-level thermal analysis tool and conducted several experimental studies for power converter thermal design. This work also contributes to the effort of thermal management for electrical systems and complements the research conducted at CPES.

The goal of this research was to develop strategies for finding the optimal cooling of systems of integrated circuits. Section 1.2 presented the specific objectives of this research that were established to accomplish this goal. The following presents the objectives that were accomplished and the contributions made to electronics cooling research.

Achievement of best-case fan arrangement. A system-level computational model was developed in I-DEAS and used for the thermal design of an IPEM-based DC-DC front-end power converter. The model was used to conduct a parametric study that investigated the system's thermal response to fan location and direction. The system's thermal sensitivity to heat sink fin geometry was also briefly investigated. The objective was to find the optimal fan layout that would reduce system-wide temperatures and promote an even distribution of heat. A total of eight cases were investigated in the study. The simulation results showed that the system was not sensitive to the direction of the airflow through the fans alone. However, it was found that the system was extremely sensitive to the location of the cooling fans. Although the best fan arrangement provided

temperatures that were significantly lower than the other cases by supplying the coolest air to the system's hottest region, it was not used for the final design because it conflicted with packaging restraints. Instead, the second-best arrangement was used as it sufficiently cooled the system's components and facilitated an equally sufficient distribution of temperatures. In many applications, the best electrical layout produces the worst thermal layout. But the integration of thermal, electrical, and packaging design can facilitate the efficient search for an optimal solution to these multi-objective design problems.

Experimental Analysis and model comparison. While thermal modeling is an extremely important and efficient tool in the thermal management of power electronic devices, the importance and necessity of experimental testing cannot be overlooked. Chapter 2 presented how the two can be used in sequence to enhance the other and to improve the efficiency and accuracy of thermal design. In this work, an experiment was conducted on a physical prototype of the converter. This test was used to investigate the device's true and transient temperature response. Furthermore, the results of this test were used to compare to the results of the computational model. Although the model did not accurately predict the specific component temperatures because of errors due to model simplification and estimates in input parameters, it was able to predict the general spread of heat in the system and accurately locate the system's hot spots. Predicted temperatures were within 31% of measured temperatures.

Development of an improved modeling approach. This objective was motivated by the need for a more accurate and efficient method of system-level thermal modeling. The zoom-in approach to thermal modeling was applied to the design of the power converter and expanded in order to overcome many of the computational modeling limits associated with modeling large, multi-scale electrical systems. This work investigated zooming-in and zooming-out from a base model to divide large system models into sub-models that can be computationally easier to manage. It was determined that clusters of components could be accurately represented as simple blocks with applied heat loads for general system-level modeling. Furthermore, many models can be further simplified by

eliminating components that do not significantly contribute to the thermal response or the air movement of the system. It was also determined that dividing a system-level model into upstream and downstream models can significantly reduce the complexity of system-level modeling and increase the efficiency of thermal analysis.

This work is intended to be a guideline of cooling strategies and design techniques in order to increase the efficiency and effectiveness of thermal management at CPES. Future work should continue where the present work left off, primarily in the area of multi-scale thermal modeling. The multi-scale modeling study that was presented in this work established a foundation for future work to build upon. Future work should focus upon the continued expansion of the zoom-in approach and the investigation of improved modeling techniques for large-scale electrical systems. This modeling methodology should be applied to data center thermal research in order to increase the accuracy and efficiency of computational analysis.

Because of the industry's push toward higher power densities and smaller device packages, thermal management is becoming increasingly important in power electronic devices. Future research should also focus upon the integration of thermal design with electrical and packaging design early in the design process. Thermal management should not be overly restricted by electrical and packaging design constraints. Instead, thermal design should coincide with electrical and packaging design in order to find the best solution to a multi-objective design problem. Thermal problems must be detected and addressed early in the design stage and thermal issues should significantly contribute to the electrical design and packaging layout of power electronic devices.

Fans and air-cooled heat sinks remain the industry's standard method for cooling power electronic devices. Furthermore, until it becomes significantly cheaper to use alternative cooling methods, fans and heat sinks will likely remain the standard. For this reason, it is warranted to further investigate how to get the most out of their use (e.g., flow diversion analysis). Having said this, it is likely that today's standard cooling methods will be unable to meet the demands of tomorrow's cooling requirements. To address this issue, new and alternative cooling methods should continue to be explored and investigated through computational and experimental analysis. Furthermore,

additional reliability issues (such as thermal stresses and load cycles) should be computationally and experimentally investigated.

The power electronics industry faces many obstacles in keeping up with current demands and technology trends. Today more than ever, there is a great emphasis being placed upon thermal management in power electronic devices. Researchers are working to develop improved design methods and techniques to address thermal management issues. This work contributes to that effort by showcasing the application of state-of-the-art modeling techniques and strategies to overcome many of the thermal issues that challenge the advancement of power electronics technology.

References

Andreozzi, A., Jaluria, Y., and Manca, O., 2003, "Transient Analysis of Natural Convection Between Inclined Parallel Plates," *ASME International Mechanical Engineering Congress & Exposition (IMECE), 2003*, Paper # 41271.

Aung, W., 1988, *Cooling Technology for Electronic Equipment*, (New York: Hemisphere Publishing Corporation).

Azar, K., and Rogers, P., 2001, "Visualization of Air Flows in Electronic Systems," http://www.electronics-cooling.com/html/2001_may_a1.html (Southborough, MA: Electronics Cooling Magazine, May 2001).

Azar, K., 1997, *Thermal Measurements in Electronics Cooling* (Boca Raton: CRC Press).

Belady, C. L., Kelkar, Kanchan M., and Patankar, S. V., 1999, "Improving Productivity in Electronic Packaging with Flow Network Modeling (FNM)", *Electronics Cooling Magazine*, January 1999, Article 4, pp. 36-40.

Bhavnani, S. H., Fournelle, G., and Jaeger, R. C., 2001, "Immersion-Cooled Heat Sinks for Electronics: Insight From High-Speed Photography," *IEEE Transactions on Components, Packaging, and Manufacturing Technologies*, Vol. 24, No. 2, pp. 166-176.

Biber, C., and Belady, C., 1997, "Pressure Drop Prediction for Heat sinks: What is the Best Method?" *Proceedings of InterPACK'97 Conference*, ASME.

Bose, B.K., 2000, "Energy, Environment, and Advances in Power Electronics," *IEEE Transactions on Power Electronics*, Vol. 15, No. 4, pp. 688-701.

Breier, A. and Schlenk, M., 2002, "Cooling of Telecom Systems – Thermal Optimization Using CFD Methods," *Proceedings of the IEEE International Telecommunications Energy Conference (INTELEC)*, pp. 486-490.

Centrum Komputerowe, 2004, "Electronic System Cooling for 3-D Flow and Thermal Simulation of Electronic, Automotive, and Industrial Systems", www.ideas.pl/katalog/elecool.pdf.

Chen, J.Z., Wu, Y., Gence, C., Boroyevich, D., and Bøhn, J.H., 2001, "Integrated Electrical and Thermal Analysis of Integrated Power Electronic Modules Using iSIGHT", *Proceedings of the CPES Power Electronics Seminar*, pp. 141-145.

Cole, R., Dalton, T., Punch, J., Davies, M., and Grimes, R., 1999a, "A Thermal Design Methodology for Electronic Systems – Part I: Board and Component Level," *Proceedings of the 33rd ASME National Heat Transfer Conference*, Paper # 152.

Cole, R., Dalton, T., Punch, J., Davies, M., and Grimes, R., 1999b, "A Thermal Design Methodology for Electronic Systems – Part II: System Level," *Proceedings of the 33rd ASME National Heat Transfer Conference*, Paper # 153.

Cook, R., Malkus, D., Plesha, M., and Witt, R., 2002, *Concepts and Applications of Finite Element Analysis*, 4th edition (New York: John Wiley & Sons).

Copeland, D., Behnia, M., and Nakayama, W., 1997, "Manifold Microchannel Heat Sinks: Isothermal Analysis," *IEEE Transactions on Components, Packaging, and Manufacturing Technologies – Part A*, Vol. 20, No. 2, pp. 96-102.

Copeland, D., 2000, "Optimization of Parallel Plate Heatsinks for Forced Convection," *Proceedings of 16th IEEE SEMI-THERM Symposium*, pp. 266-272.

Dong, W., Lu, B., Yang, B., Lu, Z., Lee, F., Pang, Y., and Scott, E., 2003, "Integrated High Frequency DPS Front-End Converter," *Proceedings of the CPES Power Electronics Seminar*, pp. 131-136.

Electronic Data Systems Corporation (EDS), 2003, "I-DEAS ESC Electronic System Cooling Reference Manual," *from I-DEAS Help Library*.

Grimes, R., and Davies, M., 2002, "The Effect of Fan Operating Point and Location on Temperature Distribution in Electronic Systems," *Proceedings from IEEE Inter- Society Conference on Thermal Phenomena,* pp. 677-684.

Grimes, R., Davies, M., Punch, J., Dalton, T., and Cole, R., 2001, "Modeling Electronic Cooling Axial Fan Flows," *Transactions of the ASME Journal of Electronic Packaging*, Vol. 123, pp. 112-119.

Gupta, A., 2002, "Modeling Large-Scale Electronic Systems Using Computational Fluid Dynamics Through a "Zoom-In" Approach", *Proceedings from IEEE Inter- Society Conference on Thermal Phenomena*, pp. 495-500.

Harlow, J.E., III, 2003, "Toward Design Technology in 2020: Trends, Issues, and Challenges," *Proceedings of the IEEE Computer Society Annual Symposium on VLSI (ISVLSI'03)*.

I-DEAS, 2003a, Version 9, from Electronic Data Systems (EDS)

I-DEAS, 2003b, ESC Help Library, from Electronic Data Systems (EDS)

Icoz, T., and Jaluria, Y., 2003, "Design of Cooling Systems for Electronic Equipment Using Both Experiment and Numerical Inputs," *ASME International Mechanical Engineering Congress & Exposition (IMECE),* Paper # 42098.

International Technology Roadmap For Semiconductors (ITRS), 2003, "Executive Summery," *http://public.itrs.net*.

Ishizuka, M., and Kitamura, Y., 2003, "A Study on the Effect of Inclination on Thermal Behaviors of Natural Convection Inside Thin Electronic Equipment Casing," *ASME International Mechanical Engineering Congress & Exposition (IMECE),* Paper # 42406.

Issa, J.S., and Ortega, A., 2002, "Experimental Measurements of the Flow and Heat Transfer of a Square Jet Impinging on an Array of Square Pin Fins," *ASME International Mechanical Engineering Congress & Exposition (IMECE),* Paper # 39244.

Jiang, L., Mikkelsen, J., Koo, J., Huber, D., Yao, S., Zhang, L., Zhou, P., Maveety, J. G., Prasher, R., Santiago, J. G., Kenny, T. W., and Goodson, K. E., 2002, "Closed-Loop Electroosmotic Microchannel Cooling System for VLSI Circuits," *IEEE Transactions on Components and Packaging Technologies*, Vol. 25, No. 3., September 2002, pp. 347-355.

Jiang, L., Mikkelsen, J., Koo, J., Huber, D., Yao, S., Zhang, L., Zhou, P., Maveety, J. G., Prasher, R., Santiago, J. G., Kenny, T. W., and Goodson, K. E., 2001, "Two-Phase Microchannel Heat Sinks for an Electrokinematic VLSI Chip Cooling System," *Seventeenth IEEE SEMI-THERM Symposium*, pp. 153-157.

Joshi, Y., 2002, "Emerging Thermal Challenges in Electronics Driven by Performance, Reliability, and Energy," *Presentation for Therminic 2002.*

Joshi, Y., Baelmans, M., Copeland, D., Lasance, C., Parry, J., and Rantala, J., 2001, "Challenges in Thermal Modeling of Electronics at the System Level: Summary of Panel Held at the Therminic 2000," *Microelectronics Journal 32*, 2001, pp. 797-800.

Karki, K.C., Patankar, S.V., and Radmehr, A., 2003, "Techniques for Controlling Airflow Distribution in Raised-Floor Data Centers", *Proceedings of the Pacific Rim/ASME International Electronic Packaging Technical Conference and Exhibition (IPACK),* Paper # 35282.

Kendo, Y., Matsushima, H., and Komatsu, T., 2000, "Optimization of Pin-Fin Heat Sinks for Impingement Cooling of Electronic Packages," *Transactions of the ASME Journal of Electronic Packaging, Vol. 122*, September 2000, pp. 240-246.

Kim, S., and Kuznetsov, A., 2002, "Optimization of Pin-Fin Heat Sinks Using the Two Medium Anisotropic Porous Model," *ASME International Mechanical Engineering Congress & Exposition (IMECE),* Paper # 33786.

Kim, S., and Webb, R., 2003, "Thermal Performance Analysis of Fan-Heat Sinks for CPU Cooling," *ASME International Mechanical Engineering Congress & Exposition (IMECE),* Paper # 42172.

Lee, F., 2000, "The State-of-the-Art Power Electronics Technologies and Future Trends," *Proceedings of the 2000 CPES Power Electronics Seminar*, pp. 1229-1232.

Lee, S., 1995, "Optimum Design and Selection of Heat Sinks," *IEEE Transactions on Components, Packaging and Manufacturing Technology – Part A*, Vol. 18, No. 4, December 1995, pp. 812-817.

Lee, S., 1998, "Calculating Spreading Resistances in Heat Sinks," http://www.electronics-cooling.com/Resources/EC_Articles/JAN98/article3.htm (Southborough, MA: Electronics Cooling Magazine, January 1998).

Lee, T.Y., and Mahalingam, M., 1994, "Application of a CFD Tool for System-Level Thermal Simulation," *IEEE Transactions on Components, Packaging, and Manufacturing Technology – Part A*, Vol. 17, No. 4, pp. 564-571.

Linton, R., and Agonafer, D., 1995, "Course and Detailed CFD Modeling of a Finned Heat Sink," *IEEE Transactions on Components, Packaging, and Manufacturing Technologies – Part A*, Vol. 18, No. 3, pp. 517-520.

Mahalingam, R., and Glezer, A., 2002, "Air Cooled Heat Sinks Integrated With Synthetic Jets," *Proceedings from IEEE Inter- Society Conference on Thermal Phenomena,* pp. 285-291.

Maveety, J.G., and Jung, H. H., 2002, "Heat Transfer From Square Pin-Fin Heat Sinks using Air Impingement Cooling," IEEE Transactions on Components, Packaging, and Manufacturing Technologies, Vol. 25, No. 3, pp. 459-469.

Minichiello, A., and Belady, C., 2002, "Thermal Design Methodology for Electronic Systems", *Proceedings of the ITHERM 2002 Conference*, pp. 696-704.

Minichiello, A., and Belady, C., 2003, "Effective Thermal Design for Electronic Systems", *Electronics Cooling Magazine*, May 2003, Article 1, pp. 16 – 21.

Minter, D. L., Pang, Y. F., and Scott, E. P., 2003, "The Effects of Various Cooling Scenarios on a System of Integrated Circuits," *Proceedings of ASME International Mechanical Engineering Congress & Exposition (IMECE),* Paper # 41667.

Mohan, N., Undeland, T., and Robbins, W., 1995, *Power Electronics: Converters, Applications, and Design*, 2nd edition (New York: John Wiley & Sons).

Montgomery, Z., Minter, D. L., and Scott, E. P., 2004, "Analysis of Airflow Diversion in a System of Integrated Electrical Components," *Proceedings of the ASME Heat Transfer/Fluids Engineering Summer Conference (HT2004)*, Paper # HTFED2004-56319.

Nagulapally, M., and Karimanal, K., 2002, "Use of Shell Conduction Plates for Compact Models of Extruded Heat Sinks in Forced Convection Environments," *Proceedings from IEEE Inter- Society Conference on Thermal Phenomena,* pp. 330-334.

Pang, Y.F., 2002, *Integrated Thermal Design and Optimization Study for Active Integrated Power Electronic Modules (IPEMs)*, M. S. Thesis, Virginia Tech.

Pang, Y. F., and Scott, E. P., 2003, "Thermal Characterization and Optimization of Active System IPEM," *Proceedings of the 2003 CPES Power Electronics Seminar*, pp. 622-627.

Pang, Y. F., Chen, J., Scott, E. P., and Thole, K., 2002, "Electrical and Thermal Layout Design and Optimization Considerations for DPS Active IPEM," *ASME International Mechanical Engineering Congress & Exposition (IMECE),* Paper # 2-16-6-3.

Patankar, S., (1980) *Numerical Heat Transfer and Fluid Flow*, (New York: Taylor & Francis).

Patel, C., Sharma, R., Bash, C., and Beitelmal, A., 2002, "Thermal Considerations in Cooling Large Scale High Compute Density Data Centers", *Proceedings from IEEE Inter Society Conference on Thermal Phenomena,* pp. 797-776.

Power Source Manufacturers Association (PSMA), 2003, "A 5-Year Power Technology Roadmap," A Summary of the PSMA Workshop, www.psma.com.

Queipo, N., Devarakonda, R., and Humphrey, J.A.C., 1994, "Genetic Algorithms for Thermosciences Research: Application to the Optimized Cooling of Electronic Components," *International Journal of Heat and Mass Transfer*, Vol. 37, No. 6, pp. 893 – 908.

Rambo, J., and Joshi, Y., 2003, "Multi-Scale Modeling of High Power Density Data Centers", *Proceedings of the Pacific Rim/ASME International Electronic Packaging Technical Conference and Exhibition (IPACK),* Paper # 35297.

Remsburg, R., 1998, *Advanced Thermal Design of Electronic Equipment*, (New York: International Thomson Publishing).

Ridley, R., Reynell, M, and Kern, S., 1993, "Thermal Considerations for Distributed Power Converter Systems," *Proceedings of Applied Power Electronics Conference and Exposition (APEC)*, pp. 866-872.

Saini, M., and Webb, R., 2002, "Heat Rejection Limits of Air Cooled Plane Fin Heat Sinks for Computer Cooling," *Proceedings of 2002 Inter-Society Conference on Thermal Phenomena*, pp. 1-8.

Schmidt, R., and Cruz, E., 2003, "Cluster of High Powered Racks Within a Raised Floor Computer Data Center: Effect of Perforated Tile Flow Distributed on Rack Inlet Air Temperatures", *ASME International Mechanical Engineering Congress & Exposition (IMECE),* Paper # 42240.

Schmidt, R., and Cruz, E., 2002, "Raised Floor Computer Data Center: Effect on Rack Inlet Temperatures When High Powered Racks Are Situated Amongst Lower Powered Racks", *ASME International Mechanical Engineering Congress & Exposition (IMECE),* pp. 297-308.

Schmidt, R., 2003, "Hot Spots in Data Centers," *http://www.electronics-cooling.com/html/2003_august_a2.html,* (Southborough, MA: Electronics Cooling Magazine, August 2003).

Sewall, E., 2002, *Development of a Thermal Management Methodology for a Front-End DPS Power Supply*, M.S. Thesis, Virginia Tech.

Sewall, E., Thole, K.A., and Odendaal, W. G., 2002, "General Guidelines for Thermal Management of High-Power Components Relative to a DC/DC Converter," *Proceedings of 2002 CPES Power Electronics Seminar*, pp. 533-538.

Shah, A., Carey, V., Bash, C., and Patel, C., 2003, "Exergy Analysis of Data Center Thermal Management Systems", *ASME International Mechanical Engineering Congress & Exposition (IMECE),* Paper # 42527.

Sharma, R., Bash, C., Patel, C., Friedrich, R., and Chase, J., 2003, "Balance of Power: Dynamic Thermal Management for Internet Data Centers", *HP Laboratories Palo Alto.*

Simons, R., 1996, "Direct Liquid Immersion Cooling for High Power Density Microelectronics," *http://www.electronics-cooling.com/Resources/EC_Articles/May96/May96_04.htm* (Southborough, MA: Electronics Cooling Magazine, May 1996).

Simons, R., 2003, "Estimating Parallel Plate-Fin Heat Sink Thermal Resistance," *Electronics Cooling Magazine*, February 2003, pp. 8-9.

Simons, R., 2004, "Estimating the Effect of Flow Bypass on Parallel Plate-Fin Heat Sink Performance," *Electronics Cooling Magazine*, February 2004, pp. 6-8.

Vafai, K., and Zhu, L., 1999, "Analysis of Two-Layered Micro-channel Heat Sink Concept in Electronic Cooling," *International Journal of Heat and Mass Transfer 42*, pp. 2287-2297.

Yeh, L.T., and Chu, R.C., 2002, *Thermal Management of Microelectronic Equipment*, (New York: ASME Press)

Yeh, L., 2003, "A System Level Thermal Analysis of Large Telecommunication Racks," *ASME International Mechanical Engineering Congress & Exposition (IMECE),* Paper # 42416.

Appendix A – Thermal Model Boundary Conditions

Section 3.5 of this work outlined the procedure that was used to build the thermal model of the power converter in I-DEAS. The I-DEAS ESC application software was used to apply boundary conditions to the meshed model. The power losses for each electrical component and the fan curve of the system's cooling fans were already listed in Chapter 3. This appendix lists the flow blockages that were defined in the model and the resistance values that were used to represent the contact resistance between surfaces of components. Also included in this appendix is the electrical layout of the converter.

Table 1 The list of flow blockages in the thermal computational model.

Component Name	Convective Flow Blockage
heat sink	yes
passive IPEM	yes
active IPEM Heat Spreader	yes
Component 11 (high snubber)	yes
Component 12 (high diode)	yes
Component 13 (high diode)	yes
Component 14 (capacitor)	yes
Component 15 (capacitor)	yes
Component 16 (low snubber)	yes
Component 17 (low diode)	yes
Component 18 (low diode)	yes
Output Filter Heat Spreader	yes
rectifier top coating	yes
capacitor 1 (DC-DC)	no
capacitor 2 (PFC)	no
inductor	no
EMI Filter	no

Table 2 The list of thermal contact resistances defined in the thermal model.

Component Name		Resistance Value (^{o}C/W)
Bottom	Top	
Component 1 (MOSFET)	DC-DC Trace	0.0392
Component 2 (MOSFET)	DC-DC Trace	0.0392
Component 3 (DC Gate)	DC-DC Trace	0.496
Component 4	PFC Trace	1.276
Component 5	PFC Trace	1.276
Component 6 (CoolMOS)	PFC Trace	0.09375
Component 7 (PFC Gate)	PFC Trace	4.472
Component 8 (CoolMOS)	PFC Trace	0.09375
DC-DC Trace	Active IPEM base	0.001
PFC Trace	Active IPEM base	0.001
Active IPEM base	Active IPEM heat spreader	0.0016
Active IPEM heat spreader	Heat sink	0.056
Passive IPEM	Heat sink	0.0291
Component 11 (high snubber)	Output filter heat spreader	1.123
Component 12 (high diode)	Output filter heat spreader	0.776
Component 13 (high diode)	Output filter heat spreader	0.776
Component 14 (capacitor)	Output filter heat spreader	0.498
Component 15 (capacitor)	Output filter heat spreader	0.498
Component 16 (low snubber)	Output filter heat spreader	1.123
Component 17 (low diode)	Output filter heat spreader	0.776
Component 18 (low diode)	Output filter heat spreader	0.776
Output Filter Heat Spreader	Heat sink	0.026
Component 19 (rectifier diode)	Rectifier base	0.073
Component 20 (rectifier diode)	Rectifier base	0.073
Component 21 (rectifier diode)	Rectifier base	0.073
Component 22 (rectifier diode)	Rectifier base	0.073
rectifier base	Heat sink	0.157

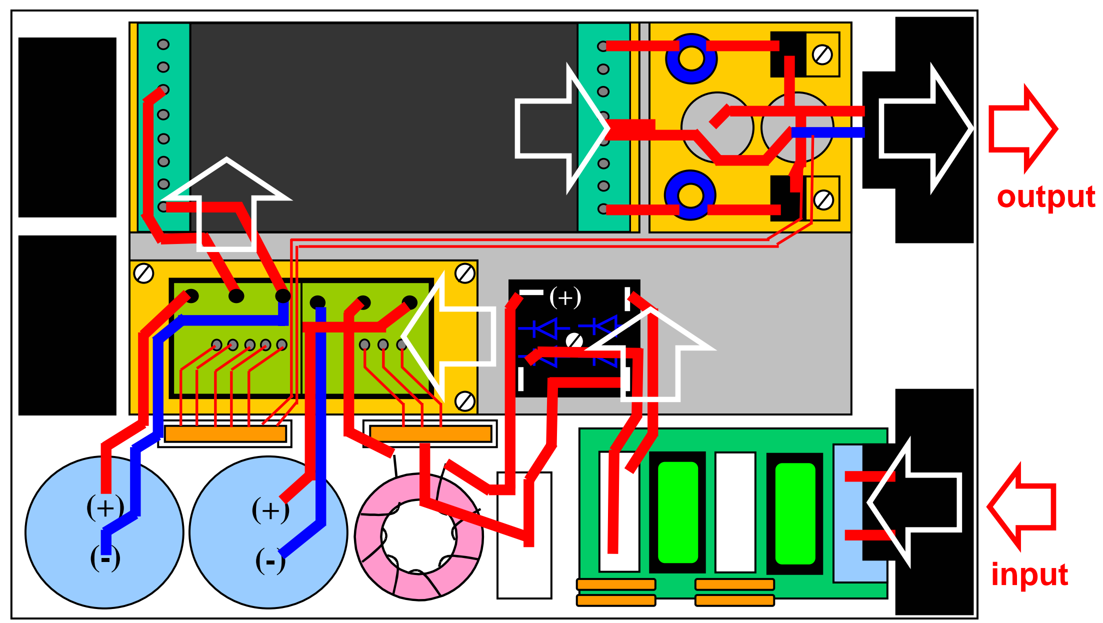

Figure 1 The system-level flow of power in the electrical layout.

Appendix B – I-DEAS Simulations

I-DEAS ESC software generates a simulation message file called escmsg.dat during the solution run. This file lists information concerning element count, boundary conditions, and solver options input by the user. It also records the details of the solution iteration process and the convergence history of the model. This appendix presents the simulation message file for the original (fully-detailed) model and the simplified base model of Chapter 5 (Model B).

B.1 Original Model

This section lists the ESC file of the original (fully-detailed) model presented in Chapter 3 and analyzed in Chapter 4.

```
Thermal/Flow Analysis Software
==============================
MAYA Heat Transfer Technologies Ltd.


TMG/ESC Version 9.0.492   Feb 21, 2003


ESCRR - Convert analysis results
======================================================================
Time: Tue Dec 23 18:05:19 2003


+---------------------------------------------------------------------+
|                          Solution Summary                           |
+---------------------------------------------------------------------+


Results Summary       Maximum       Minimum       Average
----------------------------------------------------------------------
Fluid Temperature     8.378E+01     5.000E+01     5.861E+01 C
          at node         42248         24978
Fluid Velocity        6.505E+03     8.803E+00     2.674E+03 mm/s
          at node         53717         49761
Fluid Pressure        3.299E-02    -1.727E-02     4.382E-03 mN/mm^2
          at node         62933         48603
Solid Temperature     1.158E+02     7.679E+01     9.213E+01 C
Y+                    2.648E+01     5.685E-01     1.263E+01
Heat Trans. Coef.     8.606E+01     4.410E+00     3.312E+01 mN/mm-s-C
```

```
----------------------------------------------------------------------


Volume/Mass Flow Summary
(Values < 0 are outflow)     Volume Flow          Mass Flow
----------------------------------------------------------------------
FAN 1                        6.275E+06 mm^3/s     6.858E-03 kg/s
FAN 2                        6.636E+06 mm^3/s     7.253E-03 kg/s
VENT 1                      -1.329E+07 mm^3/s    -1.411E-02 kg/s
----------------------------------------------------------------------


Flow Solver:
Heat Convected To/From Fluid
(Values < 0 are outflows)    Positive Side        Negative Side
----------------------------------------------------------------------
PASSIVE_TOP                  7.214E+06 mN-mm/s    0.000E+00 mN-mm/s
PASSIVE_SIDES                3.854E+06 mN-mm/s    0.000E+00 mN-mm/s
OUTPUT_HS                    2.643E+06 mN-mm/s    0.000E+00 mN-mm/s
OUTPUT_HS_SIDES              3.891E+05 mN-mm/s    0.000E+00 mN-mm/s
11_TOP                       6.597E+04 mN-mm/s    0.000E+00 mN-mm/s
16_TOP                       4.225E+04 mN-mm/s    0.000E+00 mN-mm/s
15_TOP                       2.974E+05 mN-mm/s    0.000E+00 mN-mm/s
14_TOP                       3.218E+05 mN-mm/s    0.000E+00 mN-mm/s
13_TOP                       2.284E+05 mN-mm/s    0.000E+00 mN-mm/s
13_SIDES                     1.521E+05 mN-mm/s    0.000E+00 mN-mm/s
18_TOP                       2.092E+05 mN-mm/s    0.000E+00 mN-mm/s
18_SIDES                     1.453E+05 mN-mm/s    0.000E+00 mN-mm/s
17_TOP                       2.005E+05 mN-mm/s    0.000E+00 mN-mm/s
17_SIDES                     1.447E+05 mN-mm/s    0.000E+00 mN-mm/s
12_TOP                       2.114E+05 mN-mm/s    0.000E+00 mN-mm/s
12_SIDES                     1.403E+05 mN-mm/s    0.000E+00 mN-mm/s
ACTIVE_HS_TOP                3.217E+06 mN-mm/s    0.000E+00 mN-mm/s
ACTIVE_HS_SIDES              5.562E+05 mN-mm/s    0.000E+00 mN-mm/s
PLASTIC_TOP                  9.017E+05 mN-mm/s    0.000E+00 mN-mm/s
PLASTIC_SIDES                5.191E+05 mN-mm/s    0.000E+00 mN-mm/s
HEATSINK_TOP                 1.153E+07 mN-mm/s    0.000E+00 mN-mm/s
HEATSINK_OUTER_SIDES         3.427E+06 mN-mm/s    0.000E+00 mN-mm/s
HEATSINK_BASE_BOTTOM         8.767E+06 mN-mm/s    0.000E+00 mN-mm/s
HEATSINK_INNER_SIDES         8.688E+07 mN-mm/s    0.000E+00 mN-mm/s
HEATSINK                     9.321E+05 mN-mm/s    0.000E+00 mN-mm/s
PASSIVE                      1.227E+06 mN-mm/s    0.000E+00 mN-mm/s
OUTPUT_HS                    8.466E+04 mN-mm/s    0.000E+00 mN-mm/s
11                           1.677E+03 mN-mm/s    0.000E+00 mN-mm/s
16                           1.300E+03 mN-mm/s    0.000E+00 mN-mm/s
15                           4.734E+05 mN-mm/s    0.000E+00 mN-mm/s
14                           5.164E+05 mN-mm/s    0.000E+00 mN-mm/s
13                           3.855E+04 mN-mm/s    0.000E+00 mN-mm/s
18                           3.236E+04 mN-mm/s    0.000E+00 mN-mm/s
17                           3.214E+04 mN-mm/s    0.000E+00 mN-mm/s
12                           3.335E+04 mN-mm/s    0.000E+00 mN-mm/s
ACTIVE_HS                    1.200E+05 mN-mm/s    0.000E+00 mN-mm/s
PLASTIC                      1.995E+05 mN-mm/s    0.000E+00 mN-mm/s
----------------------------------------------------------------------
Total Heat Convected to Fluid                     1.357E+08 mN-mm/s
```

```
Thermal Solver: Heat Flow
----------------------------------------------------------------------
Total heat load on non-fluid elements            1.357E+08 mN-mm/s
Heat flow from temperature B.C.s                 0.000E+00 mN-mm/s
Heat flow into temperature B.C.s                 1.600E+01 mN-mm/s
Heat convected to fluid                          1.357E+08 mN-mm/s
Heat convected from fluid                        0.000E+00 mN-mm/s
----------------------------------------------------------------------
Total Heat Imbalance                             2.880E+02 mN-mm/s

Solver Convergence
----------------------------------------------------------------------
Thermal solver - Maximum temperature change      8.357E-02 C
Flow solver - Momentum imbalance                  -0.00021 Percent
Flow solver - Mass imbalance                      -0.00005 Percent
Flow solver - Energy imbalance                     0.28421 Percent
Coupled solution - Maximum temperature change    8.357E-02 C
Coupled solution - Normalized Heat Imbalance     1.014E-05
----------------------------------------------------------------------




+--------------------------------------------------------------------+
|                                END                                 |
+--------------------------------------------------------------------+

Solution elapsed time: 01 min 04 sec
```

B.2 Model B of Chapter 5

This section lists the ESC simulation file for Model B of Chapter 5.

```
Thermal/Flow Analysis Software
==============================
MAYA Heat Transfer Technologies Ltd.


TMG/ESC Version 9.0.492   Feb 21, 2003


ID2ESC - Thermal/flow model file builder
======================================================================
Time: Mon Feb  2 14:28:37 2004


+--------------------------------------------------------------------+
|                           Model Summary                            |
+--------------------------------------------------------------------+

Finite Element Model
```

```
--------------------

Model File: none
Current FE Model: Fem1
Current FE Study: DEFAULT FE STUDY

Number of nodes in thermal model:                        4740
Number of elements in thermal model:                    18262

Number of nodes in flow model:                           4778
Number of elements in flow model:                       12696

Solution Options
----------------

Steady-State Analysis
Solution Method:                                    Concurrent
Communication Frequency:                                     5
Solving Flow
Solving Thermal

Ambient Temperature:                                5.000E+01 C
Ambient Pressure:                                   1.014E+02 mN/mm^2

Fluid buoyancy:                                     Off
Gravity Acceleration:                               9.810E+03 mm/s^2
Gravity Vector:   X: 0.000E+00  Y: 0.000E+00  Z:-1.000E+00

Flow laminar/turbulent model:                       Mixing length
  Length scale is auto calculated

Flow solver iteration limit:                             1000
Flow converged when RMS residual less than:         2.000E-04
Flow solver physical time step:                     5.000E-01 s
Flow solver heat imbalance:                         2.000E-02

Advection Scheme Momentum:                          First Order
Advection Scheme Energy (if Solve_Energy):          First Order

Global Relaxation Factor:                           7.500E-01
Mass Relaxation Factor:                             7.500E-01
Fluids Relaxation Factor:                           9.000E-01
Fan Curves Relaxation Factor
     Inlet, Outlet and Internal Fans:               1.000E+00
     Recirculation Fans:                            5.000E-01

Thermal Boundary Conditions
---------------------------

Number of thermal boundary  conditions:                   4

Thermal Boundary Condition     Type         Value              FSF TCP
----------------------------------------------------------------------
  1 - PASSIVE                  Heat Load    3.000E+07 mN-mm/s  No  No
  2 - OUTPUT                   Heat Load    4.100E+07 mN-mm/s  Yes No
  3 - RECTIFIER                Heat Load    1.464E+07 mN-mm/s  No  Yes
  4 - ACTIVE                   Heat Load    5.011E+07 mN-mm/s  No  No
```

```
----------------------------------------------------------------------

Thermal Couplings
-----------------

Number of thermal couplings:                              4

Thermal Coupling                   Type         Value
----------------------------------------------------------------------
  1 - PASSIVE_HEATSINK             Resistance   2.910E-08
      Primary Area:  4.370E+03 mm^2
      Secndry Area:  1.916E+04 mm^2
  2 - OUTPUT_HEATSINK              Resistance   2.600E-08
      Primary Area:  3.316E+03 mm^2
      Secndry Area:  1.916E+04 mm^2
  3 - ACTIVE_HEATSINK              Resistance   5.600E-08
      Primary Area:  1.438E+03 mm^2
      Secndry Area:  1.916E+04 mm^2
  4 - RECT_HEATSINK                Resistance   1.570E-07
      Primary Area:  8.123E+02 mm^2
      Secndry Area:  1.916E+04 mm^2
----------------------------------------------------------------------

Flow Surfaces
-------------

Number of flow surfaces:                                  9

Flow Surface                        Surface Properties     Elements
                                    +ve side / -ve side   Surfc Atchd
----------------------------------------------------------------------
  1 - PASSIVE_TOP                  SURFACE PROPERTY 1        92     0
      Area:  4.370E+03 mm^2        SURFACE PROPERTY 1
  2 - PASSIVE_SIDES                SURFACE PROPERTY 1        68     0
      Area:  2.870E+03 mm^2        SURFACE PROPERTY 1
  3 - OUTPUT_TOP                   SURFACE PROPERTY 1        68     0
      Area:  3.316E+03 mm^2        SURFACE PROPERTY 1
  4 - OUTPUT_SIDES                 SURFACE PROPERTY 1        24     0
      Area:  3.840E+02 mm^2        SURFACE PROPERTY 1
  5 - HEATSINK_TOP                 SURFACE PROPERTY 1       414     0
      Area:  1.916E+04 mm^2        SURFACE PROPERTY 1
  6 - HEATSINK_OUTER_SIDES         SURFACE PROPERTY 1       132     0
      Area:  5.904E+03 mm^2        SURFACE PROPERTY 1
  7 - HEATSINK_INNER_SIDES         SURFACE PROPERTY 1      3564     0
      Area:  1.240E+05 mm^2        SURFACE PROPERTY 1
  8 - RECT_TOP                     SURFACE PROPERTY 1        74     0
      Area:  8.122E+02 mm^2        SURFACE PROPERTY 1
  9 - RECT_SIDES                   SURFACE PROPERTY 1        44     0
      Area:  6.270E+02 mm^2        SURFACE PROPERTY 1
----------------------------------------------------------------------

Flow Blockages
--------------

Number of flow blockages:                                 9

Flow Blockage                      Type         Loss Coeff
```

```
  1 - CAP1                              Solid        0.000E+00  1/mm
      Volume:  3.315E+04 mm^3
  2 - CAP2                              Solid        0.000E+00  1/mm
      Volume:  3.315E+04 mm^3
  3 - INDUCTOR                          Solid        0.000E+00  1/mm
      Volume:  1.633E+04 mm^3
  4 - FILTER                            Solid        0.000E+00  1/mm
      Volume:  7.220E+04 mm^3
  5 - HEATSINK                          Auto-convect 0.000E+00  1/mm
      Volume:  2.052E+05 mm^3
  6 - PASSIVE                           Auto-convect 0.000E+00  1/mm
      Volume:  7.436E+04 mm^3
  7 - OUTPUT                            Auto-convect 0.000E+00  1/mm
      Volume:  9.949E+03 mm^3
  8 - ACTIVE                            Auto-convect 0.000E+00  1/mm
      Volume:  6.676E+03 mm^3
  9 - RECTIFIER                         Auto-convect 0.000E+00  1/mm
      Volume:  8.935E+03 mm^3
----------------------------------------------------------------------

Fans
----

Number of fans:                                            2

Fan                                 Type         Value
----------------------------------------------------------------------
  1 - Inlet  - FAN 1                Fan Curve
      Area:  1.600E+03 mm^2
  2 - Inlet  - FAN 2                Fan Curve
      Area:  1.600E+03 mm^2
----------------------------------------------------------------------

Vents
-----

Number of vents:                                           1

Vent                                Type
----------------------------------------------------------------------
  1 - VENT 1                        Specified temperature and pressure
      Area:  7.040E+03 mm^2

      Pres:  1.014E+02 mN/mm^2
----------------------------------------------------------------------


+--------------------------------------------------------------------+
|                          Solution Summary                          |
+--------------------------------------------------------------------+


Results Summary      Maximum       Minimum       Average
----------------------------------------------------------------------
Fluid Temperature    9.065E+01     5.000E+01     6.560E+01 C
          at node         2061          1233
Fluid Velocity       5.694E+03     2.277E+01     2.534E+03 mm/s
```

```
          at node          1864          1736
Fluid Pressure        2.975E-02    -8.825E-03     5.233E-03 mN/mm^2
          at node          3683          1698
Solid Temperature     9.550E+01     7.686E+01     8.783E+01 C
Y+                    6.996E+01     9.553E-01     1.404E+01
Heat Trans. Coef.     7.096E+01     9.121E+00     4.409E+01 mN/mm-s-C
----------------------------------------------------------------------



Volume/Mass Flow Summary
(Values < 0 are outflow)     Volume Flow          Mass Flow
----------------------------------------------------------------------
FAN 1                        6.360E+06 mm^3/s     6.952E-03 kg/s
FAN 2                        6.705E+06 mm^3/s     7.328E-03 kg/s
VENT 1                      -1.345E+07 mm^3/s    -1.428E-02 kg/s
----------------------------------------------------------------------



Flow Solver:
Heat Convected To/From Fluid
(Values < 0 are outflows)    Positive Side        Negative Side
----------------------------------------------------------------------
PASSIVE_TOP                  5.449E+06 mN-mm/s    0.000E+00 mN-mm/s
PASSIVE_SIDES                3.198E+06 mN-mm/s    0.000E+00 mN-mm/s
OUTPUT_TOP                   2.317E+06 mN-mm/s    0.000E+00 mN-mm/s
OUTPUT_SIDES                 3.127E+05 mN-mm/s    0.000E+00 mN-mm/s
HEATSINK_TOP                 1.253E+07 mN-mm/s    0.000E+00 mN-mm/s
HEATSINK_OUTER_SIDES         5.444E+06 mN-mm/s    0.000E+00 mN-mm/s
HEATSINK_INNER_SIDES         8.202E+07 mN-mm/s    0.000E+00 mN-mm/s
RECT_TOP                     6.643E+05 mN-mm/s    0.000E+00 mN-mm/s
RECT_SIDES                   5.616E+05 mN-mm/s    0.000E+00 mN-mm/s
HEATSINK                     1.889E+07 mN-mm/s    0.000E+00 mN-mm/s
PASSIVE                      1.185E+06 mN-mm/s    0.000E+00 mN-mm/s
OUTPUT                       1.892E+05 mN-mm/s    0.000E+00 mN-mm/s
ACTIVE                       2.399E+06 mN-mm/s    0.000E+00 mN-mm/s
RECTIFIER                    2.855E+05 mN-mm/s    0.000E+00 mN-mm/s
----------------------------------------------------------------------
Total Heat Convected to Fluid                     1.354E+08 mN-mm/s


Thermal Solver: Heat Flow
----------------------------------------------------------------------
Total heat load on non-fluid elements             1.357E+08 mN-mm/s
Heat flow from temperature B.C.s                 -1.874E-02 mN-mm/s
Heat flow into temperature B.C.s                  0.000E+00 mN-mm/s
Heat convected to fluid                           1.357E+08 mN-mm/s
Heat convected from fluid                         1.864E+02 mN-mm/s
----------------------------------------------------------------------
Total Heat Imbalance                             -1.600E+01 mN-mm/s

Solver Convergence
----------------------------------------------------------------------
Thermal solver - Maximum temperature change       8.629E-02 C
Flow solver - Momentum imbalance                   -0.00002 Percent
Flow solver - Mass imbalance                       -0.00007 Percent
Flow solver - Energy imbalance                      0.18530 Percent
Coupled solution - Maximum temperature change     8.629E-02 C
```

Vita

Dion Len Minter was born in Roanoke, Virginia, in 1978. He graduated from Roanoke Valley Christian Schools in 1996. In 1999, he earned his Associate in Engineering from Virginia Western Community College in Roanoke, Virginia and, in 2002, he earned his Bachelor of Science in Mechanical Engineering at Virginia Tech in Blacksburg, Virginia. He joined CPES in the fall of 2002 and conducted his master's research in heat transfer in power electronics under Dr. Elaine Scott's supervision. He earned his Master of Science in Mechanical Engineering in Spring 2004.